Physico-chemical, electrical and optical properties of regiorandom and regioregular MDMO-PPV

Proefschrift voorgelegd tot het behalen van de graad van
Doctor in de Wetenschappen, richting Scheikunde,
te verdedigen door

Tom MUNTERS

Promotor : Prof. dr. D. Vanderzande
Co-promotor: Prof. dr. L. De Schepper

INSTITUUT VOOR MATERIAALONDERZOEK

LIMBURGS UNIVERSITAIR CENTRUM
PARTNER IN DE UNIVERSITEIT LIMBURG

Voorwoord

Er was een tijd dat wetenschappers zich steeds dieper en dieper in hun discipline ingroeven. Dit opsluiten in het eigen vakgebied was vaak noodzakelijk door de toegenomen kennis en specialisatie. Vandaag echter wordt een omgekeerde beweging waargenomen. De nieuwe ontdekkingen en inzichten vinden vooral plaats op raakvlakken tussen twee of meer disciplines. Zo is er ook het domein van de 'plastiek elektronica' gesitueerd op het raakvlak van vaste-stof fysica, polymeer chemie, micro-elektronica techniek, enz. Het samenbrengen van fysici, scheikundigen en ingenieurs is dan ook cruciaal gebleken voor de steile voortgang in dit onderzoeksdomein de voorbije 15 jaar. Deze nieuwe benadering vergt dan ook naast de al eerder erkende vaardigheden zoals inspiratie en transpiratie ook vaardigheden zoals communicatie. Zelf mocht ik dit aan den lijve ondervinden door met een sterk chemische achtergrond een doctoraatsthesis te maken op het fysica departement van het 'Instituut voor Materiaal Onderzoek' (IMO) onderdeel van het 'Limburgs Universitair Centrum' (LUC). Illustratief zijn de vele malen dat die gekke tekeningetjes (structuurformules) moesten worden verklaard. Nu, op het eindpunt van dit doctoraat, beschouw ik dit functioneren in een multidisciplinaire omgeving dan ook als de grootste vaardigheid opgedaan gedurende deze jaren. Deze multidisciplinaire omgeving was dan ook vaak inspirerend en erg plezierig om in te werken. Een enkele lezer zal misschien opmerken dat dit werk geen typische scheikunde of natuurkunde thesis is daar de nadruk vooral ligt op de relaties tussen beide gebieden en de toepassingen. Desalniettemin was dit een uitdagende manier van onderzoeken.

Heel wat mensen hebben dan ook een bijdrage geleverd aan het tot stand komen van dit werk. Ik ben hen dan ook een woordje van dank verschuldigd.

In de eerste plaats zou ik mijn promotoren Prof. dr. Dirk Vanderzande en Prof. dr. Luc De Schepper willen bedanken omdat ze mij de kans hebben gegeven om dit onderzoek binnen de infrastructuur van het IMO uit te voeren. Beide zijn dan ook geen 'ivoren toren' professoren maar personen

die een multidisciplinaire benadering van het onderzoeksdomein 'plastiek elektronica' reeds lang promoten.

De leden van mijn doctoraatscommissie moet ik eveneens bedanken voor hun interesse en tijd om dit werk te beoordelen.

Een speciaal woordje van dank zou ik willen richten naar Prof. dr. Jean Manca. Niet enkel voor de gedegen wetenschappelijke begeleiding van dit werk maar ook voor de gemoedelijke en warme manier waarop hij met zijn mensen wist om te gaan. Ik dank hem dan ook voor het grote vertrouwen in mij en wens hem dan ook veel succes toe in de verdere uitbouw van de 'organic electronic materials' (OEM) onderzoeksgroep.

De naaste collega's Tom Martens en Ludwig Goris wil ik veel succes toewensen met hun doctoraatswerk en verdere loopbaan. De pogingen om de glove-box proper te houden bleken een verspilling van tijd, niet zo voor de vele aangename gesprekken en discussies. Ludwig wens ik verder nog een kopie van Sharon Stone en/of Antje De Boeck. Graag vermeld ik hier ook de mensen die steeds een oplossing brachten voor de kleine en grote glove-box problemen. Ik dank Johnny, Dany, Jan en Erik dan ook voor hun inzet.

Ook wil ik mijn waardering uitdrukken voor de hulp van Jan D'Haen bij het TEM werk. Zijn toewijding en kennis maken van hem niet enkel een succesfactor in dit werk maar in vele hieraan voorafgaande thesissen en ongetwijfeld ook aan vele volgende thesissen.

Laurence Lutsen en haar synthesemedewerkers Veerle en Iris zou ik willen bedanken voor de materialen. Hilde en Peter wil ik eveneens bedanken voor het karakteriseren van deze materialen. Daarnaast wil ik de gehele organische onderzoeksgroep van de scheikunde bedanken voor de aangename tijd en het uitwisselen van de experimentele en theoretische weetjes o.a. op de sfeervolle BPG bijeenkomsten.

De collega's van het fysicadepartement van het IMO wil ik ook bedanken voor hun getoonde interesse in dit werk en vele leuke momenten en discussies. Het feit dat enkelen naast collega ook vriend(in) genoemd mogen worden is illustrerend voor de toffe werksfeer.

De mogelijkheden om verder te kijken dan de muren van de eigen onderzoeksgroep, zowel in projecten als gedurende stages heb ik steeds als zeer boeiend en verrijkend ervaren.

Mijn dank gaat dan ook uit naar Arjan Bernsten en de mensen van Philips, Natlab om in hun interne keuken te mogen mee draaien. Het opbouwen van de fotoluminescentie efficientie meetopstelling was een boeiende ervaring.

The traineeship at the Christian Doppler Laboratory for Plastic Solar Cells headed by Prof. dr. Serdar Sariciftci, Johannes Kepler University (Linz, Austria) was an enriching experience in one of the top research groups in the field of organic photovoltaic devices. More especially I would like to thank Christoph Brabec for his clarifying insights. I am convinced he will play an omnipresent role in the future commercial success of the plastic solar cells. It was a pleasure working together with him.

Contents

CHAPTER 6 STRUCTURE-PROPERTY RELATIONS AND CONCLUSIONS 151

SUMMARY 167

SAMENVATTING 171

Chapter 1
General introduction

In chapter 1, a general introduction to this work is given. In the first section, the aim and outline of this thesis are presented. It will be shown that a multidisciplinary approach is needed to tackle the central scientific questions of this thesis, namely: 'what is the influence of sp^3 defects and regioregularity on the semiconductor properties of a 'workhorse' conjugated polymer, MDMO-PPV?' In the next sections a brief introduction on conjugated polymers is given. Besides a short description of the synthetic principles to obtain the most common conjugated polymers, the electronic structure of these disordered semiconductors and some of their applications are discussed.

1.1   Aim and outline of the thesis

In the recent wave of breakthroughs in the field of 'organic' electronics, successful results are being obtained in the development of light emitting diodes, full color displays thin film transistors, (bio-) sensors and solar cells based on organic materials, e.g. conjugated polymers or small organic molecules. The polymeric approach yields a potential to develop a large-scale (low cost) roll-to-roll production on flexible substrates. Conjugated polymers combine properties of classical macromolecules, such as low weight, good mechanical behavior and an easy processing with (semi)-conductor properties arising from their electronic structure. The scientific community has explicitly acknowledged the importance of this class of materials by awarding the pioneers in this field Alan Heeger, Alan MacDiarmid and Hideki Shirakawa with the year 2000 Nobel Prize for chemistry. In the seventies, they observed an increase in conductivity by several orders of magnitude for a poly(acetylene) film, oxidized with iodine vapour[1].
The chemical structures of several common conjugated polymers are shown

in figure 1.1: poly(acetylene) (PA), poly(aniline) (PANI), poly(pyrole) (PPy), poly(p-phenylene) (PPP), poly(p-phenylenevinylene) (PPV) and poly(thiophene) (PT).
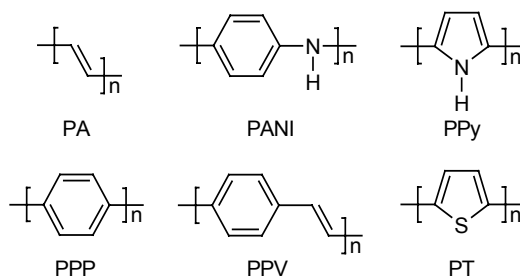
figure 1.1 Several common conjugated polymers

Conjugated polymers possess a delocalized π-electron system along the polymer backbone. In general they are constructed from aromatic units and/or multiple bonds alternating with single bonds. The overlap of adjacent atomic p_z-orbitals yields lower energy bonding (π) and higher energy anti-bonding (π*) molecular orbitals. The difference in energy between the highest occupied molecular orbital (HOMO) and lowest unoccupied molecular orbital (LUMO) is called bandgap (E_g) (typical between 1-4 eV). This energy difference plays a crucial role in making these materials suitable for electronic applications.

One of the advantages of organic materials is the possibility of unlimited chemical modifications. As a consequence, in many cases the reader tends to get lost in elaborate enumerations of many derivatives and their properties. Therefore, in section 1.2 a brief summary of the polymerization chemistry of the common basic conjugated polymers, as depicted in figure 1.1, is given. Within the scope of this thesis, one will focus on precursor routes towards PPV. In section 1.3 a description of the electronic structure of conjugated polymers and their corresponding electrical properties will be given. Finally in section 1.4 the major applications of conjugated polymers will be discussed.

Since the beginning of the nineties, at the 'Instituut voor Materiaal Onderzoek' (IMO) of the 'Limburgs Universitair Centrum' (LUC), research is performed on the development of precursor routes to synthesize semiconducting polymers. Besides the successful development of a new synthetic precursor route, the sulfinyl route, chemical and physical characterization techniques are used to obtain a better understanding of the structure-property relationship.

It is shown that this synthetic procedure is based on a highly selective chemistry. This feature allows future organic semiconductor materials with a better-controlled structure and number of chemical defects. It is good to

notice that the term defect, within the context of this thesis, is used as a deviation of the conjugated polymer from its monomeric representation. At asymmetrically substituted PPV-derivatives, such as the 'workhorse' material MDMO-PPV, two type of defects can be distinguished: defects related to interruptions of the conjugated system at the vinylene double bond (**single bond defects**) and defects related to the position of the side-chains (**regioregularity**). The sulfinyl route can control both defects.

However, some new basic scientific questions appear, namely: 'How to use these new synthetic possibilities to obtain high performance semiconducting organic polymers? What is the influence of regioregularity on the semiconductor properties? What is the influence of sp^3 defects (single bond defects) in the conjugated chain on the semiconductor properties?' Therefore, the aim of this thesis is to clarify the relation between both mentioned chemical defects of a commonly used 'workhorse' conjugated polymer, MDMO-PPV and the performance of devices made with this material.
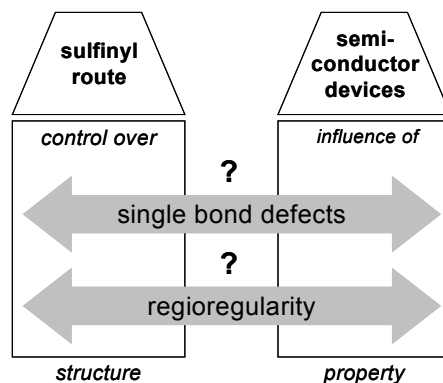
figure 1.2 Overview of the two main scientific questions within the scope of this work, namely: 'What is the influence of single bond defects on MDMO-PPV semiconductor devices?' and 'What is the influence of regioregularity on MDMO-PPV semiconductor devices?'

It is clear that the best strategy to gain correct insights in this structure-property relation is a multidisciplinary approach, combining chemistry, physics and device engineering.

Within this work the influence of both mentioned effects (e.g. regioregularity and single bond defects) on the semiconducting properties of MDMO-PPV becomes progressively clear. This insight will be used to orient future extensions of the sulfinyl route to produce high performance conjugated polymers.

This thesis is divided into six individual chapters. In the present chapter a general introduction on conjugated polymers and the aim and outline of this thesis are given. In chapter 2, a brief discussion about the different defects as expected for two precursor routes used within the scope of this

thesis to synthesize the 'workhorse' material MDMO-PPV is presented. Besides a description of the basic synthetic procedure and chemical characterization of the MDMO-PPV materials and films, a matrix with five model compounds will be defined. This characterization of this matrix can be considered as the thread of this thesis. In chapter 3 this set of materials is used as semiconductor layer in field effect transistors (FET). The corresponding characteristics yield information on the FET-mobility of the charge carriers. In chapter 4, an extended optical characterization is carried out on this matrix, thereby focusing on photoluminescence efficiency measurements and time-resolved photoluminescence experiments, to evaluate the nature and lifetime of the excitons. During a six week traineeship at Philips, Natlab (Eindhoven, The Netherlands) a new experimental set-up to determine correct values of the photoluminescence efficiency was built and tested. This set-up is described in section 4.2.1. To evaluate the performance of the defined matrix in a more complicated application, the photovoltaic responses of the different materials are discussed in chapter 5. During an eight week traineeship at the Christian Doppler Laboratory for Plastic Solar Cells, Johannes Kepler University (Linz, Austria) a comparison between solar cells based on MDMO-PPV prepared via the reference precursor route and prepared via the sulfinyl route was carried out. These results are presented in section 5.3.1 and 5.3.2. In chapter 6, a conclusive discussion is presented regarding the two central scientific questions, namely: 'What is the influence of single bond defects on MDMO-PPV semiconductor devices?' and 'What is the influence of regioregularity on MDMO-PPV semiconductor devices?'

1.2   Chemistry of conjugated polymers

At first, the poor process possibilities and the environmental instability of the conductive polymers hampered commercial success. Excitement on conjugated polymers was renewed during the eighties when chemists learned how to make these materials soluble, while maintaining their electrical properties. Nowadays, (some) conjugated polymers can be produced like the common polymers of the plastic industry. They can be molded into parts, drawn into long fibers and cast onto flexible films offering a potential for substantial cost-savings compared to traditional semiconductors.

In this section, a brief summary of the general synthetic principles of the common, basic conjugated polymers will be given. However, within the scope of this thesis, an extended survey on precursor routes towards PPV is presented.

1.2.1   Synthetic principles

Poly(acetylene) (PA) was first prepared as a linear, high molecular weight crystalline polyconjugated polymer with a regular structure by Natta et al. who polymerized acetylene in hexane using $Al(Et)_3/Ti(OpPr)_4$ as initiator system[2]. PA was considered of little interest because independently on the preparation method only an air-sensitive, infusible and insoluble black powder could be obtained. An increased attention towards PA was shown after the development of a simple method for the preparation of thin film samples by Shirakawa et al[3]. Treatment of these films with oxidizing agents exhibited an enormous increase in conductivity[1].

The preferred catalyst among other Ziegler-Natta catalysts[4] is a combination of $Ti(O-n-C_4H_9)_4$ and $(C_2H_5)_3Al$ yielding (when used in high concentrations) mechanically strong films[3]. Besides the use of Ziegler-Natta catalysts, other catalyzing systems are reported in literature[5]. A typical noncatalytic polymerization of acetylene can be performed electrochemically[6].

The inherent insolubility of most conjugated polymers combined with a strong oxygen sensitivity imposes a barrier to an easy processing. A common formalism to overcome this problem is to work with soluble polymeric analogues that can be transformed in a conjugated polymer. These so-called precursor methods are also developed for the synthesis of PA. A first example using this approach to synthesize PA, is a dehydrohalogenation of poly(vinyl chloride)[7]. Feast et al. developed an alternative, rather complex method to thermally convert prepolymers to PA[8].

The mentioned distinction between on one hand direct polymerization routes and on the other hand precursor routes can also be applied for all other common conjugated polymers depicted in figure 1.1.

Although a wide variety of direct polymerization procedures towards conjugated polymers can be found, a majority of the presented preparation methods can be classified in three categories. Firstly, there are direct synthetic routes based on a chemical oxidation of a monomer towards the conjugated polymer as mentioned in literature for PANI[9], PPy[10], PPP[11] or PT[12]. A second class of direct polymerization chemistry towards conjugated polymers is based on the well-known organo-metallic coupling reactions. Typical examples used to synthesize PPP or PT are Ni catalyzed coupling reactions[13,14] and Pd catalyzed reactions (Suzuki coupling)[15,16]. Finally, beside chemical oxidation, electrochemical oxidation is used to synthesize PANI[17], PPy[18], PPP[19] and PT[20]. A potential advantage is the possibility to obtain patterned circuitry by means of area-selected electro-polymerization[21].

To overcome the major drawbacks of direct synthetic procedures towards conjugated polymers (e.g. difficult processing due to a lack of solubility), precursor routes are developed. Typical examples, beside the well-known precursor routes towards PPV as discussed in section 1.2.2, are the ICI procedure[22] (using a diester-cyclohexadiene monomer) and the Grubbs method[23] (using a dihydroxycyclohexadiene monomer) to synthesize PPP.

An extended survey of the the literature on the polymerization chemistry towards the common, basic conjugated polymers PA[24], PANI, PPy[25], PPP[26] and PT[27] is presented in several review articles and specialized books.

1.2.2   Synthesis of poly(p-phenylenevinylene)

Poly(p-phenylenevinylene) (PPV) is widely used in its non-doped state, mainly as an active semiconductor layer in electronic devices. Research boosted after the discovery by Burroughes et al. of electroluminescence in a light emitting diode (LED) with PPV as the emissive layer[28]. As usual, the insolubility of the extended conjugated systems needs to be overcome either by working with soluble derivatives (e.g. alkoxy side chains) or by using precursor methods. Major advantage of the side chain approach is that the conjugated polymer is directly solution processable into thin films. Disadvantage of this approach is the reduction of mechanical properties e.g. reduced glass-transition temperature (T_g).

Direct synthesis towards PPV occurs mostly through poly-condensation-like polymerization based on well-known coupling reactions: Wittig olefination (e.g. coupling between a bisphosphonium salt and a bisaldehyde)[29], McMurray coupling (e.g. deoxygenative coupling of an aromatic dialdehyde)[30], Knoevenagel condensation (e.g. coupling between aromatic dialdehyde and dinitrile)[31], Heck reaction (e.g. coupling between aromatic dibromide and ethylene)[32]. PPV can also be prepared in a direct

way by an electrochemical polymerization of different types of monomeric compounds[33]. Essentially, these routes lead to insoluble, infusible and low molecular weight material, making them not interesting for commercial applications.

The alternative approach is to work with soluble (easy processible) polymeric analogues that can be transformed in a conjugated polymer. These so-called precursor methods to synthesize PPV are subject to an enormous amount of research.

Besides the already mentioned advantage of precursor methods, namely making conjugated polymers processable; an additional advantage is the change in solubility during the transformation of non-conjugated polymeric analogue to the conjugated material. Soluble conjugated polymers can be easily affected by applying another polymer layer from solution. On the other hand, a precursor polymer becomes insoluble after conversion, allowing the application of an additional layer spincasted from solution. This feature makes precursor techniques extremely interesting, especially when building multi-layer devices.

Besides these general advantages of precursor methods some synthetic precursor approaches yield a better control of chemistry.

The major precursor routes towards PPV and its derivatives, namely: the sulphonium precursor route, the alkoxy precursor route, the xanthate precursor route, the Gilch precursor route and the sulfinyl precursor route, will be discussed.

1.2.2.1 Sulphonium precursor route

Wessling and Zimmerman patented the sulphonium precursor route towards PPV in 1968, therefore often also referred as Wessling-Zimmerman precursor route[34]. The synthesis is modified and optimized by several groups and is schematically depicted in figure 1.3.
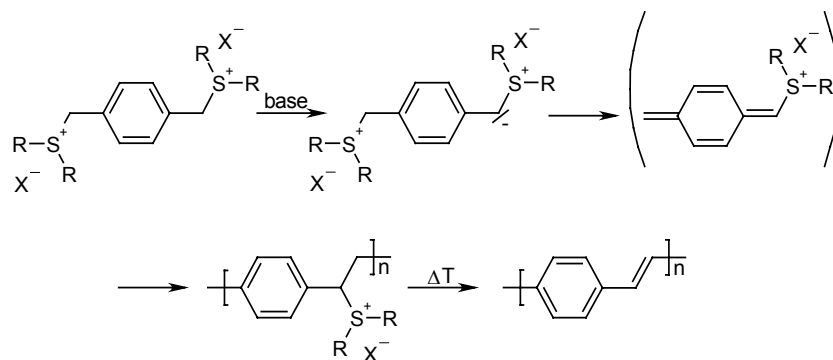
figure 1.3 Synthetic scheme of the sulphonium precursor route

The formation of the precursor polymer is obtained by a base induced polymerization of a bissulfonium p-xylylene salt in aqueous solution. Conversion from PPV analogue towards PPV is obtained by a heat treatment causing elimination of a dialkylsulfide and a hydrogenhalide.

The starting monomers in the initial synthesis are dimethyl and diethyl p-xylylene sulfonium salts with either chlorine or bromine as counter ions. Cyclic derivatives (e.g. tetrahydrothiophenium derivative), instead of linear thioethers, are examined to be more stable and give rise to a decreasing amount of side reactions during conversion[35].

Polymerization under optimized reaction conditions involves the use of low temperature (T ≤ 0°C), dilute monomer solutions (0.05 mol l^{-1}) and slightly less than equimolar (to monomer) base concentration[36]. After polymerization, the mixture is neutralized and dialyzed against distilled water to remove inorganic and low molecular weight organic impurities. Typical values for the yield are reported between 20-91%[37]. However, these high yields (> 57%) are obtained by starting with higher monomer concentrations (0.2 mol l^{-1}) leading to a not processable gel-like polymer. Interaction between the ionic precursor and chromatographic columns makes it difficult to determine molecular weights. However the sulphonium group is commonly substituted by reaction with phenylthiolate ions[38] or by extended heating in methanol[39]. Resulting polymers are soluble in tetrahydrofurane and show typical molecular weights ≥ 10^5 g mol^{-1} [39].

The polymerization mechanism is studied by a number of research groups. The first step involves deprotonation and 1,6-elimination of the sulfide group to form a reactive p-xylylene derivative with a quinoidal character. The formation of the quinoidal p-xylylene intermediate can easily be monitored by the appearance of a peak around 310 nm in the ultraviolet (UV) spectrum[40]. This p-xylylene derivative, which is the actual monomer, polymerizes either by an anionic or a radical mechanism. Cho et al. confirmed recently that the sulphonium route occurs by an elimination free radical polymerization[40], although the exact nature of the initiator is not clear. It may involve spontaneous coupling of two quinoidal p-xylylene intermediates to form a biradical.

Polymerization of PPV derivatives, using the sulphonium route still occurs with a wide variety of substituents on the aromatic ring (e.g. aromatic[41], alkoxy[42], alkyl[42a,43], silyl[44] and halogen[45] groups).

Sulphonium precursor polymers are soluble in polar solvents (e.g. water, methanol) and can be spincasted onto substrates to form thin films. Conversion of the precursor polymer to the PPV occurs by heating under vacuum or inert atmosphere in a temperature range of 160-300 °C during 2-20 hours[46].

Although the sulphonium precursor route offers a relatively quick and cheap production towards PPV, there are several drawbacks, limiting its use in a commercially successful chemistry. The hydrogen halide (HX) formed during elimination may react with indium tin oxide (ITO)

electrodes commonly used as transparent conducting oxides (TCO) in semiconductor devices[47]. Another drawback is the limited solubility of precursor polymer in good spincasting solvents (e.g. toluene or chlorobenzene) making it difficult to obtain high quality pinhole-free films. Further, the relative instability of the polyelectrolytes leads to a number of side reactions during polymerization and storage of the precursor polymer. Further, elimination shows a number of competing reactions leading to an additional amount of chemical defects.
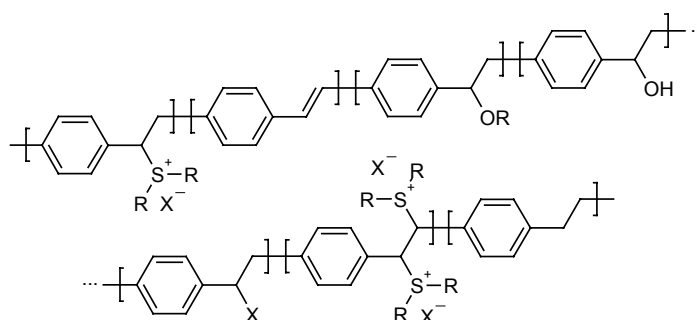
figure 1.4 Schematic structure of the possible defects in a sulphonium precursor polymer

In figure 1.4 a possible defect structure[48] of the sulphonium synthesized PPV precursor is depicted.

1.2.2.2 Alkoxy precursor route

The alkoxy precursor route can be seen as an extension of the sulphonium route, eliminating some major drawbacks of the latter. The general synthetic scheme is represented in figure 1.5.
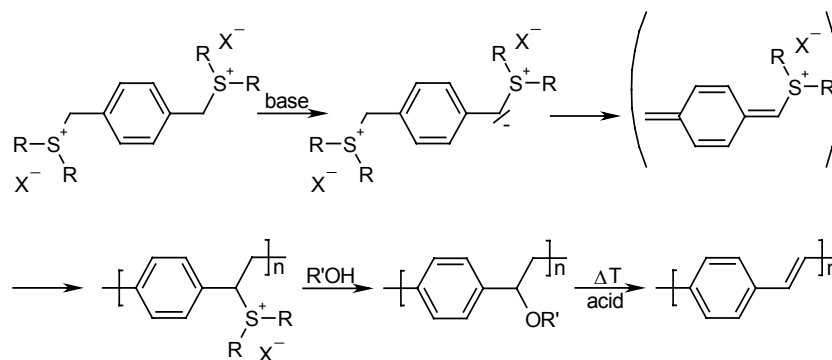
figure 1.5 Synthetic scheme of the alkoxy precursor route

The alkoxy precursor route is completely identical as the sulphonium precursor route till the formation of the sulphonium precursor polymer. Sulphonium precursor polymers can be converted to alkyloxy-substituted polymers, which are soluble in organic solvents[49] and show an enhanced stability at room temperature. Elimination occurs under heating in presence of an acid catalyst[42a]. Although some drawbacks of the sulphonium route are partially solved, the alkoxy precursor route does not satisfy for commercial applications.

1.2.2.3 Xanthate precursor route

Son et al. developed a modification of the sulphonium precursor route in an attempt to circumvent the already mentioned drawbacks of the latter[50]. A general synthetic scheme for the xanthate precursor route is depicted in figure 1.6.
A base induced polymerization in tetrahydrofurane (THF) at 0 °C of a symmetric xanthate substituted p-xylylene monomer yields the xanthate precursor polymer[51]. A typical molecular weight determined by size exclusion chromatography against polystyrene standard is 6 10^5 g mol^{-1} [52]. The conversion of the precursor PPV analogue towards PPV is performed under an argon atmosphere in a temperature range of 160-250 °C.
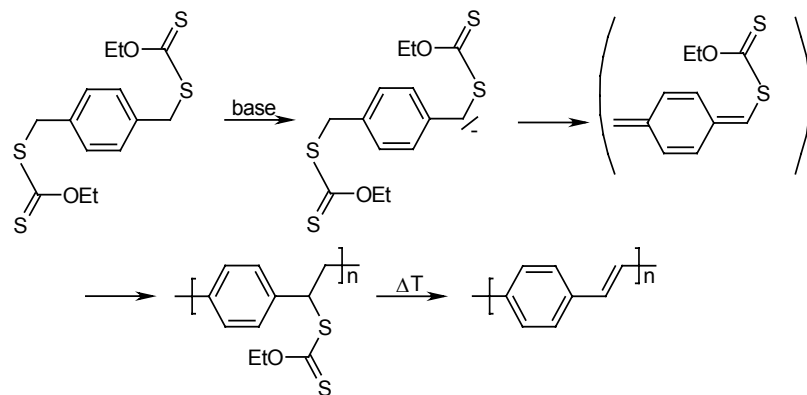
figure 1.6 Synthetic scheme of the xanthate precursor route

The presence of cis-bonds is demonstrated by infrared (IR) spectroscopy, although the frequency is not well defined in literature[53]. The authors claim that the occurrence of these cis-bonds decrease the degree of order in PPV and thus explain the observed increase of internal electroluminescence efficiency. It should be mentioned that the observed IR signal can also be induced by alkyl signals due to incomplete elimination.
The xanthate route offers certain advantages compared to the sulphonium route. The non-ionic precursor is stable during storage at room temperature

and can easily be dissolved in organic solvents (e.g. THF, chloroform, toluene). Although the number of publications is still limited, it is not yet clear if this synthetic approach will ever fulfill the needs of commercial synthesis.

1.2.2.4 Gilch precursor route

Gilch and Wheelwright investigated with success a procedure to polymerize dichloro-p-xylylene with a large excess of potassium tert-butoxide (t-BuOK) towards PPV in organic solvents[54]. To prevent premature precipitation the modification to use one equivalent of base was presented[55]. This procedure leads to the formation of a chlorine precursor polymer that can be converted to PPV. However this chlorine precursor polymer is insoluble in common organic solvents (e.g. acetone, chloroform, THF). Therefore, intermediate soluble halide-substituted polymers have been prepared[56]. Substituents used to give solubility include phenyl, alkoxy and alkyl groups. However, the intermediate precursor polymer may not be very stable. A general schematic scheme of the Gilch route is presented in figure 1.7. The reaction mechanism is related to the sulphonium precursor procedure[57].
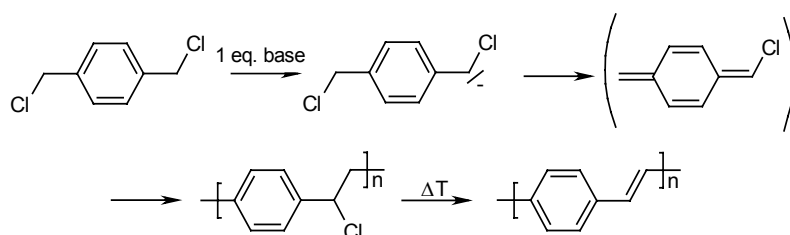
figure 1.7 Synthetic scheme of the Gilch precursor route

Conversion of the chlorine precursor polymer towards PPV can be obtained by heat treatment (300 °C, 1 h). Contrary to the sulphonium route, the elimination can also easily be completed by the addition of an excess of base.

The Gilch route is commonly used in industry because of the easy entry into a large range of substituted high molecular weight organic soluble PPV derivatives[58]. In this case, due to the addition of an excess of base, no real precursor polymer is isolated and transformed afterwards into PPV, but the whole process is taking place in one batch like the originally proposed procedure. In literature no real distinction is made between the direct (excess of base) and precursor polymerization (1 equivalent of base) towards PPV via the Gilch procedure.

1.2.2.5 Sulfinyl precursor route

All routes already described in section 1.2.2 make use of symmetrical premonomers (e.g. chemical identical functionalities on both benzylic positions). Efficient monomer formation leads to the use of good leaving groups, such as sulphonium groups or chlorine substituents. On the other hand, to produce stable precursor polymers, a weak leaving group capacity has to be introduced. These contradictory demands, lead to all kind of side reactions, when working with symmetrically premonomers, as illustrated for the sulphonium route. Therefore Vanderzande et al. developed a procedure that uses a differentiation between both functionalities[59]. As leaving group halides (X) are chosen because of their high leaving group capacity and the lack of enhancement of the acidity of the benzylic position. Sulfinyl groups on the other hand, behave in an opposite way and fulfill the function of polarizer. A three-fold function is attributed to this group: preferential stabilization of the anion, polarization of the p-quinodimethane (p-QM) system and provision of the chemistry to form the double bond. A schematic representation of this synthetic approach is depicted in figure 1.8.
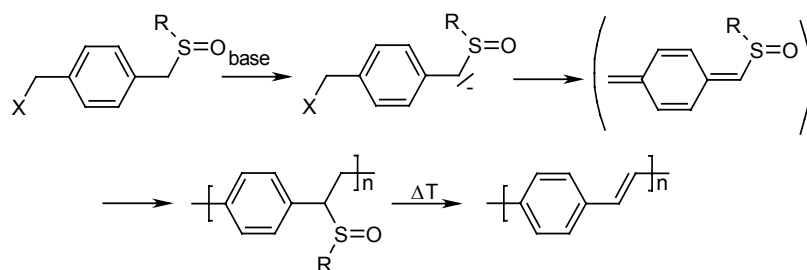
figure 1.8 Synthetic scheme of the sulfinyl precursor route

Addition of a base (1-1.3 equivalents) leads to a selective deprotonation at the side of the sulfinyl group and the formation of the reactive p-xylylene derivative, the actual monomer. The monomers polymerize spontaneously with the formation of a stable high molecular weight precursor polymer. An additional advantage of the sulfinyl route is the tunable solubility of the precursor polymer by a variation of the R-group at the sulfinyl functionality[60]. A wide range of solvents is available, both polar (e.g. alcohols) and apolar (e.g. toluene). Especially alcohols can be interesting in commercial synthesis because of environmental issues.
The precursor polymer can be converted towards the fully conjugated PPV by means of a well-known conversion from the sulfinyl group to a double bond[61]. According to recent in-situ IR and UV-visible (vis) spectroscopy measurements, conversion occurs at low temperature (70-100 °C) under inert atmosphere or vacuum[62].

The polymerization occurs by a radical mechanism responsible for the formation of a higher molecular weight polymer[63]. Also an anionic polymerization mechanism can take place under certain circumstances, yielding an oligomeric fraction[64].

The sulfinyl precursor route is a versatile procedure, which can be used to synthesis a broad range of PPV derivatives. Electron withdrawing substituents (e.g. Cl, CN, NO_2) and electron donating groups (e.g. alkyl, alkoxy) on the aromatic ring are allowed and result in high molecular weight precursor polymers[65]. Even monomers with an extended aromatic system (e.g. 4,4' biphenylring, 2,6-naphtyl ring) can be polymerized[66].

1.2.2.6 Comparison of the precursor routes

The earlier discussed precursor routes are based on a similar chemistry and can be described by a general scheme, consisting of three steps, depicted in figure 1.9. A profound understanding of this scheme will lead to a better understanding of the type and number of defects that can be expected based on differences in chemistry using the mentioned precursor routes.
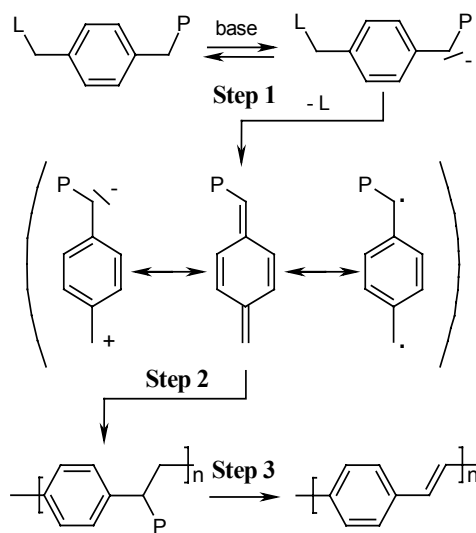
figure 1.9 General synthetic scheme of the PPV precursor routes

The first step is a base induced 1,6-elimination from a p-xylylene derivative leading to an in-situ formation of the actual monomer, the p-quinodimethane (p-QM) system. This formation is generally adopted to be an E_{1cb} mechanism. Although this is experimentally observed for the sulphonium route[67], no studies are available for the Gilch and xanthate precursor route. A study of the sulfinyl precursor route[63] shows a dependency of the polymerization on the polarizer and no dependency of

the polymerization on the leaving group, negating the other plausible mechanism (e.g. E_2).

The intermediate p-QM system is the actual monomer of the polymerization reaction and can be presented by three structures contributing differently to the character of the molecule[68].

The polymerization to the precursor polymer (step 2) occurs spontaneously. This is a chain polymerization evidenced by the presence of high molecular weights at low monomer conversion[69,54]. Arguments about the mechanism (either anionic or radical) are still ongoing however a radical mechanism seems to be more favorable.

In the third step the conjugated structure is obtained either directly or by a thermal treatment depending on the specific chemical structure of the starting monomer and the polymerization conditions.The choice of polarizer and leaving group will determine in some way or the other the ultimate quality of the conjugated polymer. A big variety of defects are induced by the chemistry related to side reactions of the presented general synthetic scheme. These side reactions can be either enhanced or suppressed by the specific properties of the leaving group and polarizer.

An overview of the specific polarizer and leaving group for the mentioned precursor routes towards PPV is presented in table 1.1.

Notice that the sulfinyl route differs from the other routes because of the chemical differentiation between leaving group and polarizer.

Precursor route:	Leaving group (L):	Polarizer (P):
Sulphonium	$^+SR_2X^-$	$^+SR_2X^-$
Alkoxy	$^+SR_2X^-$	$^+SR_2X^-$ (OR')
Xanthate	SC(S)OEt	SC(S)OEt
Gilch	Cl	Cl
Sulfinyl	X	S(O)R

table 1.1 Overview of the specific polarizer and leaving group for various precursor routes

As mentioned before, the function of the polarizer is three-fold: stabilization of the anion formed in the first step, polarization of the p-QM system in such a way that regular head-to-tail addition results and providing the ability to form after an elimination step a double bond to complete conjugation.

In general, efficient monomer formation is induced by a good leaving group capacity. This can be a drawback of the xanthate route.

The weak polarizing ability of the chlorine group leads to the formation of head-to-head additions yielding single and triple bonds in the ultimate conjugate polymer. This specific drawback of the Gilch route will be discussed in chapter 2. The sulphonium route (and to some extend the

alkoxy route) suffers from the weak stability of the polyelectrolytes inducing side reactions as already depicted in figure 1.4. Finally, a potential drawback, when working with insoluble PPV derivatives, is the weak solubility in good spincasting solvents of the Gilch precursor polymer and the sulphonium precursor polymer.

1.3   Electrical properties of conjugated polymers

The formation of the allowed valence and conduction band, with in between the forbidden energy gap in inorganic semiconductors (e.g. silicon) is caused by the delocalisation of the electronic states, induced by a strong coupling between the constituting atoms and the long-range order. Free charge carriers (e.g. free electrons in the conduction band or free positively charged holes in the valence band) can be created either by photoexcitation or thermal activation. Transport is described in the traditional quantum mechanical language of Bloch functions, k-space and dispersion relations[70].

Chemical or structural defects in the crystal introduce states in the forbidden energy gap, spatially localized at that defect. At such a defect state a mobile carrier can get trapped and no longer contributes to the conductivity until, it is released again. The carriers can also tunnel directly from one localized state to another when the electronic wave functions of the defect states have a sufficient overlap. This mechanism of phonon-assisted tunneling, or 'hopping' is originally introduced by Conwell[71] and Mott[72]. Miller and Abrahams calculated the transition rates for this hopping process[73]. The hopping rate is strongly dependent on both the positions and the energies of the localized states, while the hopping transport is extremely sensible to structural as well as energetic disorder. An overview about phonon-assisted tunneling in disordered media can be found in several review articles[74].

In organic conjugated polymers, a distinction between intramolecular and intermolecular interactions has to be considered. Interactions located at one molecule are covalent and generally rather strong. Contrary, interactions between adjacent chains are much weaker van der Waals forces. As a result the transport bands are much narrower than in inorganic systems, and the band structure is easily disrupted by disorder in the system. So although in principle the π–conjugated system can extend the whole polymer chain, allowing delocalized states in one direction, the concept of allowed energy bands (semiconductor band model) is limited. In the molecular exciton model, the electronic structure of the material is described as a Gaussian distribution of localized states. In this way, a generated exciton at a specified site will execute a random walk while relaxing within this density of states. A review concerning arguments in favor with one or the other model can be found in literature[75].

1.3.1   Semiconductor band model

Su, Schrieffer and Heeger[76] studied the interaction of an excitation with an ideal one-dimensional lattice neglecting Coulomb interactions and disorder defects.

Polymers with a degenerated ground state, exhibit no change in energy when single and double bonds are interchanged. The typical example is PA. However, most polymers have a non-degenerated ground state. Interchange of double and single bonds leads the formation from the aromatic (e.g. for PPV, three double bonds in phenyl-ring) to a higher energy quinoidal state (e.g. for PPV, two double bonds in phenyl-ring).   Application of the semiconductor band model leads, in addition to direct hole and electron excitations, to localized bond 'double-defects', called polarons, upon excitation.

aromatic state

quionoid state

neutral soliton (radical)
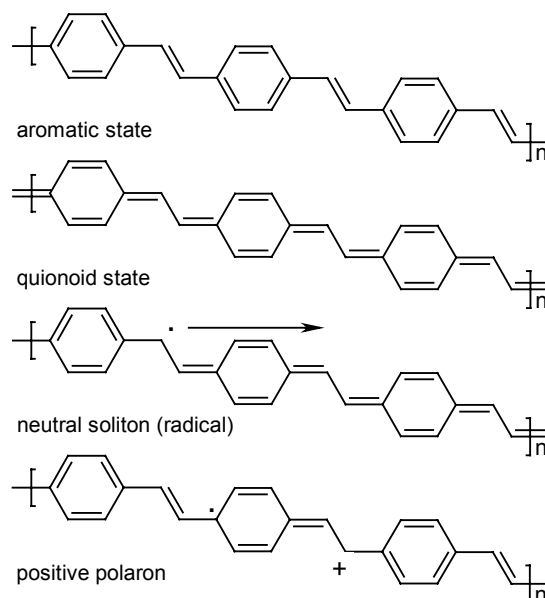
positive polaron

figure 1.10 Chemical representation of the aromatic ground state of PPV, the quinoidal state of PPV, a neutral soliton driven to the chain ends and a positive polaron

In a non-degenerated system, a localized defect in the conjugation (soliton) (either a radical, positive or negative charge) separates a low-energy (aromatic) and high-energy (quinoid) region. As a result, the single defect is unstable and will be driven to the chain ends. To stabilize conjugational defects bond 'double-defects' have to be created, minimizing the length of the quinoidal part. However the remaining distortion of the conjugation leads to the formation of mid-gap states. In figure 1.10 the aromatic and

quinoidal structure for PPV are represented. Further, it is shown that a neutral soliton (localized radical) separates a high and low energy region and can only be stabilized by merging an exemplary positive soliton, creating a 'double-defect' (e.g. positive polaron).

A polaron is characterized by two states in the gap. Besides the in figure 1.10 indicated examples, other combination of defects, pushed towards each other are possible[76]. Energetic representations of some different soliton combinations (polarons) are given in figure 1.11.

| positive bipolaron | positive polaron | singlet polaron-exciton | triplet polaron-exciton | negative polaron | negative bipolaron |
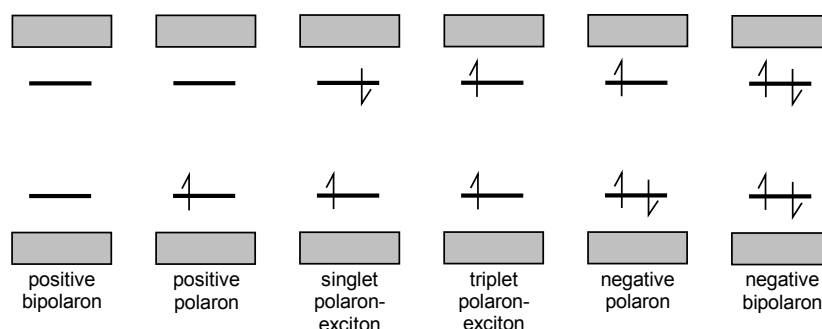
*figure 1.11 Energy scheme of polarons in non-degenerated polymers
(the grey bands correspond with the valence and conduction band,
the intra-gap states can be occupied by none, one or two electrons)*

Roth et al give an overview concerning properties of one-dimensional metals[77]. In most common conjugated polymers disorder plays an omnipresent role, disrupting an eventual band structure. However, some concepts of the semiconductor band model are certainly useful and this approach is often used to describe qualitatively the behavior of polymer electronic devices.

1.3.2   Exciton model

Spectroscopic studies of conjugated polymers show many features, characteristic for disordered molecular systems[78]. Bässler et al.[79] described conjugated polymers with a Gaussian distribution of localized states. These localized states can be attributed to conjugated polymer chain parts separated by mechanical (e.g. twists, kinks) or chemical defects (e.g. single bonds, cross links, carbonyl groups). Since there is only a weak coupling between the conjugated parts in these materials the conjugated segments behave as individual molecules.

The primary excitation is a neutral exciton, a bound electron hole pair. Different type of excitons, found in literature are: Frenkel exciton[80] (the electron-hole pair is confined to not more than one molecular unit), Mott-Wannier exciton[81] (with a distance between hole and electron much greater

than the molecular units) and charge-transfer exciton[82] (the electron-hole pair extends a few adjacent molecular units).

Due to the low dielectric permittivity in organics, the interaction between the electron in the LUMO and the hole in the HOMO is rather strong. The reported binding energies range from 0.4 eV[83] to 1 eV[84] and therefore, the primary exciton is believed to be of the Frenkel type. The exciton may decay radiative, nonradiative or migrate. Under influence of an electric field or in presence of an acceptor molecule, the exciton can even dissociate by transferring one of its charges to this neighboring molecule or conjugated segment (intra or interchain). These different processes are schematically represented in figure 1.12.
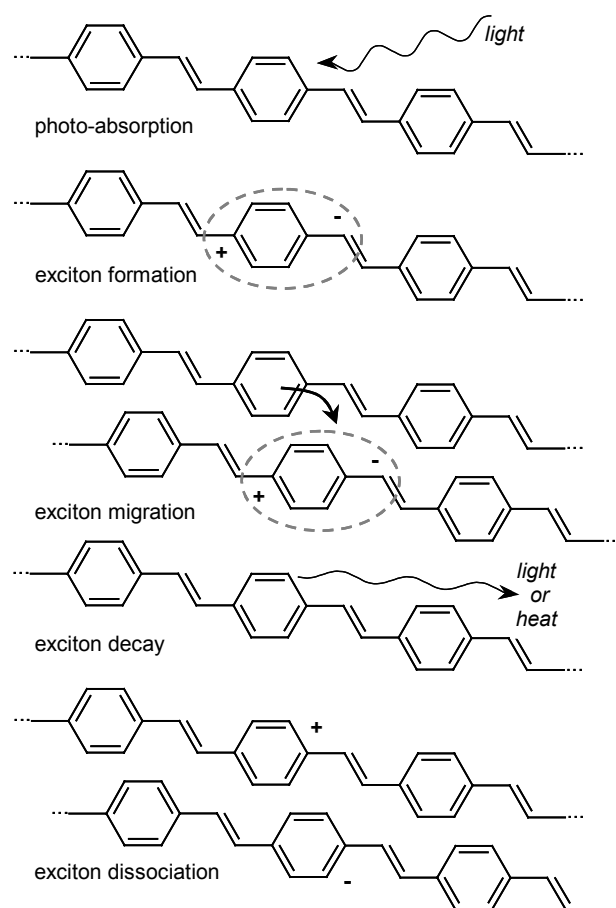
figure 1.12 Schematic representation of the exciton dynamics in a disordered organic solid containing conjugated segments

Transport occurs via a sequence of charge transfer steps (hopping) from one conjugated segment towards another. The red shift between absorption and

emission is attributed to an incoherent random walk of the excitons towards an available lower energy conjugated segment site.

The incoherent dynamics of charge carriers as well as excitons are described by a kinetic equation known as the master equation.

$$\frac{\partial}{\partial t} f_i(t) = -\sum_{j \neq i} W_{ji} f_i(t)\left[1 - f_j(t)\right] + \sum_{j \neq i} W_{ij} f_j(t)\left[1 - f_i(t)\right] - \lambda_i f_i(t)$$

equation 1.1 Master equation describing the incoherent dynamics of excitons and charge carriers

In this equation $f_i(t)$ is the occupational probability of site i (position R_i and energy ε_i) at time t. The transition from site j towards site i is described by the rate W_{ij}. The factor (1-f) limits an eventually double occupied state. Decay processes are described through the rates λ_i (λ_i equals zero in case of charge carriers). This non-linear equation is linearized by either assuming small deviations from equilibrium or by assuming uncorrelated particles. The different approaches for solving the linearized version of the master equation are the resistor network method[73] combined with effective medium techniques[85] or percolation techniques[86], the continuous-time random walk method[87] and the Green function method[88].

Vissenberg[89] et al. used the described procedure to study the mobility data of organic field-effect transistors, polymer light emitting diodes and time-of-flight measurements, thereby succeeding to relate the in the past for disordered molecular solids observed field and temperature dependency (equation 1.2 empirical relation by Gill[90] et al.) of the mobility (μ) with energetic and structural disorder.

$$\mu = \mu_0 \exp\left(\frac{-\Delta}{kT}\right) \exp\left(B\left(\frac{1}{kT} - \frac{1}{kT_0}\right)\sqrt{E}\right)$$

equation 1.2 Empirical relation by Gill et al. to express the field and temperature dependence of the mobility

Numerous experiments on moleculary doped polymers, pendant group polymers, amorphous molecular glasses and conjugated polymers have revealed a similar behaviour, with typical parameter values of the activation energy $\Delta \sim 0.5$ eV, a field dependent parameter B $\sim 3~10^{-5}$ eV(m/V)$^{1/2}$ and a temperature where above a change of sign in the field dependency is indicated $T_0 \sim 600$K[91].

The essential difference between the different models describing exciton and charge dynamics in conjugated polymers is related to the relative importance of the contribution of either disorder and Coulomb interactions or intramolecular deformation energy. The hopping model assumes that the coupling of the charge to inter (or intra)-molecular modes is weak. The

activation energy reflects basically the static energy disorder of the hopping sites. The polaron model, on the other hand, considers the disorder energy to be unimportant to the intramolecular deformation energy. This may be true for highly ordered organic crystals but not for the amorphous polymer materials studied within the framework of this thesis.

1.4   Applications of conjugated polymers

Conjugated polymers are promising candidates for numerous applications. A detailed description of the wide range of applications of organic conducting materials can be found in specialized books[92].

A distinction is made between organic conductors and organic electronic devices. In this section both groups of applications will be briefly discussed. Within the scope of this thesis one will focus on transistors, light emitting diodes and solar cells. A detailed description of these devices can be found in the next chapters: in chapter 3 for the transistors, in chapter 4 for the light emitting diodes and in chapter 5 for the solar cells.

1.4.1   Organic conductors

The most straightforward application is the use of conjugated polymers in their doped state, yielding high conductivity values[93]. Especially transparent layers, consisting at poly(ethylenedioxythiophene) (PEDOT) are currently used as antistatic layer in photographic materials[94]. Typically values required for the conductivity in antistatic applications[95] are in the range of 10^{-8} to 10^{-6} S cm^{-1}. Besides the use in antistatic applications, organic materials are used to shield against electromagnetic radiation. Typically values for the conductivity needed in this type of applications[96] are in the range of 10^{-4} and 10^{-2} S cm^{-1}.

A high potential application of conjugated polymers is corrosion inhibition[97]. In this regard, coatings of metals with PANI, PT and PPy have been extensively investigated. Especially PANI seems to be quite successful by forming an impenetrable oxide layer.

Finally, conjugated polymers are used as (transparent) electrodes that might serve as an alternative for ITO[98]. PEDOT for example is used as electrode for polymer light emitting diodes[99], photovoltaic[100] and electro chromic devices[93]. Not all applications require electrodes with high transparencies. Area selective electro polymerization, photochemical patterning, micro molding, screen-printing, micro contact printing, inktjet-printing are reported techniques to obtain a spatial deposited electrode pattern with conjugated polymers (e.g. PPy, PANI, PEDOT, …)[21]. An important advantage is the implementation of the patterned conjugated polymer electrodes with the active conjugated polymer semiconductor layer, yielding potentially cost savings.

1.4.2   Organic electronic devices

Amongst more advanced organic based electronic devices, there are batteries capacitors, light emitting diodes (LED's), a wide range of sensors, optical devices (e.g. wave guides, lasers), electrochromic windows, solar cells, photodiodes and transistors.

Conjugated polymers can repeatedly undergo electrochemical doping and dedoping processes, involving an amount of charges, making them attractive as electro active materials for batteries and capacitors[101]. An electrode with an open structure and a charge-discharge process controlled by the diffusion of counter-ions in and out the matrix will lead to high performance capacitors[101].

Some conjugated polymers can be electrochemically switched between the doped and undoped state with a high contrast in color. This property makes conjugated polymers excellent candidates as active layer for electrochromic devices such as 'smart windows' with controllable light- and heattransit[101].

Efficient laser action was observed for a PPV derivative in the liquid state[102]. Later, in sub-μm thick conjugated polymer films lasing evidence was founded by a collapse of the emission line width above a certain pump energy threshold[103].

A number of sensors based on conjugated polymers are reported: conductometric, potentiometric, voltametric, gravimetric, optical, pH based and incorporated-receptor-based.

The mentioned applications show exemplary the enormous potential of conjugated polymers to produce, with considerable cost savings, plastic electronic devices. However within the scope of the thesis one will focus on the most representative semiconductor applications being: transistors, solar cells and LED's. A detailed description of these devices can be found in the following chapters, however the performance of today's devices is briefly discussed within this section.

Research towards Polymer light emitting diodes (PLED's) was boosted after the discovery, of electroluminescence (EL) of the conjugated polymer PPV, sandwiched between two injecting electrodes[28]. Due an easy processing and mechanical flexibility, conjugated polymers are promising candidates for large area display applications. Additional advantages are low power consumption, low voltage operation, fast response times, a wide range of available colors, light weight, the absence of a viewing angle dependency and high contrast and resolution.

A typical PLED consists of four layers. An ITO layer is used as transparent anode. On top, an additional conjugated polymeric anode layer is used to increase stability and lifetime. In a next step, the semiconducting conjugated polymer layer is spincoated on top of this anode. Finally a low

work-function metal such as Ca is evaporated as cathode. The total set-up is encapsulated to prevent diffusion of water and oxygen into the active area. Current PLED's reach a brightness[a] of 100 Cd m[-2] at 2.5 V[104], external efficiencies[b] of 4 Lm/W[104] and a lifetime of more than 10000 hours[105] for the orange PPV-based emitter. Prototypes of passive matrix and active matrix monochrome and full color displays are presented by a number of companies[106].

Research to use simple and cheap electronics in areas where standard silicon is too expensive is an attractive application of conjugated polymers. The construction of organic field effect transistors (OFET's), both as discrete devices and as integrated circuits plays a crucial role in this context[107]. Commercial applications such as wireless radio frequency identification tags (e.g. active bar-codes, bank- and phone cards, personal identification, …) are almost within range.
Recent, an impressive increase in mobility is shown either by the synthesis of new materials or by an improvement of the deposition parameters of the semiconductor layer[108]. Typical transistor characteristics[109] yield a temperature and gate-bias dependency, which is interpreted either by a multiple trapping and release-model[110] or by model based on a hopping transport in the tail of a density-of-states[111]. The latter is more favorable in amorphous organic films such as used within the scope of this thesis.

The need to develop inexpensive renewable energy sources stimulates the research towards low cost photovoltaic devices. As such, efficient plastic solar cells can sustain that need. Aside from possible economic advantages, polymeric materials posses low specific weight and mechanical flexibility, properties that are desirable for a solar cell. The discovery of ultra fast photoinduced electron transfer in a composite of conjugated polymers as donors and buckminsterfullerene (C_{60}) as acceptor[112] provided a molecular approach to high efficient photovoltaic conversion. Because the time scale for photoinduced charge transfer is three orders of magnitude faster (< 100 fs) than the radiative or nonradiative decay of photoexcitation, the quantum efficiency from donor to acceptor is close to unity[112]. Early devices, based on a conjugated polymer/C_{60} bilayer, yield monochromatic efficiencies of 0.1 %[113]. A major increase in efficiency was obtained by blending the conjugated polymer directly with a soluble

---

[a] *Brightness expressed in Candela per m[2] (Cd m[-2]) is an alternative expression also used to determine the efficiency of a LED. The value of 100 Cd m[-2] is comparable to the typical brightness of a LCD (Liquid Crystal Display) computer screen.*
[b] *The luminous efficiency is the product of the power conversion efficiency and the luminous efficacy. The latter is a conversion factor taking into account the spectral sensitivity of the human eye as defined by the 'Commission Internationale de L'Eclairage' (CIE)*

methanofullerene[114] in order to form a large interfacial region. Because any photoexcitation in the composite is within a few nanometers of a donor-acceptor interface, these devices are named as donor-acceptor bulk hetero junction solar cells. Large area (3600 mm^2) flexible plastic solar cells based on this concept of bulk hetero junction of a blend of an alkoxy PPV-derivative (MDMO-PPV) and a soluble fullerene derivative (PCBM), are reported with efficiencies (about 1%) equal to similar small area (typically 6 mm^2) photovoltaic devices[115], proving the ability for an easy up-scaling.

Today's organic solar cells based on PCBM and MDMO-PPV reach efficiencies of about 3%. Thiophene based photovoltaic devices exhibit even an increased efficiency up to 5%[116].

In the next chapter a matrix of semiconducting polymers will be defined. The properties of these materials are evaluated in transistors (chapter 3), PLED's (chapter 4) and solar cells (chapter 5).

1.5   References

[1]   a) H. Shirakawa, E.J. Louis, A.G. MacDiarmid, C.K. Chiang, A.J. Heeger, *J. Chem. Soc., Chem. Commun.* (**1977**) 579. b) C.K. Chiang, C.R. Fincher, Y.W. Park, A.J. Heeger, H. Shirakawa, E.J. Louis, S.C. Gau, A.G. MacDiarmid, *Phys. Rev. Lett.* (**1977**) 39, 1098.

[2]   G. Natta, G. Mazzanti, P. Coraddini, *Atti. Acad. Naz. Lincei. Rend. Cl. Sci. Fis. Mat. Natur.* (**1958**) 25, 3.

[3]   T. Ito, H. Shirakawa, S. Ikeda, *J. Pol. Sci. Polym. Chem. Ed.* (**1974**) 12. 11.

[4]   H. Shirakawa, *Handbook of Conducting polymers, (eds. T.A. Skotheim, R.L. Elsenbaumer, J.R. Reynolds)* Dekker, New York (**1998**) 197.

[5]   a) L.B. Luttinger, *J. Org. Chem.* (**1962**) 27, 1591. b) M. Aldissi, C. Linaya, J. Sledz, F. Schué, L. Giral, J.M. Fabre, M. Rolland, *Polymer* (**1982**) 23, 243. c) J.R. Martinez, M.D. Raush, J. C. W. Chien, H.G. Alt, *Macromol. Chem.* (**1989**) 190, 1309. d) F. Cataldo, *Polym. Commun.* (**1992**) 33, 3073.

[6]   S.A. chen, H.J. Shy, *J. Polym. Sci., Polym. Chem. Ed.* (**1985**) 23, 2441.

[7]   H.J. Boweley, D.L. Gerrard, W.F. Maddams, *Macromol. Chem.* (**1985**) 186, 715.

[8]   a) W.J. Feast, M.J. Taylor, J.N. Winter, *Polymer* (**1987**), 28, 601. b) D.C. Bott, C.S. Brown, C.K. Chai, N.S. Walker, W.J. Feast, P.J.S. Foot, P.D. Calvert, N.C. Billingham, R.H. Friend, *Synth. Met.* (**1986**) 14, 245.

[9]   a) J.C. Chiang, A.G. MacDiarmid, *Synth. Met.* (**1986**) 13, 193. b) Y. Cao, A. Andeatta, A.J. Heeger, P. Smith, *Polymer* (**1989**) 30, 2305.

[10]   a) S. Machida, S. Miyata, A. Techagumpuch, *Synth. Met.* (**1989**) 31, 311. b) Y.A. Bubitsky, B.A. Zhubanov,G.G. Maresch, *Synth. Met.* (**1991**) 41-43, 375. c) E.T. Kang, K.G. Neoh, Y.K. Ong, K.L. Tan, B.T.G. Tan, *Macromolecules* (**1991**) 24, 2822.

[11]   a) P. kovacic, J. Oziomek, *J. Org. Chem.* (**1964**) 29, 100. b) J. Simizis, C. Dimopoulou, *Makromol. Chem.* (**1984**) 185, 2553. c) P. Kovacic, F.W. Koch, C.E. Stephan, *J. Polym. Sci., Polym. Chem. Ed.* (**1964**) 2. 1193.

[12]   a) K. Yoshino, D.H. Park, B.K. Park, M. Onoda, R. Sugimoto, *Solid State Commun.* (**1988**) 67, 1119. b) K. Yoshino, S. Nakajima, M. Fujii, R. Sugimoto, *Polym. Commun.* (**1987**) 28, 309. c) K. Yoshino, S. Nakajima, R. Sugimoto, *Jpn. J. Appl. Phys.* (**1987**) 26, L1038.

[13]   T. Yamamoto, *Handbook of organic conductive molecules and polymers, (Ed. H.S. Nalwa)* John Wiley & Sons, New York (**1997**) vol. 2, 171.

[14]   a) T. Yamamoto, K. Sanechika, A. Yamamoto, *J. Polm. Sci., Polym. Lett. Ed.* (**1980**) 18, 9. b) I. Colon, G.T. Kwiatkowski, *J. Polym. Sci., Polym. Chem. Ed.* (**1990**) 28, 367. c) X. Wu, T.A. Chen, R.D. Rieke, *Macromolecules* (**1995**) 28, 2101. d) T.A. Chen, X. Wu, R.D. Rieke, *J. Am. Chem. Soc.* (**1995**) 117, 233. e) T.A. Chen, R.A. O'Brien, R.D; Rieke, Macromolecules (1993) 26, 3462.

[15]   R.B. Miller, S. Dugar, *Organometallics* (**1984**) 3, 1261.

16 a) M.D. McClain, D.A. Whittington, D.J. Mitchell, M.D. Curtis, *J. Am. Chem. Soc.* (**1995**) 117, 3887. b) M.J. Marsella, T.M. Swager, *J. Am. Chem. Soc.* (**1993**) 115, 12214.

17 a) R. Noufi, A. J. Nozik, J. White, L. Watten, *J. Electrochem. Soc.* (**1982**) 129, 2261. b) E.M. Geniès, A.A. Syed, C. Tsintavis, *Mol. Cryst. Liq. Cryst.* (**1985**) 121, 181.

18 A.F. Diaz, K.K. Kanazawa, G.P. Gardini, *J. Chem. Soc., Chem. Commun.* (**1979**) 635.

19 L.M. Goldenberg, P.C. Lacaze, *Synth. Met.* (**1993**) 58, 271.

20 A.F. Diaz, *Chem. Scr.* (**1981**) 17, 142.

21 S. Holdcroft, *Adv. Mater.* (**2001**) 13:23, 1753.

22 D.G.H. Ballard, A. Courtis, I.M. Shirley, S.C. Taylor, *J. Chem. Soc. Chem. Commun.* (**1983**) 954.

23 D.L. Gin, V.P. Conticello, R.H. Grubbs, *J. Am. Chem. Soc.* (**1994**) 116, 10934.

24 a) J.C.W. Chien, *Polyacetylene : chemistry, physics and materials science*, Academic Press, Orlando (**1984**). b) W.J. Feast, J. Tsibouklis, K.L. Pouwer, L. Groendaal, E.W. Meijer, *Polymer*, (**1996**) 22, 5017. c) S. Curran, A. Stark-Hauser, S. Roth, *Organic conductive Molecules and polymers, (Ed. H.S. Nalwa)* John Wiley & Sons, New York (**1997**) vol. 2, 2. d) R. Kiebooms, R. Menon, K. Lee, *Handbook of advanced electronic and photonic materials and devices, (Ed. H.S. Nalwa)* Academic Press (**2001**) vol. 8, 1.

25 J. Rodriguez, H.J. Grande, T.F. Otero, *Handbook of organic conductive molecules and polymers, (Ed. H.S. Nalwa)* John Wiley & Sons, New York (**1997**) vol. 2, 505.

26 a) P. Kovacic, M.B. Jones, Chem. Rev. (1987) 87, 357. b)W.J. Feast, J. Tsibouklis, K.L. Pouwer, L. Groenendaal, E.W. Meijer, Polymer, (1996) 22, 5017. c) P.C. Lacaze, S. Aeiyach, J.C. Lacroix, *Handbook of organic conductive molecules and polymers, (Ed. H.S. Nalwa)* John Wiley & Sons, New York (**1997**) vol. 2, 205. d) R. Kiebooms, R. Menon, K. Lee, *Handbook of advanced electronic and photonic materials and devices, (Ed. H.S. Nalwa)* Academic Press (**2001**) vol. 8, 1.

27 a) J. Roncali, *Chem. Rev.* (**1992**) 92, 711. b) J. Roncali, *Chem. Rev.* (**1997**) 97, 173. c) J.P. Ferraris, D.J. Guerrero, *Handbook of conducting polymers (Eds. T.A. Skotheim, R.L. Elsembaumer, J.R. Reynolds)* Dekker, New York (**1998**) 259. d) R.D. McCullough, *Adv. Mater.* (**1998**) 10, 93. e) R.D. McCullough, P. Ewbank, *Handbook of conducting polymers (Eds. T.A. Skotheim, R.L. Elsembaumer, J.R. Reynolds)* Dekker, New York (**1998**) 225. f) J. Roncali, *Handbook of conducting polymers (Eds. T.A. Skotheim, R.L. Elsembaumer, J.R. Reynolds)* Dekker, New York (**1998**) 311.

28 J.H. Burroughes, D.D.C. Bradley, A.R. Brown, R.N. Marks, K. Mackay, R.H. Friend, P.L. Burn, A.B. Holmes, *Nature* (**1990**) 347, 539.

29 R.N. McDonald, T.W. Cambell, *J. Am. Chem. Soc.* (**1960**) 82, 4669.

30   M. Rehahn, A.D. Schlüter, *Makromol. Chem., Rapid Commun.* (**1990**) 11, 375.

31   a) R.W. Lenz, C.E. Handlovits, *J. Org. Chem.* (**1960**) 25, 813. b) E.G.J. Staring, R.C.J.E. Demandt, D. Braun, G.L.J. Rikken, Y.A.R.R. Kessener, A.H.J. Venhuizen, M.M.F. Knippenberg, M. Bouwmans, *Synth. Met.* (**1995**) 71, 2179.

32   a) R.F. Heck, *Org. React.* (**1982**) 27, 345. b) A. Greiner, W. Heitz, *Makromol. Chem., Rapid Commun.* (**1988**) 9, 581.

33   a) W.P. Chang, W.T. Whang, P.W. Lin, *Polymer* (**1996**) 37, 1513. b) H. Nishihara, M. Tateishi, K. Aramaki, T. Ohsawa, O. Kimura, *Chem. Lett.* (**1987**) 539.

34   a) R.A. Wessling, R.G. Zimmerman, *U.S. Pat.* (**1968**) 3 401 152. b) R.A. Wessling, R.G. Zimmerman, *U.S. Pat.* (**1968**) 3 404 132. c) R.A. Wessling, R.G. Zimmerman, *U.S. Pat.* (**1970**) 3 532 643. d) R.A. Wessling, R.G. Zimmerman, *U.S. Pat.* (**1972**) 3 706 677.

35   R.W. Lenz, C.C. Han, J. Stenger-Smith, F.E. Karasz, *J. Pol. Sci., Polym. Chem.* (**1988**) 26, 3241.

36   D.D.C. Bradley *J. Phys. D : Appl. Phys.* (**1987**) 20, 1389.

37   a) R.A. Wessling, *J. Polym. Sci., Polym. Symp.* (**1985**) 72, 55. b)R. Garay, R.W. Lenz, *Makromol. Chem. Suppl.* (**1989**) 15, 1.

38   J.M. Machado, F.R. Denton, J.B. Schlenoff, F.E. Karasz, P.M. Lahti, *J. Polym. Sci. Part B: Polym. Phys.* (**1989**) 27, 199.

39   D.R. Halliday, P.L. Burn, R.H. Friend, D.D.C. Bradley, A.B. Holmes, *Synth. Met.* (**1993**) 55, 902.

40   B.R. Cho, Y.K. Kim, M.S. Han, *Macromolecules* (**1998**) 31, 2098.

41   R. Garay, F.E. Karasz, R.W. Lenz, *J. Macromol. Sci.-Pure Appl. Chem. A* (**1995**) 32, 905.

42   a) P.L. Burn, D.D.C. Bradley, R.H. Friend, D.A. Halliday, A.B. Holmes, R.W. Jackson, A. Kraft, *J. Chem. Soc. Perkin. Trans. 1* (**1992**) 3225. b) I. Murase, T. Ohnishi, T; Noguchi, M. Hirooka, *Synth. Met.* (**1987**) 17, 639. c) K.Y. Yen, L.W. Shacklette, R. Else,baumer, *Synth. Met.* (**1987**) 22, 179. d) S.A. Askari, S.D. Rughooputh, F. Wudl, *Synth. Met* (**1989**) 29, 129.

43   Y. Sonada, K. Kaeriyama, Bull. Chem. Soc. Jpn. (**1992**) 65, 853.

44   a) D.H. Hwang, H.K. Shim, J.I. Lee, K.S. Lee, *J. Chem. Soc. Chem. Commun.* (**1994**) 2461. b) S. Höger, J.J. McNamara, F. Wudl, *Chem. Mater.* (**1994**) 6, 171.

45   R.K. McCoy, F.E. Karasz, *Chem. Mater.* (**1991**) 3, 941.

46   a) R.O. Garay, U. Baier, C. Bubeck, K. Mullen, *Adv. Mater.* (**1993**) 5, 561. b) C. Zhang, D. Braun, A.J. Heeger, *J. Appl. Phys.* (**1993**) 73, 5177.

47   a) W. Brutting, M. Meier, M. Herold, S. Karg, M. Schwoerer, *Synth. Met.* (**1997**) 163. b) M. Herold, J. Gmeimer, C. Drummer, M. Schwoerer, *J. Mater. Sci.* (**1997**) 32, 5709.

48   a) T. Momii, S. Tokito, T. Tsutsui, S. Saito, *Chem. Lett.* (**1988**) 1201. b) H.V. Shah, A.R. McGhie, G.A. Arbuckle, *Thermochimica acta* (**1996**) 287, 319. c) B.R. Hsieh, H. Antoniadis, M.A. Abkowitz, H. Stolka, *Polym.*

Prep. (**1992**) 33, 414. d) M. Herold, J. Gmeimer, W. Riess, M. Schwoerer, *Synth. Met.* (**1996**) 76, 109. e) P.M Lahti, A. Sarker, R.O. Garay, R.W. Lenz, F.E. Karasz, *Polymer* (**1994**) 35, 1312.

49 S. Tokito, T. Momii, H. Murata, T. Tsutsui, S. Saito, *Polymer* (**1990**) 31, 1137.

50 S. Son, A. Dodabalapur, A.J. Lovinger, M.E. Galvin, *Science* (**1995**) 269, 376.

51 S. son, A.J. Lovinger, M.E. Galvin, *Polym. Mater. Sci. and Engin.* (**1995**) 72, 567.

52 a) J. Yang, H. Hong, M.E. Thompson, *Polym. Prepr.* (**1999**) 40(2), 1244. b) G. Arbuckle-Keil, Y. Liszewski, J. Peng, B. Hsieh, *Polym. Prepr.* (**2000**) 41(1), 826. c) S.C. Lo, A.K. Sheridan, I.D.W. Samuel, P.L. Burn, *J. Mater. Chem.* (**1999**) 9, 2165.

53 a) R. Gowri, D. Mandal, B. Shivkumar, S. Ramakrishan, *Macromolecules* (**1998**) 31, 1819. b)J.I. Jin, C.K. Park, H.K. Shim, *Macromolecules* (**1993**) 26, 1799.

54 H.G. Gilch, W.L. Wheelwright, *J. Pol. Sci., Part A: Polym. Chem.* (**1966**) 4, 1337.

55 W.J. Swatos, B. Gordon, *Polym. Prepr.* (**1990**) 31(1), 505.

56 a) D. Braun, E.G.J. Staring, R.C.J.E. Demandt, G.L .J. Rikken, Y.A .R.R. Kessener, A.H.J. Venhuizen, *Synth. Met.* (**1994**) 66, 75. b) B.R. Hsieh, W.A. Field, *Polym. Prepr.* (**1993**) 34, 410. c) G.J. Sarnecki, P.L. Burn, A. Kraft, R.H. Friend, A.B. Holmes, *Synth. Met.* (**1993**) 55-57, 914.

57 a) B.R. Hsieh, Y; Yu, G.M. Schaaf, W.A. Feld, *Polym. Prepr.* (**1998**) 32, 72. b) B.R. Hsieh, W.C. Wan, Y. Yu, Y. Gao, T.E. Goodwin, S.A. Gonzalez, W.A. Feld, *Macromolecules* (**1998**) 31, 651. c) B.R. Hsieh, Y; Yu, E.W. Forsythe, G.M. Schaaf, W.A. Feld, *J. Am. Chem. Soc.* (**1998**) 120, 231. d) B.R. Hsieh, W.C. Wan, Y. Yu, Y. Gao, T.E. Goodwin, S.A. Gonzalez, W.A. Feld, *Macromolecules* (**1998**) 31, 631.

58 H.H. Hörhold, J. Gottschaldt, J. Opfermann, *J. Prakt. Chem.* (**1977**) 139, 611.

59 a) F. Louwet, D. Vanderzande, J. Gelan, Synth. Met. (1992) 52, 125. b) F. Louwet, D. Vanderzande, J. Gelan, J. Mullens, *Macromolecules* (**1995**) 28, 1330. c) F. Louwet, D. Vanderzande, J. Gelan, *Synth. Met.* (**1995**) 69, 509.

60 A. van Breemen, *Ph.D Dissertation* (**1999**) Limburgs Universitair Centrum.

61 a) J.R. Shelton, K.E. Davis, *Int. J. Sulfur Chem.* (**1973**) 8(2), 205. b) C.A. Kingsbury, D.J. Cram, *J. Am. Chem. Soc.* (**1960**) 82, 1810.

62 E. Kesters, L. Lutsen, D. Vanderzande, J. Gelan, T.P. Nguyen, P. Molinié, *Thin Solid Films* (**2002**) 120, 404.

63 A. Issaris, D. Vanderzande, P. Adriaensens, J. Gelan *Macromolecules* (**1998**) 31(14), 4426.

64 L. Hontis, *Ph.D Dissertation* (**2002**) Limburgs Universitair Centrum.

65 M. Van der Borght, D. Vanderzande, J. Gelan, *Synth. Met.* (**1997**) 84, 399.

66   M. Van der Borght, D. Vanderzande, J. Gelan, *Polymer* (**1998**) 39, 4171.

67   a) B.R. Cho, Y.K. Kim, M.S. Han, *Macromolecules* (**1998**) 31, 2098. b) B.R. Cho, M.S. Han, Y.S. Suh, K.J. Oh, S.J. Jeon, J. Chem. Soc., Chem. Commun. (1993) 564. c) P.M. Lahti, D.A. Modarelli, F.R. Denton, R.W. Lenz, F.E. Karasz, *J. Am. Chem Soc.*, (**1988**) 110, 7258.

68   a) P.C. Hiberty, P. Karafiloglou, *Theoret. Chim. Acta (Berl.)* (**1982**) 61, 171. b) D. Döhnert, J. Koutecky, *J. Am. Chem. Soc.* (**1980**) 102(6), 1789. c) C.R. Flynn, J. Michl, *J. Am. Chem. Soc.* (**1974**) 96(10), 3280.

69   F. Louwet, *Ph.D Dissertation* (**1993**) Limburgs Universitair Centrum.

70   Vaste stof fysica boek.

71   E.M. Conwell, *Phys. Rev.* (**1956**) 103, 51.

72   N.F. Mott, *Canadian J. Phys.* (**1956**) 34, 1356.

73   A. Miller, E. Abrahams, Phys. Rev. (**1960**) 120, 745.

74   a) B.I. Shklovskii, A.L. Efros, *Electronic properties of doped semiconductors*, Springer-Verlag, Berlin (**1984**). B) H. Böttger, V.V. Brysksin, *Hopping conduction in solids*, Akademie-Verlag, Berlin (**1985**).

75   *Primary photoexcitations in conjugated polymers: molecular exciton versus semiconductor band model (Ed. N.S. Sariciftci)*, World Scientific, Singapore (**1997**).

76   A.J. Heeger, S. Kivelson, J.R. Schrieffer, W.P. Su, *Rev. Mod. Phys.* (**1988**) 60, 781.

77   S. Roth, *One-dimensional metals*, VCH Verslagsgesellschaft mbH, Wienheim (**1995**)

78   U. Rauscher, H. Bässler, D.D.C. Bradley, M. Hennecke, *Phys. Rev. B* (**1990**) 42, 9830.

79   H. Bässler, Phys., *Status Solidi B* (**1993**) 175, 15.

80   a) J. Frenkel, *Phys. Rev.* (**1931**) 38, 309. b) R. Peierls, *Ann. Phys.* (**1932**) 13, 905.

81   a) N.F. Mott, *Trans. Faraday Soc.* (**1938**) 34, 500. b) G.H. Wannier, *Phys. Rev.* (**1937**) 52, 191.

82   K.C. Kao, W. Hwang, *Electrical Transports in solids – with particular reference to organic semiconductors*, Pergamon Press, Oxford (**1981**).

83   A) R.N. Marks, J.J.M. Halls, D.D.C. Bradley, R.H. friend, *J. Phys.: Cond. Mat.* (**1996**) 6, 1379. b) P.G.D. Costa, E.M. Conwell, *Am. Phys. Soc. Rap. Comm.* (**1993**) 48, 1993.

84   M. Chandross, S. Mazumdar, S. Jeglinski, X. Wei, Z.V. Vardeny, E.W. Kwock, T.M. Miller, *J. Phys. Cond. Matter* (**1994**) 6, 1379.

85   S. Kirkpatrick, *Rev. Mod. Phys.* (**1973**) 45, 574.

86   V. Ambegaokar, B.I. Halperin, J.S. Langer, *Phys. Rev. B* (**1971**) 4, 2612.

87   H. Scher, E.W. Montroll, *Phys. Rev. B* (**1975**) 12, 2455.

88   a) B. Movaghar, W. Schirmacher, *J. Phys. C* (**1981**) 14, 859. b) D. Bourbie, *Phil. Mag. B* (**1996**) 73, 201.

89   M.C.J.M. Vissenberg, *PhD Dissertation* (**1999**) Universiteit Leiden.

90   W.D. Gill, *J. Appl. Phys.* (**1972**) 43, 5033.

[91] a) P.W.M. Blom, M.J.M. de Jong, M.G. Munster, Phys. Rev. B (1997) 55, R656. b) S.J. Santos Lemus, J. Hirsch, *J. Phil. Mag. B* (**1986**) 53(1), 25.

[92] P. Chandrasekhar, *Conducting polymers, fundamentals and applications,* Kluwer Academic publishers, Boston (**1999**).

[93] M.G. Kanatzidis, *Chemical & engineering news* (**1990**) 68(49), 36.

[94] J. Roncali, *Chem. Rev.* (**1997**) 97, 173.

[95] E. Van Thillo, G. defieuw, W. De Winter, *Bull. Soc. Chim. Belg.* (**1990**) 99(11-12), 981.

[96] C. Klason, D.H. Mcqueen, J. Kubat, *Macromolecular Symposia* (**1996**) 108, 247.

[97] M.K. Lu, S. Basak, R.L. Elsenbaumer, *Handbook of conducting polymers (Eds. T.A. Skotheim, R.L. Elsembaumer, J.R. Reynolds)*, Dekker, New York (**1998**) vol. 1, 881.

[98] M. Onoda, H. Nakayama, K. Tada, S. Morita, K. Yoshino, *Mol. Cryst. Liq. Cryst.* (**1994**) 256, 657.

[99] a) V.G. Kulkarni *Handbook of conducting polymers (Eds. T.A. Skotheim, R.L. Elsembaumer, J.R. Reynolds)*, Dekker, New York (**1998**) vol. 1, 1059. b) S. Roth, *Indian J. Chem., Sect. A* (**1994**) 33A, 453.

[100] M. Pope, *Mol. Cryst. Liq. Cryst.* (**1993**) 228, 1.

[101] C. Arbizzani, M. Mastragostino, B. Scrosati, *Handbook of organic conductive molecules and polymers*, John Wiley and Sons (**1997**) vol. 4, 595.

[102] D. Moses, *Appl. Phys. Lett.* (**1992**) 60, 3215.

[103] M.A. Diaz-Garcia, F. Hide, B.J. Schwartz, M.R. Anderson, Q. Pei, A.J. Heeger, *Synth. Met.* (**1997**) 84, 455.

[104] R.J. Visser, *Philips J. Res.* (**1998**) 51, 467.

[105] A. Bernsten, Y. Croonen, C. Liedenbaum, H. Schoo, R.J. Visser, J. Vleggaar, P. van de Weijer, *Optical Materials* (**1998**) 9, 125.

[106] O. Yokoyama et al. *International Display Workshop* (**2000**)

[107] D.M. de Leeuw, E.J. Lous, *Synth. Met.* (**1994**) 65, 45.

[108] C.D. Dimitrakopoulos, D.J. Mascaro, *IBM J. Res. & Dev.* (**2001**) vol. 45(1), 11.

[109] A.R. Brown, C.P. Jarret, D.M. de Leeuw, M. Matters, *Synth. Met.* (**1997**) 88, 37.

[110] G. Horowitz, R. Hajlaoui, P. Delannoy, *J. Phys. III France,* (**1995**) 5, 355.

[111] M. Matters, D.M. de Leeuw, M.J.C.M. Vissenberg, C.M. Hart, P.T. Herwig, T. Geuns, C.M.J. Mutsaers, C.J. Drury, *Optical Materials* (**1999**) 12, 189.

[112] N.S. Saritiftci, L. Smilowitz, A.J. Heeger, F. Wudl, *Science* (**1992**) 258, 1474.

[113] G. Yu, C. Zhang, A.J. Heeger, *Appl.Phys.Lett.* (**1994**) 64, 1540.

[114] a) G. Yu, J. Gao, J.C. Hummelen, F. Wudl, A.J. Heeger, *Science* (**1995**) 270, 1789. b) L.S. Roman, M.R. Andersson, T. Yohanms, O. Inganäs, *Adv.Mat.* (**1997**) 9, 1164.

[115] C.J. Brabec, F. Padinger, J.C. Hummelen, R.A.J. Janssen, N.S. Sariciftci, *Synth. Met.* (**1999**) 102/1-3, 861.

[116] *Presseabteilung* Siemens, G. Weber (**2004**) Informationsnummer CT200309.001d

Chapter 2
MDMO-PPV: a matrix of materials

In chapter 2 a matrix of different materials with various defect levels and types (e.g. regioregularity and single bond defects) of the 'workhorse' conjugated polymer, MDMO-PPV is defined. The Gilch and sulfinyl procedure will be used to synthesize these MDMO-PPV batches. These synthetic routes are intensively discussed including side reactions causing the mentioned defects. Chapter 2 is ended with a discussion about the film and device preparation as used within the frame of this work.

2.1   Solution processable PPV

A typical electronic device based on conjugated polymers desires a high quality thin film, making solution processing by spincoating the most appropriate preparation technique. As poly(p-phenylenevinylene) (PPV) is insoluble, intractable and infusible, the dilemma of the easy processing is conveniently resolved by using solution-processible precursor polymers as quoted in section 1.2.2.

Early light emitting diodes (LED's) based on this approach with a configuration consisting at a transparent Indium Tin Oxide (ITO) layer, an emissive PPV layer and Al as a cathode layer (ITO/PPV/Al), yielded an external quantum efficiency of 0.01%[1]. Present, reported values of the luminous efficiency for devices based on PPV prepared via a precursor film, ranges 2 lmW^{-1} (lumens per watt)[2].

So although fairly good results are obtained, the use of an additional conversion step on the thin spincoated precursor film can be seen as a major drawback of the precursor approach. Indeed, this additional thermal treatment during device fabrication often complicates the performance and

the production[3]. So following the discovery of electroluminescence in (PPV)[4], light emitting diodes based on PPV derivatives, soluble in the conjugated form were independently reported by Ohnishi et al.[5] and Braun et al.[6]

The introduction of substituents on the PPV-skeleton not only allows the modification of the electronic properties (e.g. bandgap, electron affinity and ionization potential) but also enables the generation of PPV's that are soluble in organic solvents. Typical structures reported in literature are based on poly((2,5-dialkoxy-1,4-phenylene)vinylene) with at least one solubilizing alkoxy side chain: e.g. 2-ethylhexyloxy, 3,7-dimethyloctyloxy, 2-methylpentyloxy or dodecyloxy[5,6,7].

MEH-PPV   MDMO-PPV
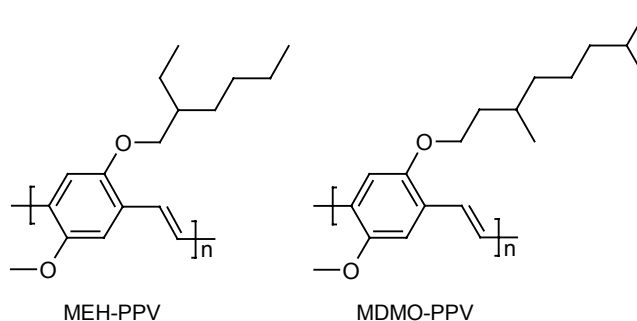
figure 2.1 Examples of soluble dialkoxy-substituted PPV derivatives

The in figure 2.1 depicted examples of soluble dialkoxy-substituted PPV derivatives, namely poly(2-methoxy-5-(2'-ethylhexyloxy)-p-phenylenevinylene) (MEH-PPV) and poly(2-methoxy-5-(3'-7'-dimethyloctyloxy)-p-phenylenevinylene) (MDMO-PPV) are typical representatives of this class of materials and are used as standard materials in conjugated polymer research and development.

Besides the solubilizing function of the alkoxy side-chains, a change in electronic properties (e.g. a bathochromical shift in emission and absorption spectra) is observed. The value of the bandgap (E_g) is decreased from $E_{g(PPV)}$ 2,3 eV to typical $E_{g(dialkoxy-PPV)}$ 2.1 eV. Furthermore, long side chains separate the polymeric chains and hence impede non-emissive relaxation[1].

MEH-PPV applied as an emissive layer in a simple LED (ITO/MEH-PPV/Ca) achieves a respectable value for the external quantum efficiency of 1,0 %[6a,8]. Currently, values of the luminous efficiency of multi-layer devices ranging 3-4 lmW^{-1} are reported[9].

A related polymer, MDMO-PPV, often also referred as OC_1C_{10}-PPV, has been the subject of investigation by workers at Philips and Covion[10]. A high value for the external quantum efficiency obtained in single layer devices (ITO/MDMO-PPV/Ca) is reached namely 2.1 %[10]. MDMO-PPV has a luminous efficiency value of 3 lmW^{-1} and a brightness of 100 Cd m^{-2}.

34

Although the mentioned conjugated polymers are historically developed during research towards organic LED's and played in this field the role of 'workhorse' material for many years, MDMO-PPV and MEH-PPV are also subject of extensive research in other organic electronoc devices, e.g. solar cells.

Typical photovoltaic devices consist of a hetero junction between a p-type and an n-type material either planar or dispersed in the bulk as described in chapter 5. Planar, organic/organic, p/n junctions can be realized by spincoating MEH-PPV, followed by an evaporation of C_{60}[11]. Solar cells based on MDMO-PPV and PCBM are today's reference photovoltaic devices based on an organic/organic bulk p/n junction. A value for the efficiency under AM1.5 illumination, ranging 2.5 %, is reported[12]. However, one should notice that these promising results can not completely be attributed to this specific set of materials but are also the result of an enhanced optimization of the processing and device configuration (e.g. choice of electrodes, spincoating parameters, …).

Due to the excellent solubility properties of the dialkoxy-PPV's, the in section 1.2.2 mentioned precursor routes are not insurmountable anymore to process these materials. However, they still yield fairly good chemical results and as such are used to synthesize MDMO-PPV and MEH-PPV.

Although, MDMO-PPV and MEH-PPV will never be the ultimate conjugated polymers in fully commercial applications, it is clear that they play the role of 'workhorse' already for many years in this field. As such, a considerable knowledge on the synthesis, properties and processing parameters, is gathered in recent years. However still important questions concerning these materials remain unanswered.

Within the scope of this thesis, one will focus on one of both materials namely MDMO-PPV. The basic idea of this thesis is to clarify a relation between the chemical defects occurring in the chemical structure of MDMO-PPV induced by difference in synthetic approach, and the performance of devices made with this material, via physical parameters.

In section 2.2 a typical choice of two synthetic routes towards MDMO-PPV, used in this work, (e.g. Gilch route and sulfinyl route) is presented and justified. A more profound overview as found in literature and experimentally determined within our group is shown in section 2.3. Thereby, a strong focus on the main reaction, side reaction and aspects of regioregularity with a correlation to defects in the chemical structure is presented. The obtained information leads to the definition of a matrix of MDMO-PPV materials with differences in conjugational defects and regioregularity ratios that will be studied systematically in the course of this thesis. A description of this matrix will be the subject of section 2.4. Furthermore in this chapter, the preparation of the devices out of these polymer materials will be briefly discussed. Besides a limited description of the pilot line to produce all organic semiconductor devices under inert

atmosphere, section 2.5 will mainly discuss the film preparation for the defined matrix of materials.

2.2 Synthesis of MDMO-PPV

In this thesis, the relation between defects in the chemical structure of a 'workhorse' conjugated polymer, namely MDMO-PPV and the performance in electronic devices via physical parameters, is investigated.

So although the already mentioned precursor approach is not insurmountable anymore to process soluble dialkoxy-PPV's, it yields good results and is as such used to synthesize MDMO-PPV.

As indicated in figure 2.2, a distinction can be made between precursor routes and direct routes.
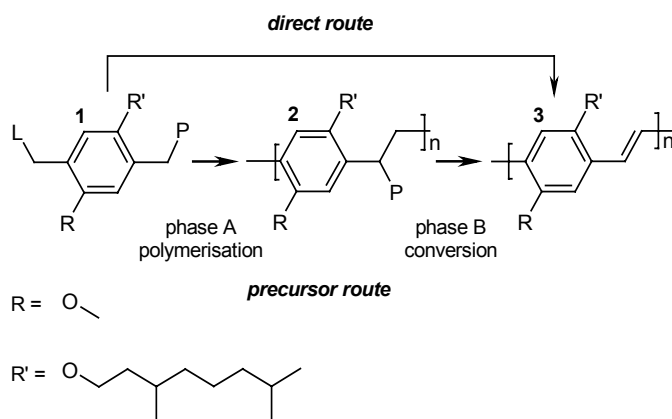
figure 2.2 Schematic representation of direct routes and precursor routes used to synthesize MDMO-PPV

The direct solution polymerization from monomer (**1**) towards conjugated polymer (**3**) is a synthetic approach, often used in industry. When working with precursor routes, two typical phases occurring at the synthesis can be observed, namely: the polymerization (A) from monomer (**1**) towards non-conjugated precursor polymer (**2**) and the conversion (B) from precursor polymer (**2**) towards conjugated polymer (**3**). An overview of the exact nature of the polarizer (P) and leaving group (L) for the different precursor routes can be found in table 1.1 at section 1.2.2.6.

Synthesizing of solution processible conjugated polymers (e.g. MDMO-PPV) via precursor routes, allows the conversion (B) either to be executed in film or in solution. In the latter case, precipitation and purification of the conjugated polymer (**3**) can be performed. After redissolving, a high quality thin film can be obtained via spincoating of the conjugated polymer (**3**), thereby reducing the typical drawbacks of a conversion (B) in film. The major drawback of the latter is a strong increase in surface roughness due to the elimination products escaping as gaseous compounds the thin film.

This reduced film quality often influences the performance of the devices. An evaluation via atomic force microscopy of the influence of this conversion step on the film properties can be found in section 2.5.3.

Within the scope of this work, an evaluation of MDMO-PPV prepared via two synthetic procedures (e.g. Gilch route and sulfinyl route) is presented. The typical choice to work with both procedures can be justified by the use of the Gilch route as a standard procedure in industry and the already promising results obtained for the sulfinyl route developed at the 'Limburgs Universitair Centrum'.

In figure 2.3, a schematic representation of the Gilch[13] route and the sulfinyl[14] route used to synthesize MDMO-PPV, is depicted.

figure 2.3 Schematic representation of the Gilch route and the sulfinyl route used to synthesize MDMO-PPV

The Gilch route is presented as a direct route without any isolation of a precursor polymer. This is indeed the procedure as proposed by Gilch and Wheelwright to obtain, starting from a 1,4- bis(halomethyl)benzene-monomer (**1**) via a polydehydrohalogenation[13] the fully conjugated polymer (**4**) by adding a large excess of base. As will be indicated in section 2.3, when focusing on the main reaction, a distinction between three steps (e.g. formation of the active monomer, a p-quinodimethane system, a polymerization of a 'precursor' polymer and the further conversion to the conjugated polymer), similar to the three typical steps of a precursor route can be made. Indeed the proposal to use only on equivalent of base was already presented by Swatos et al[15], converting the Gilch route into a sort of precursor route, although the intermediate chlorine precursor polymer has only a limited stability.

A first issue when working with the sulfinyl route is to convert the by Covion[16] commercially available 2,5-bis(chloromethyl)-1-((3,7-

dimethyloctyl)oxy)-4-methoxybenzene (BCDM) (**1**) into the actual monomer, namely 2-(chloromethyl)-5-((butylthio)methyl)-1-((3,7-dimethyloctyl)oxy)-4-methoxybenzene (**2**). This asymmetrically monomer shows a differentiation between on one hand the leaving group (e.g. chlorine) and on the other hand polarizer (e.g. sulfinyl group). As polarizer and leaving group show contradictorily demands, the major advantage of this approach[14], in comparison with precursor routes starting from symmetrically substituted monomers, is a fine-tuning of both functionalities. The actual sulfinyl route starts by a solution polymerization towards the sulfinyl precursor polymer (**3**). The formation of the conjugated MDMO-PPV polymer (**4**) occurs via a thermal elimination of the sulfinyl group. This conversion is, within the scope of this thesis, performed in solution to overcome typical drawbacks of conversion in film. Because of the solubility of the MDMO-PPV, precipitation and purification of the conjugated polymer (**4**) can be performed, eliminating the presence of conversion products.

2.3   Chemical structure of MDMO-PPV

This section will give insight at the chemical structure (including side reactions and regioregularity aspects) of MDMO-PPV, as created during polymerization. Indeed, strong variations in some properties in the PLED application (e.g. lifetime in PLED), which are not related to the primary structure in an obvious way, are observed[17]. Defects such as long-chain branching, cross linking, single bonds instead of the desired double bonds, triple bond formation, substitution instead of elimination, incomplete elimination leading to conversion rates below 100%, … are conceivable[18]. These typical defects, occurring by a number of possible side reactions are expected to be also strongly dependent on the followed synthetic procedure. A better understanding about the occurrence of potential defects can be achieved via a NMR spectroscopy study of a ^{13}C-labeled MDMO-PPV. Such a study is performed by Becker et al.[19] for the Gilch polymerization of MDMO-PPV and within our group by Roex et al. for the sulfinyl polymerization.
Within the scope of this thesis, a summary of these results will be shown, however more details can be found in the appropriate literature. In the following paragraphs, for each polymerization route used in this thesis, an overview of the different steps occurring at the main reaction, possible side reactions related to defects in the chemical structure and aspects concerning the regioregularity of MDMO-PPV will be presented.

2.3.1   Gilch procedure

2.3.1.1 Main reaction and side reactions

A typical Gilch polymerization is performed under a nitrogen atmosphere with dry and degassed 1,4-dioxane as a solvent. After heating (98°C) an amount of 2,5-bis(chloromethyl)-1-((3,7-dimethyloctyl)oxy)-4-methoxybenzene (BCDM) (**1**) is added as a solid, followed by a drop wise addition of an excess (larger then 2 equivalents) of potassium tert-butoxide dissolved in 1,4-dioxane. During this addition, a change in color of the reaction mixture from colorless to orange and an increase in viscosity are observed. After cooling to 50°C, acetic acid is added, followed by a workup (precipitating in water/methanol, filtering, drying) and a purification step (dissolving in THF, precipitating in methanol, filtering, washing and drying).
Focusing on the main reaction, a schematic representation consisting at three steps similar to the three typical steps of a precursor route is depicted in figure 2.4.
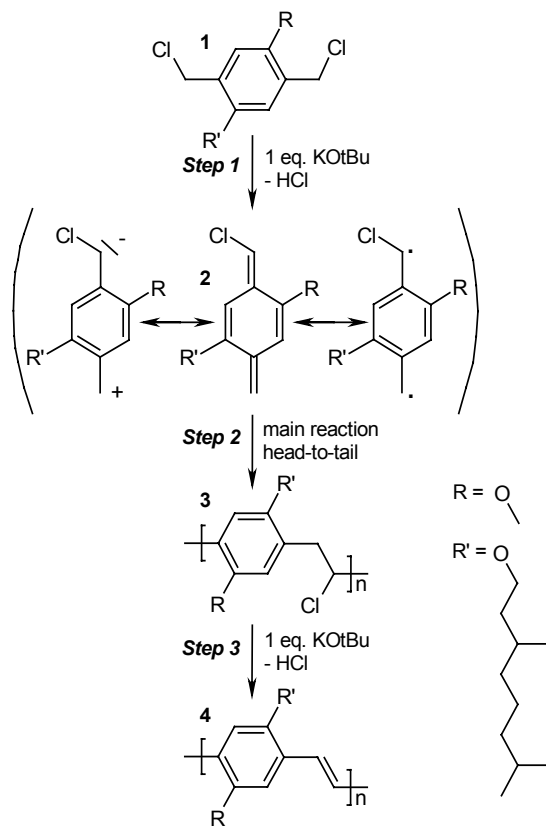
figure 2.4 Schematic representation of the main reaction of the Gilch polymerization of MDMO-PPV

The first step, similar to various precursor methods, is a base induced elimination of HCl on BCDM (**1**) which leads to the formation of the 'real monomer', a quinodimethane derivative (**2**). The second step is the polymerization itself towards a polymeric analogue of a precursor polymer (**3**). This is a chain-polymerization evidenced by the presence of high molecular weights at low monomer conversion[20,13]. Arguments about the mechanism (either anionic or radical) are still ongoing however a radical mechanism, at least responsible for the high molecular weight polymer formation, seems to be more favorable[21]. The third and last step is the polymer analogous elimination of HCl by a second equivalent of base. Indications (a residual organic chlorine in the polymers below 50 ppm) for an almost complete elimination towards MDMO-PPV (**4**) are observed by Becker et al.[19]

Defects in the 'regular' polymer chain will especially arise during steps 2 and 3. Using selectively ^{13}C labeled polymers Becker et al.[19] demonstrated

the occurrence of only one significant defect in Gilch polymerized PPV's, denoted as tolane-bisbenzyl (TBB) moiety. The observed single and triple bonds are formed via the mechanism as depicted in figure 2.5. Both bondings are related to each other and induced by a head-to-head addition during polymerization.

figure 2.5 Schematic representation of the side reaction of the Gilch polymerization[19]

From their measurements, they were not able to determine wether the two defects (e.g. single and triple bond) are located either on two adjacent monomer units or whether they are separated by one or more 'normal' double bonds. No mechanistic information could be determined from the presence of the TBB defect. It would occur in any case, independent on the polymerization mechanism, either free radical or anionic. Quantification of the amount of the TBB defect could be performed and ranges about 2 % (based on the number of monomer units) single and about 2 % triple bonds. Further structural defects could not be detected down to a level of about 0.2 %. However, at the level of the sensitivity, indications for ether-type end groups and functional groups resulting from deterioration (carbaldehyde and carboxylic acid) were found. Beside information on structural defects, evidence for almost 100 % trans double bonds could be found.

Roex et al. performed similar NMR spectroscopy experiments to clarify the chemical structure of sulfinyl and Gilch synthesized MDMO-PPV. Within

that framework, the observations of Becker et al.[19] could be reproduced qualitatively. Although a fairly good accordance could be reached, quantification of the TBB defect yielded a somewhat higher defect value ranging 11 % (e.g. 5-6 % single, 4 % triple bonds and 1% chlorovinylene bonds). No real explanation for this observed difference could be found, although the scale of polymerization is much smaller within this work. Furthermore quantification is obtained via the ^{13}C NMR spectroscopy experiments while Becker et al. uses the proton signal.

2.3.1.2 Regioregularity aspects

Although the Gilch route starts from a symmetrical monomer (BCDM), the position of the (3,7-dimethyloctyl)oxy) and methoxy side chains on the monomer units of the polymerized material shows a sort of regio-chemistry.
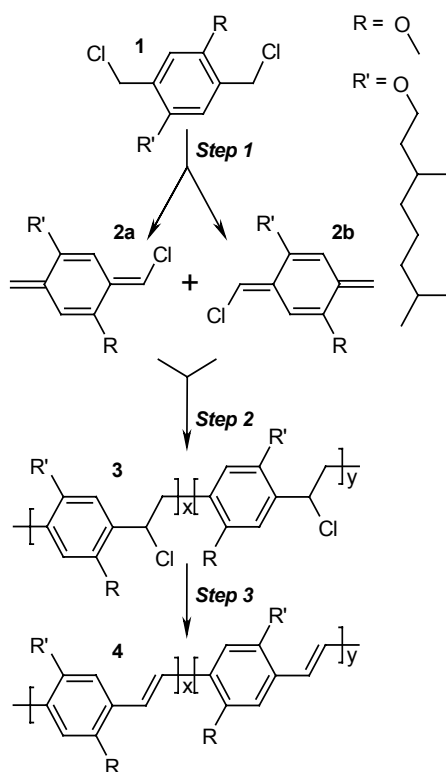

figure 2.6 Schematic representation of the reaction scheme of the Gilch polymerization including regio-chemistry

Indeed as indicated in figure 2.6, MDMO-PPV (**4**) is actually a co-polymer of two monomer isomers. This effect is to some extend induced by the

43

occurrence of two isomers (**2a** and **2b**) of the 'real' monomer, the quinodimethane derivative. An arbitrary reaction scheme based on the main reaction scheme (figure 2.4) is depicted in figure 2.6.

Cause of the instability of the quinodimethane derivative (**2a** and **2b**) and the symmetric nature of the monomer BCDM (**1**) no exclusion between both isomers can be made. MDMO-PPV obtained via the Gilch route yields in any case a random co-polymer of two monomer isomers.

Although the reactivity to extract a proton from both chloromethyl positions is not fully equal, not too much difference is expected. As such, synthesizing MDMO-PPV via the Gilch route yields a random co-polymer with a composition ratio of both isomers approaching unity.

2.3.2   Sulfinyl procedure

2.3.2.1 Asymmetric monomer synthesis

A first step when using the sulfinyl route to obtain MDMO-PPV is a conversion of BCDM (**1**) (commercially available by Covion) towards the actual monomer, namely 2-(chloromethyl)-5-((butylsulfinyl)methyl)-1-((3,7-dimethyloctyl)oxy)-4-methoxybenzene (**4**). This asymmetrically monomer shows a differentiation between on one hand the leaving group (e.g. chlorine) and on the other hand the polarizer (e.g. sulfinyl group). Although this differentiation complicates to some extend the synthesis of MDMO-PPV, it allows an increased control over the polymerization[22]. A highly selective route toward this product is developed within our group by Lutsen et al.[23] and schematically depicted in figure 2.7.
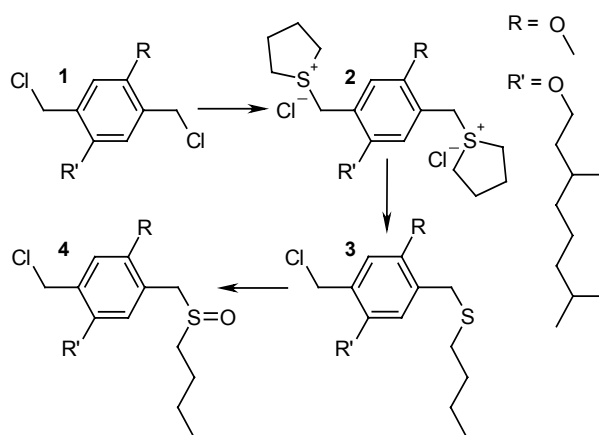

figure 2.7 Synthesis of the asymmetric monomer derived from BCDM via a highly selective route

A first step is the creation of a bis(tetrahydrothiophenium) salt (**2**) starting from BCDM (**1**) at room temperature using methanol as a solvent. A high selectivity towards the mono-butylsulfinyl-substituted product (**3**) is observed during the second reaction step by adding butanethiol and NaOtBu. A selective oxidation of the thioether by using hydrogenperoxide in combination with telluriumdioxide, a catalytic amount of hydrogen chloride in 1,4 dioxane as a solvent yields 2- (chloromethyl)-5- ((butylsulfinyl)methyl) -1-((3,7-dimethyloctyl)oxy)-4- methoxy-benzene (**4**), the actual asymmetrically substituted monomer.

This product is the actual starting product of the sulfinyl polymerization towards MDMO-PPV.

2.3.2.2 Main reaction

A typical sulfinyl polymerization is performed under a nitrogen atmosphere with s-BuOH as a solvent. The first step in the polymerization (schematically depicted in figure 2.8), is an addition of NaOtBu, to perform a base induced elimination of HCl on the monomer, namely 2- (chloromethyl)-5-((butylsulfinyl)methyl) -1-((3,7-dimethyloctyl)oxy)-4- methoxy-benzene (**1**). The difference in leaving group capacity between the chlorine and the sulfinyl group, assures a well-defined formation of the actual monomer, the quinodimethane system (**2**). The second step is the spontaneous polymerization towards the stable precursor polymer (**3**). Notice the function of the polarizer (e.g. sulfinyl group) during this step, namely a polarization of the quinodimethane system in such a way that regular head-to-tail addition occurs dominantly. Indeed the major difference between the Gilch procedure and sulfinyl procedure is the polarizing ability of the polarizer, either the chlorine group or the sulfinyl group. The mixture of solvent and precursor polymer is poured into water and neutralized. An extraction with chloroform is carried out followed by a drying step and a concentrating step of the organic layer. The isolated precursor polymer shows a high stability and can be stored as such.

The final step is the conversion of the precursor polymer (**3**) towards the fully conjugated polymer, MDMO-PPV (**4**) by a thermal elimination of the sulfinyl group. Due to the excellent solubility properties of MDMO-PPV, the conversion can be performed in solution. A typical procedure is carried out in a refluxing toluene (110 °C) for 3 hours under nitrogen atmosphere.

A schematic representation of these typical steps occurring during the solution polymerization of MDMO-PPV via the sulfinyl route is depicted in figure 2.8.
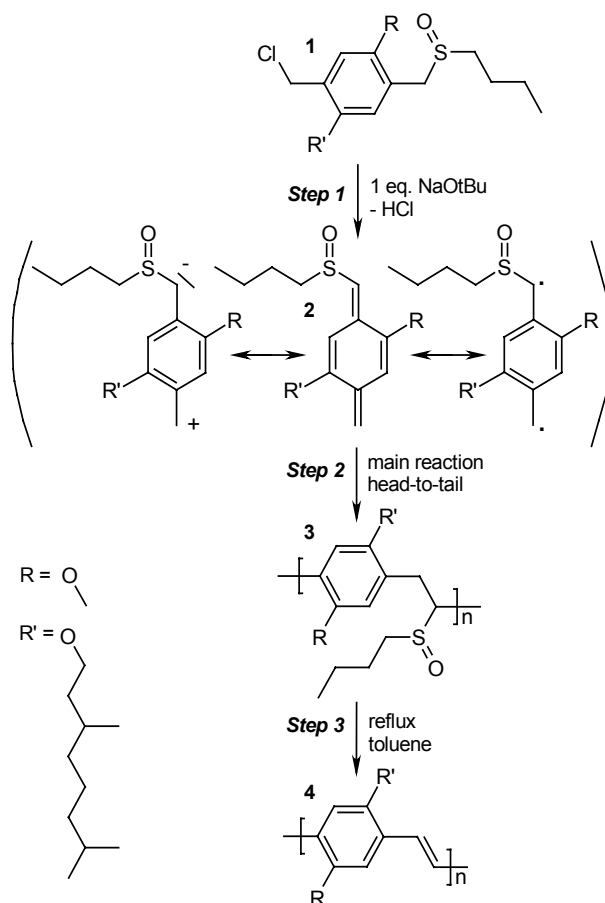
figure 2.8 Schematic representation of the reaction scheme of the sulfinyl polymerization of MDMO-PPV

Insight at the chemical structure of sulfinyl polymerized MDMO-PPV could be obtained by Roex et al. via a NMR spectroscopy study of ^{13}C labeled compounds. Within the scope of this work, an overview of the main results is presented. However a detailed description can be found in the appropriate literature.

Within the sensitivity of the experiments, the only defect that could be observed in the conjugated backbone of MDMO-PPV is the presence of a single bond. Quantification of this defect yields a percentage in comparison to the monomer units ranging 7 %. No observation of a triple bond could be performed, making the presence of a TBB defect unlikely. The single bonds can be interpreted as an incomplete elimination of the sulfinyl group. A such this defect is not a real defect. The amount of incomplete elimination can be further reduced using more appropriate thermal elimination programs. A schematic presentation of the defect structure of via the

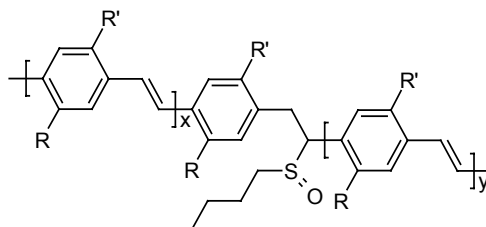sulfinyl procedure solution polymerized MDMO-PPV, is presented in figure 2.9.

*figure 2.9 Defect structure of solution polymerized MDMO-PPV with
an incomplete elimination via the sulfinyl route*

Although the presented structure corresponds with MDMO-PPV synthesized via the sulfinyl route as described in present literature[24], effort towards a reduction of this defect via an enhanced elimination was successfully made. An additional elimination after precipitating and purification of the MDMO-PPV polymer for an additional 4 hours in a refluxing toluene atmosphere yielded a defect free (within the sensitivity of the experiments < 0.5 %) polymer. This excellent result emphasizes the promising chemistry of the sulfinyl route towards conjugated polymers.

2.3.2.3   Regioregularity aspects

Contrary to the Gilch route the asymmetric nature of the monomer allows the definition of two isomers, namely: 2- (chloromethyl)-5-((butylthio)methyl) -1-((3,7-dimethyloctyl)oxy)-4- methoxy-benzene (**1a**) and 2-((butylthio)methyl)-5- (chloromethyl)-1-((3,7-dimethyloctyl)oxy)-4-methoxy-benzene (**1b**). The synthetic procedure to convert BCDM to this mixture of both monomer-isomers as presented in section 2.3.2.1 yields a typical ratio of both products approaching unity[23]. A detailed reaction scheme based on the existence of this two starting monomers is depicted in figure 2.10.

A difference in leaving group capacity of on one hand the sulfinyl group and on the other hand the chlorine group allows a controlled formation, via a base-induced elimination, of the actual monomer, the quinodimethane system (**2a** and **2b**). The excellent polarizing properties of the sulfinyl group determine a complete head-to-tail addition when the precursor polymer is formed (**3a**, **3b** and **3c**).
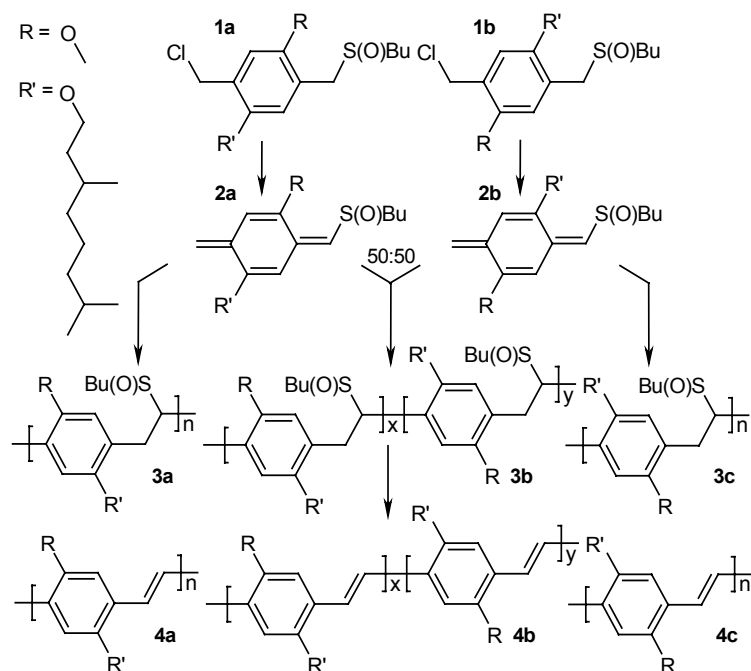
figure 2.10 Schematic representation of the reaction scheme of the sulfinyl polymerization including regio-chemistry

An important advantage of the sulfinyl route is the possibility of a chromatographic separation of both monomer-isomers (**1a** and **1b**). This allows beside the formation of a random co-polymer (**3b**) consisting at an equal ratio of both monomer-isomers, the formation of both homo-polymers (**3a** and **3c**) and even random co-polymers consisting at a desired ratio of both monomer-isomers. As the position of both alkoxy chains does not change during conversion, the precursor polymers will lead to the formation of either a homo-polymer of MDMO-PPV (**4a** and **4c**) or a random 50:50 (or any other composition ratio) co-polymer of MDMO-PPV (**4b**).

Extended information about the assignment of both monomer-isomers by NMR spectroscopy experiments and the synthesizing of homo-polymers of MDMO-PPV can be found in literature[25].

2.4 Matrix of materials

The aim of this thesis is to clarify a relation between the chemical defects of a conjugated polymer, MDMO-PPV, as discussed in the previous section and the performance of devices made with this material. As shown each synthetic route towards PPV has its own drawbacks yielding specific defects. Two type of defects related to asymmetrically substituted MDMO-

PPV can be distinguished: defects related with interruptions of the conjugated system on the vinylene double bond and defects related with the position of the side-chains (regioregularity). As indicated in the previous section, the sulfinyl route has a potential to control both mentioned synthetic defects, emphasizing the promising polymerization chemistry to conjugated polymers via the sulfinyl approach.

As a sort of thread in this work, a matrix of MDMO-PPV materials is defined and synthesized. An overview can be found in table 2.1.

Code	Synthetic route	Single bonds (%)	Triple bonds (%)	Regio – regularity (ratio)
A-SUL	sulfinyl	< 0.5	0	50:50
B-SUL	sulfinyl	7	0	50:50
C-SUL	sulfinyl	> 7 & < 10	0	50:50
N-GIL	Gilch	2	2	± 50:50
R-SUL	sulfinyl	7	0	80:20

table 2.1 Matrix of MDMO-PPV materials as used within the scope of this thesis

Because of these batches are not ^{13}C labeled MDMO-PPV, the values for the quantification of the defects should be interpreted within the reproducibility of the synthesis ranging about 1%. The Gilch material used within the scope of this thesis is directly ordered from Covion. Therefore the values of the number of defects as presented in table 2.1 are originally copied from their publication[19].

Within this matrix a first distinction can be made on the synthesis procedure, namely the Gilch and sulfinyl procedure. The three batches of sulfinyl material (A-SUL, B-SUL, C-SUL) exhibit an increasing number of defects, however none of them shows a triple bond.

The material C-SUL MDMO-PPV is prepared via an elimination of the precursor material during only 2 hours (refluxing toluene). However, no labeled ^{13}C NMR experiments were carried out on a reference batch with an elimination procedure of 120 minutes. The reference batch sulfinyl MDMO-PPV with an elimination time equal to 90 minutes yields about 10 % of single bond defects and the reference sulfinyl MDMO-PPV batch with an elimination time of 180 minutes yields 7 % defects. Therefore the C-SUL material is estimated to have a defect level of between 7 % and 10 %. In the following figures this level is indicated as 8.5 % with an error bar of 2 %. All of these batches show an almost 50:50 ratio of both isomers of the monomer unit. The MDMO-PPV material with an increased regioregularity (batch R-SUL) can as indicated in the previous section only be synthesized via the sulfinyl route. An equal number of defects in the backbone allow a comparison with batch B-SUL. The ratio of both isomers, namely 80:20 is chosen because of an optimum between on one hand solubility and on the

other hand a higher degree of regioregularity. Indeed the homo-polymer of MDMO-PPV exhibits an extremely reduced solubility[25].

In the next section, the results of a basic physico-chemical characterization are presented. As this matrix of materials will be examined and compared in semiconductor devices, some issues concerning the device preparation are discussed. The typical parameters for the different MDMO-PPV materials to prepare high quality thin films via spincoating will be given.

2.5   Device preparation

Since 1999, the 'Instituut voor Materiaal Onderzoek' possesses a small pilot line to prepare and characterize under inert atmosphere various types of organic semiconductor devices. Within the scope of this thesis a limited survey about this equipment to prepare and characterize polymer semiconductor devices is given in section 2.5.1.

As the MDMO-PPV batches are examined in active devices or in film, it is of major importance to control the film preparation step. Indeed as the different MDMO-PPV materials have different molecular weights an appropriate study on the spincoating properties is needed. Furthermore, knowledge of this step can already give some insight in the different behavior of the matrix of MDMO-PPV materials. Therefore section 2.5.2 is devoted to some relevant physico-chemical properties of the matrix of MDMO-PPV materials and a description of the film preparation via spincasting.

As both, the sulfinyl and Gilch route are precursor routes to synthesize MDMO-PPV, the intermediate precursor polymer can be spincasted and converted to MDMO-PPV in film. In section 2.5.3 these possibilities are briefly explored. However it is shown that within the framework of this thesis, this process complicates the ability to obtain high quality thin films. Therefore it will be concluded to perform all conversions in solution and spincoat the solved MDMO-PPV.

2.5.1   Pilot line

The pilot line, often denoted as glove-box consists of all necessarily equipment to produce and characterize under inert nitrogen atmosphere (<5ppm O_2 and <5ppm H_2O) all basic organic semiconductor devices. As most organic materials posses' strong oxygen sensitivity, this set-up allows to prepare high quality devices and characterize them without complicated packaging steps.

Firstly the substrates either glass or quartz substrates (when studying naked films of MDMO-PPV), glass plates with conductive ITO stripes (when studying either solar cells or PLED's) or silicon substrates with gold electrodes (when studying transistors) are cleaned. This is performed via an ultrasonic treatment of the substrates in iso-propanol. After drying under vacuum atmosphere, dust particles are removed via a flow of nitrogen gas. Next, the substrates are inserted into the glove-box.

An additional anode layer is added when studying PLED's and solar cells. This poly(dioxythiophene) (PEDOT) layer[26] has a three-fold function, namely: smoothing of the electrode surface, balancing of the charge

injection between cathode and anode, and preventing oxygen migration from the ITO. This PEDOT layer is applied via a spincoating step out of a water/iso-propanol based solution.

The next step is the spincasting of the MDMO-PPV layer. A 'Karlsuss RC8' spincoater equipped with a patented 'gyrset' cover is incorporated inside the glove-box. A detailed description of this spincoating step will be described in section 2.5.2. As already mentioned, the sulfinyl procedure allows a conversion from non-conjugated precursor polymer to MDMO-PPV in solution or in film. In the latter case, the precursor polymer is spincoated instead of MDMO-PPV and a conversion is performed via the high vacuum oven.

Finally when studying PLED's or solar cells, a metal cathode layer needs to be applied. This is performed via metal evaporation under vacuum ($<10^{-6}$ mbar). A house-build shutter combined with an oscillating crystal (Leybold XTC2) to measure the thickness allows a well-controlled deposited layer thickness (ranging between 0.5 to 200 nm) and evaporation speed (ranging 0.05 nm s^{-1} to 1 nm s^{-1}). As MDMO-PPV is a rather soft semiconductor material, a slow evaporation speed prevents metal atoms to penetrate the conjugated polymer layer. These metal particles can act as quenching sites.

A photographic representation of the pilot line at the IMO and a more detailed overview of the major process equipment are depicted in figure 2.11.
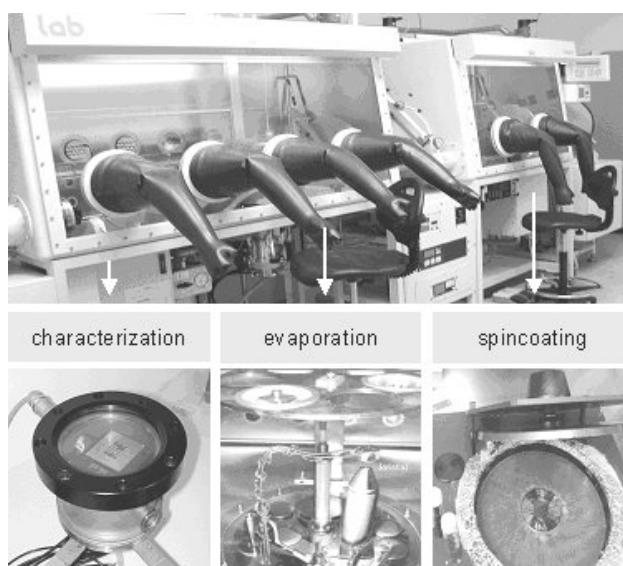
figure 2.11 Photographic representation of the pilot line at the 'Institute voor Materiaal Onderzoek' and a schematic overview of the major process steps

Beside the equipment to execute the different process steps, an electro optical characterization chamber is incorporated. This chamber has all necessarily connections to perform basic electrical measurements. Beside the electrical characterization tools, a simple spectrophotometer (Avantis AVS SD 2000, 200-1100 nm) and solar light simulator (Oriel 40-200 Watts) are present to measure optical performance and photovoltaic responses.

2.5.2   Spincasting of MDMO-PPV

An initial physicochemical characterization including determination of the molecular weight quantities and viscosity properties is presented in this section. Indeed, as typical polymer electronic devices desire a high quality thin film, a good knowledge on the viscosity properties of the batches is required to optimize the spincoating parameters. Besides an overview of the molecular weight properties the parameters and procedures to produce thin films via spincoating are presented.

2.5.2.1 Molecular weight properties

An overview of the molecular weight determination by size exclusion chromatography (SEC) against polystyrene standard for the different batches of MDMO-PPV is given in table 2.2. The properties listed are the number-average molar mass (M_n), the weight-average molar mass (M_w), the polydispersity or heterogeneity index (D) and an average number of monomer units based on M_n ($\overline{n}$).

Code	M_n (10^3 g mol^{-1})	M_w (10^3 g mol^{-1})	D (M_w/M_n)	$\overline{n}$ (units)
A-SUL	189	820	4.3	656
B-SUL	152	615	4.0	528
C-SUL	120	504	4.2	417
N-GIL	207	1386	6.7	719
R-SUL	135	554	4.1	469

table 2.2 Molecular weights as determined by SEC for the different MDMO-PPV batches

The sulfinyl material with an increased degree of regioregularity (R-SUL) has limited solubility properties making the study of this material more difficult. Therefore the determination of the molecular weight is executed on the precursor polymer and recalculated to the conjugated form.

In general the molecular weights (especially the value for M_w) of the sulfinyl materials are somewhat lower than the Gilch polymerized one. Although they can all be considered as rather high molecular with an average number of monomer units between 400 and 1000. This difference

has important consequences concerning viscosity properties. Indeed, the viscosity properties are mainly determined by the high molecular weight fraction of the polymer, yielding for the Gilch material a higher viscosity and lower gel-point induced by longer polymer chains and a broader distribution of chain lengths (making the presence of very high molecular weight chains more frequent).

An important condition for a successful spincoating is a gel-point of the polymer/solvent system at a sufficient low temperature (below room temperature for the spincoat equipment used within the scope of this thesis). Therefore a limited viscosimetric study was performed on sample B-SUL as a reference for the sulfinyl synthesized materials and N-GIL as a reference for the Gilch synthesized materials on a number of commonly used spincasting solvents.

In table 2.3 the temperature at which gelation occurs (observed as a significant increase in viscosity by a rotation-viscosimeter) during a cool-down cycle of a heated solution of 0.5 (w/v)% of MDMO-PPV (e.g. B-SUL and N-GIL) in different solvents is given.

Solvent	Gel-point B-SUL (°C)	Gel-point N-GIL (°C)
Toluene	27	12
50/50 Toluene/chlorobenzene	3	< -10
Chlorobenzene	-7	< -10

table 2.3 Gel-point of the Gilch and sulfinyl synthesized MDMO-PPV in various solvents

As expected on the difference in molecular weight, the tendency to form aggregates and a physical network is easier for the sulfinyl material. As the values for molecular weight and the distribution of the molecular weight for the other sulfinyl batches (A-SUL and C-SUL) are to some extend similar to the studied sulfinyl batch (B-SUL), results in the same order of magnitude are expected for the other sulfinyl batches.

A decreased gel-point is observed for the MDMO-PPV solved in chlorobenzene compared to toluene. It is clear that casting processes for the sulfinyl batches solved in toluene at room temperature yield a limited film quality and reproducibility. Therefore, within the scope of this thesis chlorobenzene as a solvent is used to obtain either sulfinyl or Gilch synthesized MDMO-PPV films via spincoating.

## 2.5.2.2 Spincasting parameters and conditions

The typical preparation technique to obtain high quality thin film from polymers or high molecular weight molecules is spincoating. Thereby, a

rotating plate with a substrate is covered with an amount of solved polymer. A combination of adhesion forces and centrifugal forces combined with the evaporation of the solvent allows the formation of a thin homogenous film. The film thickness[27] is determined by the rotation speed (ω), rotation time (t), density (ϱ), concentration (c) and viscosity (η) of the solution as expressed in equation 2.1.

$$\text{thickness} \sim \cfrac{c}{\sqrt{\cfrac{3\,\rho\,t\,\omega^2}{4\eta}}}$$

equation 2.1 The thickness of dependency the a thin film obtained via spincoating expressed as function of the speed (ω), rotation time (t), density (ρ), concentration (c) and viscosity (η)

As an example, the observed relation between the thickness of polymer films obtained via spincoating of Gilch synthesized MDMO-PPV solved in different solvents and the parameters (e.g. rotation speed and time) is depicted in figure 2.12.
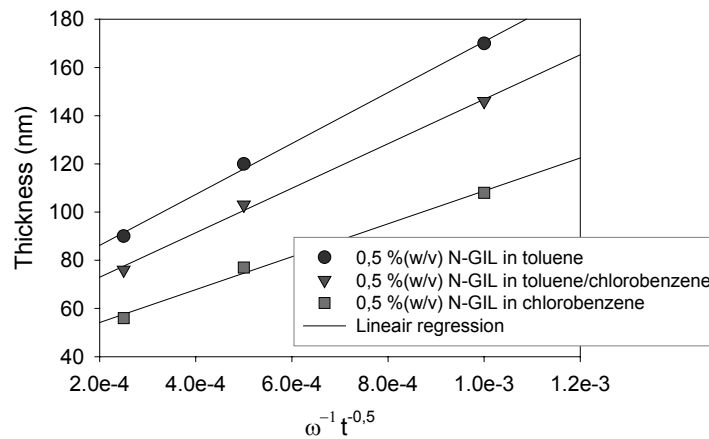
figure 2.12 Spin curve showing the relation between the thickness of a polymer film and the spincoat parameters such as rotation speed (ω) and time (t)

As shown, the observed relation between the thickness of the film and the spincoat parameters; namely: 1000 rpm/ 16 s, 1000 rpm/ 4 s, 500 rpm/ 4 s; is in accordance with equation 2.1. The decreased viscosity of the MDMO-PPV solution when working with chlorobenzene as a solvent is also expressed as a decrease in film thickness.

A thickness measurement of the polymer film is performed by making a thin scratch at the relatively soft film until the substrate is reached and a

measurement with a profilo-meter ('Sloan Dektak 3ST') perpendicular to that scratch.

Within the scope of this thesis, an empirical spincoat program is optimized to form homogenous thin films in a reproducible way. The spincoater used in this work is a 'Karlsuss RC 8' type, equipped with a patented 'gyrset' cover. By closing this cover, a solvent saturated atmosphere occurs above the substrate covered with polymer solution. Preventing solvent evaporation can be used to distinguish between the three typical steps occurring at a spincoat program, namely the addition of the polymer solution, the thickness spinning and the evaporation of the solvent. The optimized spincoat program for MDMO-PPV polymers solved in chlorobenzene is schematically depicted in figure 2.13.

Step 1 addition
cover: open
speed: 200 rpm
acceleration : 500 rpm s^{-1}
time: 4 s

Step 2 thickness
cover: closed
speed: cf. table 2.4
acceleration : 500 rpm s^{-1}
time: 4 s

Step 3 evaporation
cover: open
speed: 400 rpm
acceleration : 300 rpm s^{-1}
time: 100 s
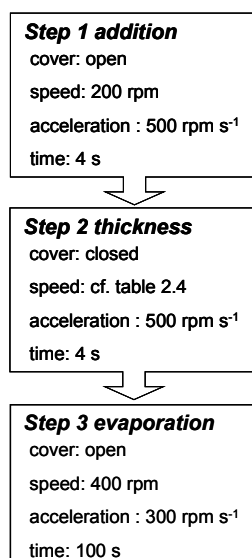
figure 2.13 Schematic representation of the optimized three-steps spincoat program

During the first step, at relatively low speed, the hot solution (50 °C) is added on the substrate. In order to prevent premature evaporation of the solvent, the duration of this step is kept as short as possible (e.g. 4 s). During the second step, at relatively high speed, the thickness of the final polymer film is determined. As the evaporation of the solvent is limited by the use of the closed 'gyrset' cover, the influence of evaporation on the film thickness is excluded.

Finally, during the last step, at low speed and with the cover in an open position, the evaporation of the solvent is performed. As the speed in this step is much lower than during the previous step, this step has no contribution to the final thickness of the polymer film.

An overview of the rotation speed needed to obtain a 100 nm thick film for the different MDMO-PPV batches as described in table 2.1 is given in table 2.4. Thereby 0.8%(v/w) solutions of MDMO-PPV in chlorobenzene are prepared and stirred for 4 hours at a temperature of 50 °C. The R-SUL material is kept at a somewhat higher temperature 70 °C to prevent premature gelation. Filtration of the solution is performed via 5 μm filters. Afterwards this filtered solution is stirred again for a couple of hours at elevated temperature (50 °C). These solutions are used to prepare thin films using the spincoat program represented in figure 2.13 and the values for the rotation speed in the thickness step represented in table 2.4.

Code	Rotation speed (rpm)
A-SUL	1290
B-SUL	1200
C-SUL	810
N-GIL	2940
R-SUL	1300

table 2.4 Rotation speed during the thickness spinning to obtain a 100 nm thick MDMO-PPV film via the spincoat program represented in figure 2.12

A clear relation between the molecular weight and the rotation speed needed to obtain a 100 nm thick film for the different MDMO-PPV batches can be observed. Indeed, a higher molecular weight yields an increased viscosity. As such an increased rotation speed is needed to obtain a 100 nm thick MDMO-PPV film. Thereby, the R-SUL material with a higher degree of regioregularity is behaving somewhat different caused by a stronger aggregation.

2.5.3   Conversion in solution or film

As already stated in section 2.2 the sulfinyl procedure allows the formation of the conjugated polymer, MDMO-PPV either in the film via spincoating of a precursor polymer followed by a thermal conversion step of this film or in solution. A more extensive overview of the synthetic reactions occurring during this step can be found in the work of Kesters et al[28].
Nevertheless the influence of the conversion step on the device preparation is preliminary examined as an introduction to this work. The evaluation criterion used is the peak-to-peak height difference (R_{PP}) of the converted MDMO-PPV film spincoated on a naked glass substrate. This value can be determined easily and accurately via atomic force microscopy (AFM).

Indeed an extremely rough film will lead to all kinds of leak paths decreasing the device performance.

Three MDMO-PPV films, exhibiting a different origin with respect to the conversion step are evaluated. Firstly, a film of B-SUL MDMO-PPV converted in solution and afterwards spincoated using the parameters in section 2.5.2 is considered as a reference sample. Secondly a MDMO-PPV film prepared via spincoating of a solution of the butyl-precursor polymer (as depicted in figure 2.3 product 3) and afterwards thermally converted according to the program described in figure 2.14 is studied. Thirdly, a MDMO-PPV film prepared via spincasting of the octyl-precursor polymer and a similar thermal conversion in film towards MDMO-PPV is examined. The latter is a derivative of the regular butyl-precursor polymer (the butylsulfinyl group is replaced by an octylsulfinyl group). As such the use of different leaving groups can be used to tune the solubility of the precursor polymer. However this leaving group has approximately double molecular weight compared to the standard material. Therefore large influences on the film properties are expected. An overview of the different examined polymer films is depicted in table 2.5.

Spincast material	Conversion in film	Molecular weight of leaving group compared to precursor monomer (%)	Film
MDMO-PPV (B-SUL)	none	/	MDMO-PPV
Butylsulfinyl precursor polymer	present	27	MDMO-PPV
Octylsulfinyl precursor polymer	present	36	MDMO-PPV

table 2.5 Overview of the three different MDMO-PPV films studied with AFM to quantify the influence of the conversion step in film

The conversion step in film is equal for all samples. In a high vacuum oven (<10^{-5} mbar) the samples are heated up till 150 °C and kept at this temperature for 120 minutes. As this oven is incorporated in the glove-box, no oxygen contamination of the samples can occur. The conversion program used is schematically depicted in figure 2.14.
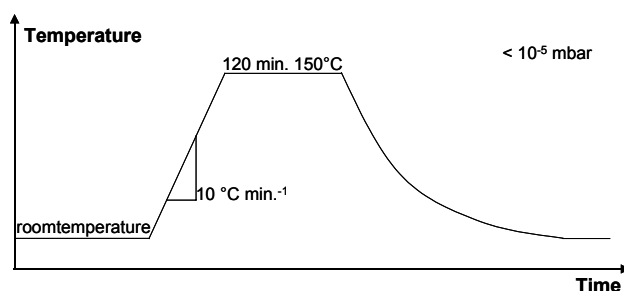
figure 2.14 Overview of the thermal conversion step applied on the precursor films

The prepared MDMO-PPV films are examined using an AFM (M5, Park Scientific Instruments/Thermomicroscopes) in noncontact mode. The cantilever used within this work is an ultra lever type 20B with stiffness of 3.2 N m^{-1} and resonance frequency of 90 kHz. A representative AFM picture (10 by 10 μm) clearly illustrating the obtained result is given in figure 2.15 for the reference MDMO-PPV material, in figure 2.16 for the MDMO-PPV film converted from the butylsulfinyl precursor film and in figure 2.17 for the MDMO-PPV film converted from the octylsulfinyl precursor film.
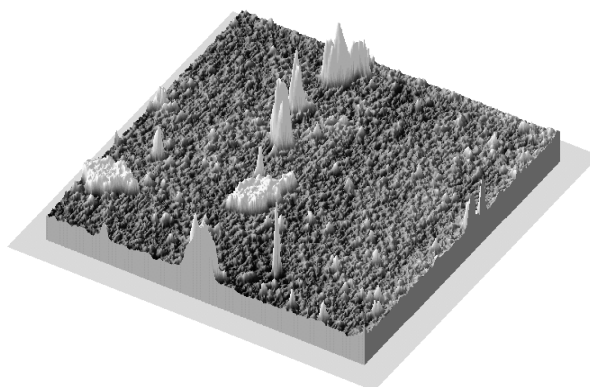
figure 2.15 AFM picture (100 μm^2) of a MDMO-PPV film with no conversion in film (e.g. conversion in solution, reference material)

As shown in figure 2.15, a rather smooth surface is obtained. The high peaks are interpreted as dust particles. The nature of these particles is not completely sure, however most likely they are induced via sample preparation and transportation from to glove-box to the AFM equipment. The average peak-to-peak height difference, ignoring the dust particles is 0.5 nm.
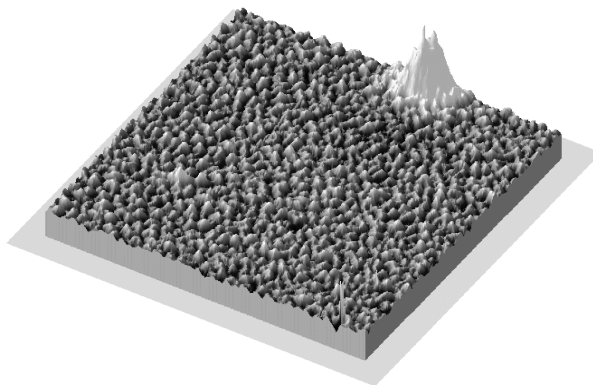
figure 2.16 AFM picture (100 μm^2) of a MDMO-PPV film prepared via thermal conversion of a butylsulfinyl precursor film

The AFM picture of the film prepared via thermal conversion of the butylsulfinyl precursor film (figure 2.16) shows clearly a much higher roughness. Typical peak-to-peak height differences ignoring the dust particle range 15 nm. The total film thickness is decreased from 100 nm to 70 nm. Note that no quantitative information about the degree of conversion and the amount of side products formed during conversion actually leaving the film is obtained.

figure 2.17 AFM picture (100 μm^2) of a MDMO-PPV film prepared via thermal conversion of an octylsulfinyl precursor film

A somewhat different picture (figure 2.17) is obtained for the MDMO-PPV film thermally converted from the octylsulfinyl precursor film. Typi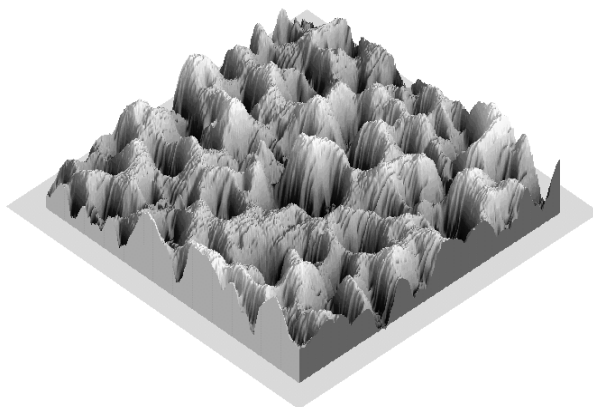cal height differences range 25 nm. Beside this increase in height difference, also the size of the regions with low and high height is increased. The reason for these observations is unclear. A hypothesis is that due to the relative high molecular weight of the leaving products in this particular case, a sort of phase separation can occur during conversion. In this case,

evaporation of the leaving products should end in a picture similar to this observations.

The total film thickness is decreased from 100 nm to 70 nm. The roughness of the precursor film is in the same order as the picture given in figure 2.15.

It can be concluded that the applied thermal conversion program for the butylsulfinyl and the octylsulfinyl precursor polymer is introducing a higher film roughness. Most likely this is caused via evaporation of the side products that originate during the conversion step. The worst film quality is obtained for the MDMO-PPV films originating from the octylsulfinyl precursor polymer films. Diode preparation based on these films indicated a limited decrease in rectification factor for the MDMO-PPV samples based on butyl- and octylsulfinyl precursor polymer films.

As the scope of this thesis is to compare different batches of MDMO-PPV with various defect levels and regioregularity ratios, it is useful to prepare all MDMO-PPV film via a conversion in solution (comparable to the reference sample). The conversion in film seems to be influencing the morphology of the film, yielding additional variables complicating the obtained results. Additionally, no comparable NMR spectroscopy experiments were performed to evaluate the completeness of the conversion and thus the number of sp^3 defects.

However from this result it is not excluded that a dedicated thermal conversion program can give smooth films. However this optimization is beyond the scope of this thesis. Therefore all studied samples in chapter 3, 4 and 5 are prepared via MDMO-PPV already converted in solution.

2.6   References

[1]   U. Mitschke, P. Bäuerle, *J. Mater. Chem.* (**2000**) 10, 1471.

[2]   R.H. Friend, R.W. Gymer, A.B. Holmes, J.H. Burroughes, R.N. Marks, C. Taliani, D.D.C. Bradley, D.A. Dos Santos, J.L. Brédas, M. Lögdlund, W.R. Salaneck, *Nature* (**1999**) 137, 121. A. Kraft, A.C. Grimsdale, A.B. Holmes, *Angew. Chem. Int. Ed.* **(1998)** 37, 402.

[3]   a) M. Herold, J. Gmeiner, C. Drummer, M. Schwoerer, *J. Mater. Sc.* (**1997**) 32, 5709. b) W. Brutting, M. Meier, M. Herold, S. Karg, M. Schwoerer, *Synth. Met.* (**1997**) 163.

[4]   J.H. Burroughes, D.D.C. Bradley, A.R. Brown, R.N. Marks, K. Mackay, R.H. Friend, P.L. Burn, A.B. Holmes, *Nature* (**1990**) 347, 539.

[5]   S. Doi, M. Kuwabara, T. Noguchi, T. Ohnishi, *Synth. Met.* (**1993**) 57, 4174.

[6]   a) D. Braun, A.J. Heeger, *Appl. Phys. Lett.* (**1991**) 58, 1982. b) D. Braun, A.J. Heeger, H. Kroemer, *J. Electron. Mater.* (**1991**) 20, 945.

[7]   a) G. Gustafsson, Y. Cao, G.M. Treacy, F. Klavetter, N. Colaneri, A.J. Heeger, *Nature* (**1992**) 357, 477. b) G.J. Sarnecki, P.L. Burn, A. Kraft, R.H. Friend, A.B. Holmes, *Synth. Met.* (**1993**) 55, 914. c) F. Wudl, P.M. Allemand, G. Srdanov, Z. Ni, D. McBranch, *ACS Symp. Ser.* (**1991**) 455. d) D. Braun, E.G.J. Staring, R.C.J.E. Demandt, G.L.J. Rikken, Y.A.R.R. Kessener, A.H.J. Venhuizen, *Synth. Met.* (**1994**) 66, 75.

[8]   I.D. Parker, *J. Appl. Phys.* (**1994**) 75, 1656.

[9]   G. Yu, *Synth. Met.* (**1996**) 80, 143.

[10]   a) J. Salbeck, *Ber. Bunsenges. Phys. Chem.* (**1996**) 100, 1666. b) H. Spreitzer, H. Becker, E. Kluge, W. Kreuder, H. Schenk, R. Demandt, H. Schoo, *Adv. Mater.* (**1998**) 10, 1340. c) G.H. Gelinck, J.M. Warman, E.G.J. Staring, *J. Phys. Chem.* (**1996**) 100, 5485.

[11]   N.S. Saraciftci, D. Braun, C. Zhang, V.I. Srdanov, A. Heeger, G. Stucky, F. Wudl, *Appl. Phys. Lett.* (**1993**) 62, 585.

[12]   S.E. Shaheen, C.J. Branec, N.S. Sariciftci, F. Padinger, T. Fromherz, J.C. Hummelen, *Appl. Phys. Lett.* (**2001**) 78, 841.

[13]   H.G. Gilch, W.L. Wheelwright, *J. Pol. Sci., Part A: Polym. Chem.* (**1966**) 4, 1337.

[14]   a) F. Louwet, D. Vanderzande, J. Gelan, *Synth. Met.* (**1992**) 52, 125. b) F. Louwet, D. Vanderzande, J. Gelan, J. Mullens, *Macromolecules* (**1995**) 28, 1330. c) F. Louwet, D. Vanderzande, J. Gelan, *Synth. Met.* (**1995**) 69, 509.

[15]   W.J. Swatos, B. Gordon, *Polym. Prepr.* (**1990**) 31(1), 505.

[16]   Covion Organic Semiconductors GmbH, Frankfurt, Germany. info@covion.com or www.covion.com

[17]   a) H. Becker, H. Spreitzer, *Adv. Mater.* (**2000**) 1430. b) I.D. Parker, *J. Appl. Phys.* (**1999**) 85, 2441.

[18] a) H. Schoo, R. Demandt, Philips J. Res. (**1998**) 51, 527. b) C. Yin, C. Yang, *Synth. Met.* (**2001**) 118, 75.

[19] H. Becker, H. Spreitzer, K. Ibrom, W. Kreuder, *Macromolecules* (**1999**) 32, 4925.

[20] F. Louwet, *Ph.D Dissertation* (**1993**) Limburgs Universitair Centrum.

[21] L. Hontis, *Ph.D Dissertation* (**2002**) Limburgs Universitair Centrum.

[22] a) M. van der Borght, J.M.J.V. Gelan, D.J.M. Vanderzande, *Synth. Met.* (**1997**) 84, 399. b) A. Issaris, D.J.M. Vanderzande, J.M.J.V. Gelan, *Polymer* (**1997**) 38, 2571.

[23] L.J. Lutsen, A.J. van Breemen, W. Kreuder, D.J.M. Vanderzande, J.M.J.V. Gelan, *Helvetica Chimica Acta* (**2000**) 83, 3113.

[24] L. Lutsen, P. Adriaensens, H. Becker, A.J. van Breemen, D. Vanderzande, J. Gelan, *Macromolecules* (**1999**) 32, 6517.

[25] A. van Breemen, *Ph.D Dissertation* (**1999**) Limburgs Universitair Centrum.

[26] H. Spreitzer, H. Becker, E. Kluge, W. Kreuder, H. Schenk, R. Demandt, H. Schoo, *Adv. Mater.* (**1998**) 10(16), 1340.

[27] a) A. Emslie, F. Bonner, L. Peck, *J. Appl. Phys.* (**1958**) 29, 858. b) D. Meyerhofer, *J. Appl. Phys.* (**1978**) 49, 3993.

[28] E. Kesters, *Ph.D Dissertation* (**2002**) Limburgs Universitair Centrum.

Chapter 3
Electrical
characterization

In chapter 3 the matrix of different materials with various defect levels and types (e.g. regioregularity and sp^3 interruptions) of the 'workhorse' conjugated polymer, MDMO-PPV is electrically characterized in field effect transistor (FET) devices. The major parameter derived from the obtained electrical characteristics is the FET-mobility. Besides a brief introduction about organic thin film transistors, a description of the models used within the scope of this work, the obtained results for the different MDMO-PPV batches and some conclusions are presented.

3.1   Field effect transistor

For more than a decade now, organic thin film transistors (TFT) based on organic molecules have been envisioned as a viable alternative to more traditional thin film transistors based on inorganic materials[1]. Especially the use of simple and cheap electronics in areas such as wireless radio frequency identification or switching devices for active matrix flat panel displays is an attractive potential application of conjugated polymers[2].

As in traditional inorganic semiconductors, organic materials can act either as p-type or n-type. However, most widely studied organic semiconductors such as MDMO-PPV are p-type.

A typical parameter limiting the performance of a field effect transistor (FET) is the mobility of the charge carriers. The highest reported values for p-type small organic molecules (e.g. pentacene[3]) at room temperature range 1-2 cm^2 V^{-1} s^{-1}. The highest mobility values for p-type conjugated polymers (e.g. poly(3-hexylthiophene[4]) range 0.1 cm^2 V^{-1} s^{-1}.

A typical path to performance increase of organic FET's (OFET's) is either the result of the application of new organic materials or an improvement of the deposition parameters. However in recent years, the individual performance-versus-time curves saturate. The evolution of the highest reported yearly mobility for conjugated polymers (mainly polythiophene and its alkyl substituted derivatives) presented in a semi-logarithmic plot is shown in figure 3.1[1,4,5]. A new value is only entered if it is higher than the preceding one.
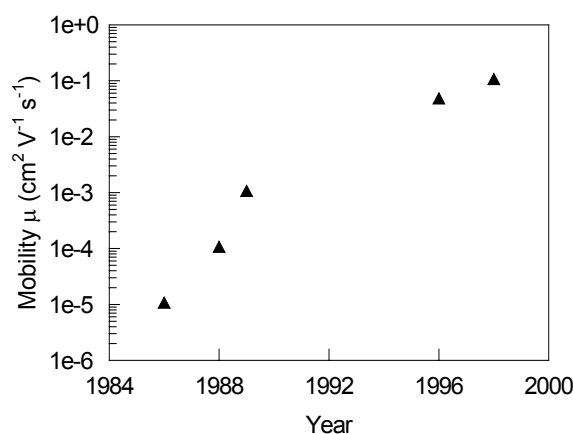

figure 3.1 Evolution of charge carrier hole mobility's for conjugated polymers[1,4,5]

Contrarily to inorganic semiconductors exhibiting band transport, disordered organic semiconductors show a carrier transport limited by a hopping mechanism between localized states. The reason for this fundamental difference is the weak intermolecular forces in organic semiconductors (e.g. van der Waals interactions) with energies smaller than 10 kcal mol^{-1} reaching a magnitude close to that of the vibrational energy of the molecules at room temperature. Materials having mobilities between 0.1 and 1 cm^2 V^{-1} s^{-1} define the boundary between band transport and hopping[6]. Although highly ordered organic semiconductors based on small molecules such as pentacene or antracene have room temperature mobilities in this intermediate range, this boundary can be seen as an upper limit for the macroscopic mobilities of conjugated polymers.

Two possible ways of eliminating this limit are on one hand increasing the intermolecular interactions without breaking of the conjugation and on the other hand replacing the intermolecular conduction by a intramolecular conduction by a reduction of the channel size[1]. The first approach would result in stiffer crystalline structures making small organic molecules more appropriate, thereby introducing a loss in processing. The second way would require a drastic change in FET design by the introduction of nano-size channels that are transcended by single molecules. Although these

strategies are extremely interesting from a fundamental point of view, executing them in a commercial process will not be present in the near future.

However one can argue that for the mentioned applications a mobility of 1 $cm^2 \, V^{-1} \, s^{-1}$ or even less, comparable to the mobility of amorphous silicon would be far more sufficient. Considering arguments with respect to an easy and cheap processing, research and development of polymeric FET's is an extremely attractive subject for fundamental and applied sciences.

A more detailed overview about organic TFT's can be found in several excellent papers and books[7].

Besides the development of high performance transistors based on either small organic molecules or conjugated polymers, FET devices are an excellent tool to determine the electrical behavior of organic semiconductors.

Within the scope of this work, MDMO-PPV is applied as an active layer in FET devices to compare values for the mobility with the presence of defects in the conjugated polymer as defined in table 2.1 for our matrix of materials.

Besides an introduction concerning mobility values of semi-conducting layers in FET devices presented in section 3.1, section 3.2 will handle the preparation, processing and configuration of the devices used in this work. Section 3.3 will describe the modeling of the electrical characteristics of the transistors. The results obtained for the different MDMO-PPV batches will be discussed in section 3.4. Chapter 3 concerning the electrical characterization will be ended with an interpretation of the results and a conclusion defined in section 3.5.

3.2   FET- configuration and preparation

Although one of the ultimate goals in this research area is the development of all-polymer electronic devices (including insulator layers, good conductive (inter-) connection layers and semiconductor layers) within the scope of this thesis TFT devices are used to study the electrical properties of the different MDMO-PPV batches. As such all-polymer test substrates can complicate a direct correlation between the observed electrical characteristics and the properties of the semi-conducting MDMO-PPV layer. Therefore in this work silicon test substrates with only one organic layer, namely the semiconductor conjugated polymer layer are used. This approach introduces an increased reproducibility and allows an improved interpretation of the results. The inorganic test substrates used for this work are mainly produced at Philips (Eindhoven, the Netherlands). The TFT's used in this investigation are actually Metal Oxide Semiconductor Field Effect Transistors (MOSFET's). A schematic representation of a vertical cross-section of such a structure is depicted in figure 3.2.
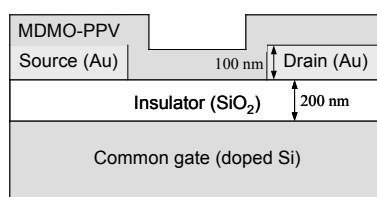
figure 3.2 Schematic representation of a vertical cross-section of a silicon test substrate as used in this work

In figure 3.2, a so-called bottom-gate architecture is represented, with from bottom to top: a heavily p-type silicon gate (common for each individual transistor), a high quality silicon oxide (typically 200 nm), 100 nm thick gold source and drain electrodes and the organic semiconductor layer, MDMO-PPV with a typical thickness ranging 50 – 80 nm. A Scanning Electron Micrograph (SEM) of a vertical cross-section of an embedded substrate is shown in figure 3.3.
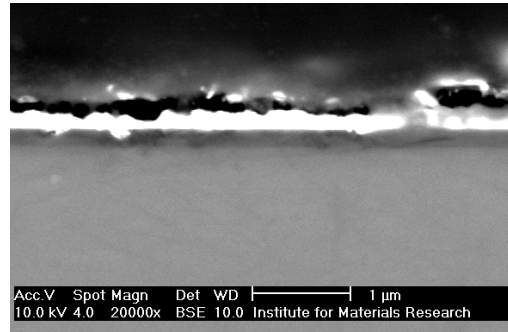
figure 3.3 Scanning Electron Micrograph (SEM) of a vertical cross-section of the silicon substrate

As shown, a clear distinction can be made between the doped common gate and the insulating oxide layer. The capacitance per unit area of this insulating layer (C_i) has a value ra nging 17 10^{-9} F cm^{-2}.

The design of both electrodes (e.g. source and drain) is a so-called interdigitated finger structure. The drain electrode is in this case completely enclosed by the source electrode. An important advantage of this set-up is the possibility to have a conductive channel between source and drain with a high channel width (W) combined with relatively small channel length (L), increasing the measurement sensitivity. Besides this increase in sensitivity, a high W/L ratio (> 10)[1] eliminates an overestimating of the mobility induced by fringe currents outside the conductive channel between source and drain.

A SEM picture of the top-view of such an electrode design is given in figure 3.4.
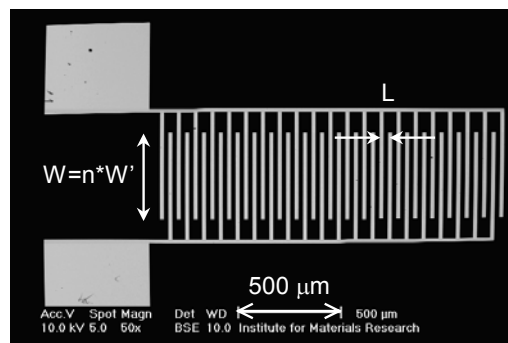

figure 3.4 Scanning Electron Micrograph (SEM) of a top-view of the source and drain electrodes of the FET's used

Contact between the measurement probes and the contact paths for the source and the drain, can be performed under a dedicated microscope (figure 3.5 A and B). As shown in figure 3.5 C, a number of individual

transistors with different channel widths and lengths, each with the common gate connected via silver past to the third measurement probe (figure 3.5B), are located on one substrate.
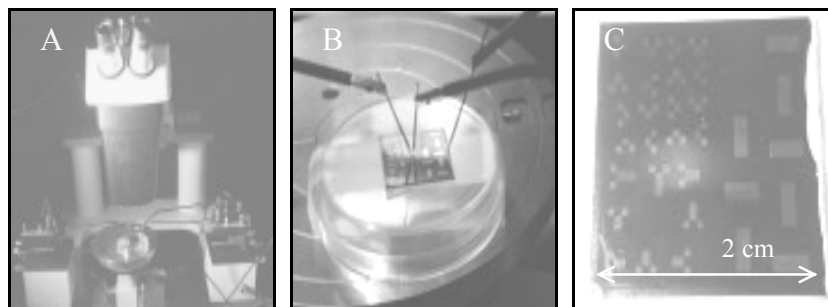
figure 3.5 A) Dedicated microscope and measurement probes B) Close-up on the measurement probes connected to the source, drain of one particular transistor and to the common gate C) Overview of the different transistors located on one substrate

The semi-conducting MDMO-PPV layer is deposit on the silicon test substrates via spincoating. Device preparation in the glove-box prevents oxygen deterioration of the conjugated polymer.

Prior to deposition, the silicon test substrates are ultra-sonically cleaned in isopropanol (pa) for 15 minutes. The 0.8 %(w/v) MDMO-PPV solutions in chlorobenzene prepared for the different batches of polymer as described in table 2.1, are stirred for 4 hours at 50 °C and deposited under a nitrogen atmosphere, using spincoat parameters comparable to the description in section 2.5.2. For each material of the MDMO-PPV matrix, individual transistors with a total channel width (W) of 10 mm and a channel length (L) of 2; 2.5; 3; 5; 7.5; 10 and 15 µm are tested.

The measurement equipment consists at two Keithley 2400 sourcemeters to control the potential difference applied between source and drain and the difference applied between source and gate. The first sourcemeter is also used to measure the drain current. Both apparatus are controlled via a homemade Labview based program.

3.3   Modeling of the electrical characteristics of organic FET's

The majority charge carriers in most organic FET's are holes. Also MDMO-PPV exhibits a p-type electrical behavior. The observed current (I) versus voltage (V) characteristics can be adequately described by models developed for inorganic semiconductors[6a,8]. Experiments have indicated a dependency of the FET-mobility on the temperature and on the applied gate-voltage[7d]. This can be understood either by a multiple trapping and release-model[9] or by a hopping transport in the tail of a density-of-states[10]. In the multiple trapping and release model the assumption is made that most of the charge carriers are trapped in localized states. The amount of released charge carries to an extended state transport level depends in this case, besides on the energy level of the localized states on the temperature and gate-bias. However this extended-state transport may occur in highly ordered films with a strong interaction between individual molecules, it is not expected to play a major role in amorphous polymer films such as MDMO-PPV.

Therefore in section 3.3.1 the classical formulas, modeling the electrical behavior of FET's and the data acquisition will be discussed. An overview of the extended model explaining the temperature and gate-bias dependency, based on a hopping transport will be the subject of section 3.3.2. Finally, the influence of a contact resistance on the derived FET-mobility is presented in section 3.3.3.

3.3.1   Classical FET-formulas and data acquisition

Field effect mobilities (μ_{FET}) can be estimated by measuring the current between source and drain (I_d) at various applied potential differences between either source and drain (drain-voltage V_d) and between source and gate (gate-voltage V_g). An ideal current-voltage characteristic for classic silicon based MOSFET's is depicted in figure 3.6.
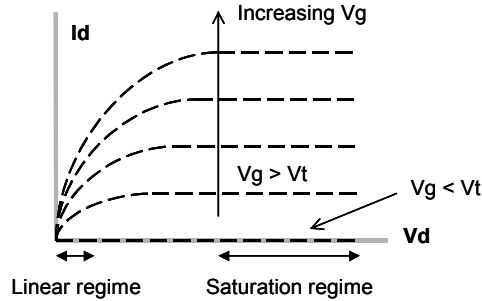
figure 3.6 Ideal current-voltage characteristic of a long channel MOSFET

A theoretical description[11] of a MOSFET transistor yields two regimes with a fairly simple expression for I_d as function of V_g, V_d and a threshold-voltage (V_t). A mathematical formula describing partly the current-voltage characteristic under these specific conditions is indicated for the so-called linear regime by equation 3.1 and for the so-called saturation regime by equation 3.2.

$$I_d = \frac{\mu_{FET} \, W \, C_i}{L} \left(V_g - V_t\right) V_d$$

equation 3.1 Expression for a MOSFET transistor current-voltage characteristic in the linear regime

In this linear regime valid for low values of V_d ($V_d \ll (V_g - V_t)$) the channel appears as an essentially linear resistor dependent on V_g.

$$I_d = \frac{\mu_{FET} \, W \, C_i}{2L} \left(V_g - V_t\right)^2$$

equation 3.2 Expression for a MOSFET transistor current-voltage characteristic in the saturation regime

The saturation regime valid for values of $V_d \cong (V_g - V_t)$ yields an essentially constant I_d for large values of V_d. This can be understood for classical MOSFET structure as a pinch–off of the channel at the drain end.

An increase of the measurement sensitivity by a large ratio of W/L, as mentioned before, is shown in equation 3.1 and equation 3.2.

The threshold-voltage can be understood for classical MOSFET devices, as the potential required turning the transistor on or off. For an ideal structure this voltage is equal to the potential required to obtain flat band conditions, then accommodate the charge in the depletion layer and finally induce an inverted region[11a].

However some important remarks can be made by applying these fairly simple models on organic FET's (OFET's). First of all OFET's operate in the

accumulation regime. In such geometry, there is no depletion layer to isolate the conducting channel from the substrate. This absence yields in principle a threshold-voltage that should be nil[12]. A comprehensive model for OFET's described by Horowitz et al.[13] introduces instead of this threshold-voltage, a zero-voltage with inverse sign of the gate-voltage (i.e., positive for a p-type semiconductor) connected to the equilibrium free carrier density. However a threshold-voltage with the same sign as the gate-voltage is often observed. This feature is attributed to a gate-voltage-dependent mobility, tentatively ascribed to the transport mechanism.

Within the scope of this thesis, a comparison of the mobility values of the matrix of MDMO-PPV batches is required. Therefore the FET-mobility is calculated from the linear regime from the transconductance (g_m), as described in equation 3.3.

$$g_m = \left(\frac{\partial I_d}{\partial V_g} \right)_{V_d \to 0} = \frac{\mu_{FET} \, W \, C_i \, V_d}{L}$$

equation 3.3 The transconductance can be used to calculate the FET-mobility in the linear regime

During a so-called gate-sweep, the drain-voltage is kept constant at –2 V and the gate-voltage is varied from +10 V to –10 V in steps of 0.1 V. Although in principle the mobility can be calculated on each point of the sweep, this is preferably done for high values of V_g (within this work at –9.7 V). The mobility of the spincoated MDMO-PPV films on the silicon test substrates (with a capacitance of the oxide ranging 17 10^{-9} F cm^{-2} and various values for W and L) is determined using equation 3.4.

$$\mu_{FET} = \frac{L}{W \, C_i \, V_d} \left(\frac{\partial I_d}{\partial V_g} \right)_{V_g = -9,7V; \, V_d = -2V}$$

equation 3.4 Determination of the FET-mobility from a so-called gate-sweep for an OFET

Besides the use of this gate-sweep to determine the mobility, another typical characterization is performed by applying a drain-sweep yielding information about the conductivity. Thereby, the gate-voltage is kept constant at 0 V and the drain-voltage is varied from –10 V to +10 V in steps of 1 V. A typical value for the conductivity (σ) (usually expressed in S m^{-1}) is determined at high values for V_d (within this work at –10 V) according to equation 3.5 corresponding to Ohm's and Pouillet's law.

$$\sigma = \frac{L}{W\,t}\left(\frac{\partial I_d}{\partial V_d}\right)_{V_g = 0V; V_d = -10V}$$

equation 3.5 Determination of the conductivity from a so-called drain-sweep for an OFET

The geometry of the electrodes (e.g. W and L) and the thickness (t) of the MDMO-PPV film between both electrodes are incorporated in this formula.

3.3.2 Gate-voltage dependency of the mobility

In amorphous organic films such as the MDMO-PPV films used in this work, an electrical transport based on a hopping mechanism is widely accepted. Matters and Vissenberg et al.[10] described theoretically the dependence of the mobility on the gate-voltage and the temperature by a model based on the variable-range hopping (VRH) of charge carriers in an exponential density of states. Within the concept of VRH, a carrier may either hop over a long distance with a low activation energy or hop over a short distance with high activation energy. Within the scope of this thesis, a short summary concerning this model is presented.

In an OFET, the applied gate-voltage leads to the accumulation of charge in the region close to the insulating oxide layer. The accumulated charge carriers fill the lower lying states of the organic semiconductor. Additional charges will occupy states at relatively high energies. Thus, they will require less activation energy to hop away to a neighboring site, resulting in a higher mobility with an increased V_g.

A study of the influence of temperature (T) and filling of states (δ) on the conductivity (σ) in a VRH system with an exponential distribution of localized-state energies ($g(\varepsilon)$ with a width T_0) under condition of low carrier densities and low T, yields equation 3.6[10b].

$$\sigma(\delta,T) = \sigma_0\left(\frac{\pi N_t\,\delta(T_0/T)^3}{(2\alpha)^3 B_c \Gamma(1-T/T_0)\Gamma(1+T/T_0)}\right)^{T_0/T}$$

equation 3.6 Influence of temperature and carrier occupation on the conductivity

Within this equation, N_t expresses the number of states per unit volume; σ_0 is a pre-factor; α^{-1} is an effective overlap parameter, which governs the tunneling process between two localized states; B_c is the critical number of bonds per site in the percolation network[14] and the gamma-function expresses $\Gamma(z) \equiv \int_0^\infty dy \exp(-y)y^{z-1}$.

However, in a transistor a certain potential perpendicular to the conduction channel is applied by a gate-voltage. This makes the charge density not

uniform but decreasing with distance x from the semiconductor-insulator interface. The occupation of carriers δ(x) depends on the distance x through the gate-induced potential V(x) as indicated by equation 3.7[10b].

$$\delta(x) = \delta_0 \exp\left(\frac{eV(x)}{k_B T_0}\right)$$

equation 3.7 The distance dependent carrier occupation

Within this equation, δ_0 is the carrier occupation far from the semiconductor-insulator interface, where V(x) equals zero. The variation of V(x) with the distance x is determined by the Poisson equation.

This distance dependent charge occupation, combined with temperature dependency as expressed in equation 3.6 allows, according to equation 3.8 the calculation of the source-drain-current, I_d in the linear regime[10b].

$$I_d = \frac{W V_d}{L} \int_0^t dx\, \sigma\big(\delta(x), T\big)$$

equation 3.8 Determination of the drain-current from the conductivity (dependent of temperature and the filling of states)

The mobility can be derived from I_d by using the formula for the transconductance (equation 3.3). Combination of equation 3.6, equation 3.7 and equation 3.8 yields an expression (equation 3.9) for the FET-mobility[10b] dependent on the gate-voltage and on the temperature. Thereby, the assumption is made that the thickness (t) of the semiconductor layer is sufficiently large that V(t) equals zero.

$$\mu = \frac{\sigma_0}{e}\left(\frac{\pi(T_0/T)^3}{(2\alpha)^3 B_c \Gamma(1-T/T_0)\Gamma(1+T/T_0)}\right)^{T_0/T} \times \left(\frac{(C_i)^2}{2k_B T_0 \varepsilon_s}\right)^{T_0/T-1} \times \left((V_g)^2\right)^{T_0/T-1}$$

equation 3.9 The temperature and gate-voltage dependency of the field effect mobility

Notice that a linear regression of a logarithmic plot of the mobility as function of the gate-voltage yields the width of the energy distribution (T_0). For more details of this model describing the gate-voltage and temperature dependency of the FET-mobility of organic semiconductors, a reference to the PhD dissertation of Vissenberg[15] is made.

3.3.3   Contact resistance

In literature, a number of FET configurations are investigated. Besides the already in section 3.2 described bottom-contact devices, top-contact devices

are used. Thereby, the gold source and drain electrodes are evaporated on top of the organic semiconductor layer spincoated on a substrate (consisting at a common silicon gate and a siliconoxide insulating layer). The observation that top-contact OFET's yield higher mobility values than bottom contact devices has been reported[16] and is attributed to an enhanced charge carrier injection from a top contact.

Within this work, a dependency of the mobility on the channel length is observed for bottom-contact devices, indicating indeed the presence of a contact resistance.

Beside differences between device architectures, observations of a dependency of the contact resistance on the solvent used to spincoat are reported for MEH-PPV LED's[17] and for MDMO-PPV OFET's[16b].

Although the nature of this contact resistance is not yet fully understood, within the scope of this thesis a simple model is presented to correct the mobility for this feature. Thereby, a constant contact resistance (R_{con}) is placed in series with the resistance of the conduction channel in the linear regime (R_{cha}) as earlier described by Jain et al[18].

When working under conditions of constant W, and variable L to determine the mobility in the linear regime (e.g. constant small V_d), an equivalent electric scheme as depicted in figure 3.7 is used. Within this work, the assumption is made that the channel resistance (R_{cha}) is linearly scaling with the channel length (L)via R'_{cha} the resistance per unit of length.

$$\boxed{R_{contact}\ (R_{con})} \quad \boxed{R_{channel}\ (R_{cha}) = L.\ R'_{cha}}$$
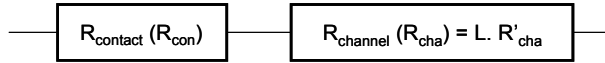
figure 3.7 Equivalent electric scheme for the conduction channel of a FET under conditions to determine the FET- mobility in the linear regime

The total resistance (R_{tot}) and potential difference between source and drain (V_{tot}) is given by equation 3.10 and equation 3.11.

$$R_{tot} = R_{con} + LR'_{cha}$$

equation 3.10 The total resistance is the sum of the contact resistance and the resistance of the conduction channel

$$V_{tot} = V_{con} + LV'_{cha}$$

equation 3.11 The potential difference between source and drain is the sum of the potential drop over the contact resistance and potential drop over the conduction channel

Within this equation, V'_{cha} is the potential drop in the conduction channel per unit of length and V_{con} is the potential drop over the contact resistance.

The in equation 3.4 notified V_d used to determine the mobility is actually V_{tot}. Combination of equation 3.4, equation 3.10 and equation 3.11 yields the dependency of the observed mobility (μ_{obs}) on the channel length (equation 3.12).

$$\mu_{obs} = \mu_{cor} \left(\frac{L}{L + R_{con}/R'_{cha}} \right)$$

equation 3.12 Dependency of the observed FET-mobility on the channel length

Within this equation, μ_{cor} is the contact resistance corrected value of the mobility. Notice that working with long channel lengths increases the accordance between μ_{obs} and μ_{cor}, but is decreasing the measurement sensitivity.
As depicted in equation 3.13, a similar trend can be derived for the channel length dependency of the observed conductivity.

$$\sigma_{obs} = \sigma_{cor} \left(\frac{L}{L + R_{con}/R'_{cha}} \right)$$

equation 3.13 Dependency of the observed conductivity on the channel length

In the next section, the proposed formulas and models will be used to compare the electrical properties of the matrix of MDMO-PPV materials.

3.4   Results and discussion

Within the scope of this thesis, a matrix of different MDMO-PPV batches with different types and amount of defects, as defined in table 2.1 is investigated as semiconductor layer in TFT's. The device architecture and preparation used is described in section 3.2. The current-voltage characteristics show a typical p-type transistor-like behavior for all examined devices. An example (e.g. R-SUL, L = 15 μm) of a set of I_d-V_d characteristics for different V_g values is shown in figure 3.8.
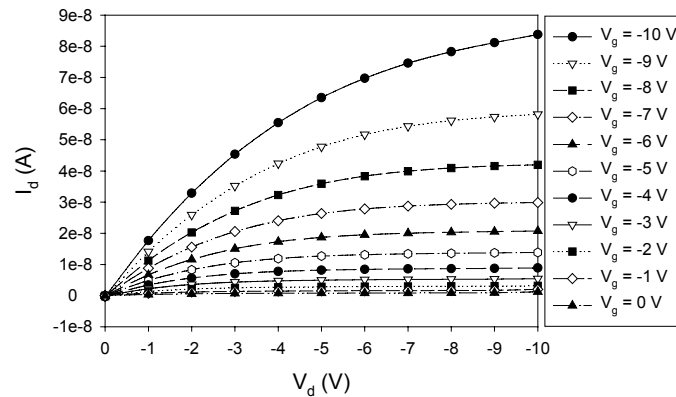

figure 3.8 Typical I_d-V_d characteristic for different V_g values for a p-type organic TFT's (e.g. R-SUL, W = 10000 μm, L = 15 μm)

Within this figure, a linear increase of I_d at low V_d is observed. I_d shows a tendency to saturate as V_d further increases. Application of a negative bias to the gate electrode (V_g) increases the number of charges in the accumulation layer, contributing to I_d. According to equation 3.4 and equation 3.5, the FET-mobility and conductivity can be determined out of these characteristics for the different devices with different channel lengths and different MDMO-PPV semiconductor layers. Beside a number of experiments performed at the IMO laboratories (Diepenbeek, Belgium) duplo-measurements are carried out at IMEC (Leuven, Belgium) and partly at Philips Natlab (Eindhoven, the Netherlands).

3.4.1   FET-Mobility results

The results of the calculation of the FET-mobility for one series of devices with different channel lengths and different MDMO-PPV semiconductor layers are summarized in figure 3.9.
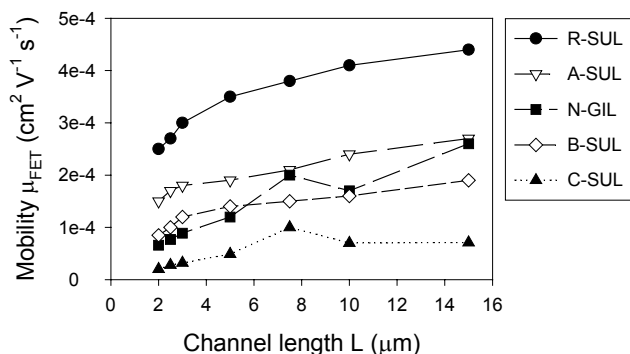
figure 3.9 FET-mobility of the charge carriers obtained via MDMO-PPV transistor measurements for different channel lengths

Within these results, a channel dependency as predicted by equation 3.12 is observed for all MDMO-PPV batches. The highest FET-mobility values approaching the contact resistance corrected mobility are observed at high channel lengths.

Although the reported values for the mobility are somewhat higher compared to earlier published values, they are in accordance with results obtained by W. Geens et al[16b]. Furthermore, a solvent induced influence[7] on the mobility should be taken into account as chlorobenzene is used as spincoat solvent instead of toluene.

The MDMO-PPV material with increased regioregularity (R-SUL) yields a considerable higher value for the mobility (e.g. $4.5 \ 10^{-4}$ cm^2 V^{-1} s^{-1}) than the MDMO-PPV batches with a random 50/50 ratio of both regioregularity forms (A-SUL, B-SUL, C-SUL and N-GIL).
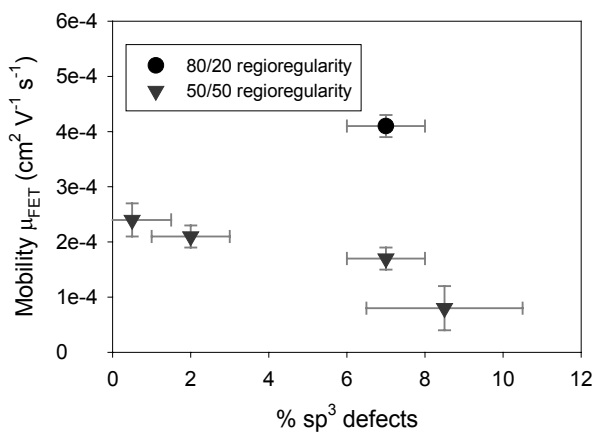

figure 3.10 Overview of the FET-mobility of the charge carriers determined via TFT's for the highest channel lengths, for the different MDMO-PPV batches

Within this group of regiorandom (50/50) MDMO-PPV materials, differences in mobility between the different batches are smaller and at the limit of reproducibility. However an important result is the decreasing mobility as function of the increasing number of single bond defects within the group of regiorandom MDMO-PPV materials as indicated in figure 3.10. The plotted mobility is an average value for all devices with a value for the channel length equal to 7.5 µm, 10 µm and 15 µm. The standard deviation of these measurements is taken as the vertical error bar.

To quantify the observed trend a first order fit is applied at the values for the A-SUL, N-GIL and B-SUL material. The C-SUL MDMO-PPV material is excluded of this process due to the high uncertainty on the defect level. The fitted trend line using least squares method is a first order function with a value for the intercept equal to $2.4 \ 10^{-4}$ cm^2 V^{-1} s^{-1} and a value for the slope equal to $-1.0 \ 10^{-5}$ cm^2 V^{-1} s^{-1} (% defects)$^{-1}$. A correlation coefficient or coefficient of determination R^2 equal to 0.95 could be obtained.

The molecular weight, considerable higher for Gilch synthesized MDMO-PPV (N-GIL) does not seem to be influencing the values of the mobility when compared to the sulfinyl synthesized MDMO-PPV batches (A-SUL, B-SUL and C-SUL).

In section 3.3.3 a fairly simple model is described, indicating the influence of a contact resistance on the observed mobility as function of the channel length. In figure 3.11, the result of a modeling of the series of transistors depicted in figure 3.9, with equation 3.12 is presented.

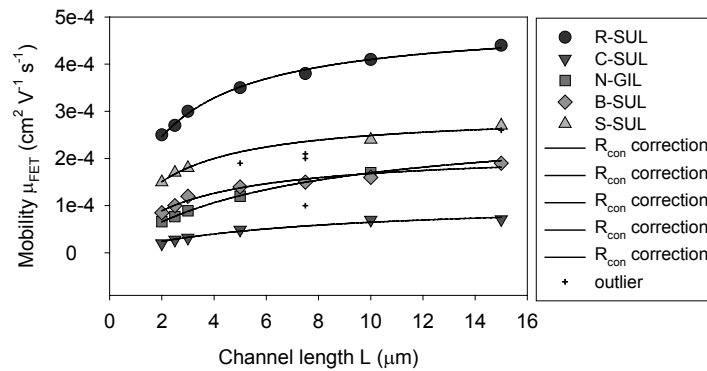*figure 3.11 Modeling of the series of transistors depicted in figure 3.9, with equation 3.12*

Although fairly good results are obtained, one has to be aware of two major assumptions made within this model, namely: a linear scaling of the channel resistor with the channel length and an equal value of the contact resistance for each individual transistor.

A summary of the results of this modeling is given in table 3.1.

Code	μ_{corr} $(10^{-4}$ cm^2 V^{-1} s^{-1})	R_{con}/R'_{cha} (μm)	R^2
A-SUL	2.97 ± 0.08	1.9 ± 0.2	0.986
B-SUL	2.1 ± 0.1	2.8 ± 0.4	0.962
C-SUL	1.1 ± 0.1	7 ± 2	0.968
N-GIL	2.81 ± 0.04	6.6 ± 0.2	0.998
R-SUL	4.91 ± 0.06	2.0 ± 0.1	0.994

table 3.1 Summary of the results of the modeling according to equation 3.12 of the mobility data for one series of transistors

Within this table, an increase of the mobility values compared to the values depicted in figure 3.10 is observed, attributed to the elimination of the influence of a contact resistance. However, no changes are observed in the order of the mobility values when correcting them for a contact resistance.

Notice that the fault on the reported values is the fault as determined by the modeling.

In figure 3.12, an overview of the contact resistance corrected values for the mobility are plotted as function of the percentage of sp^3 defects.
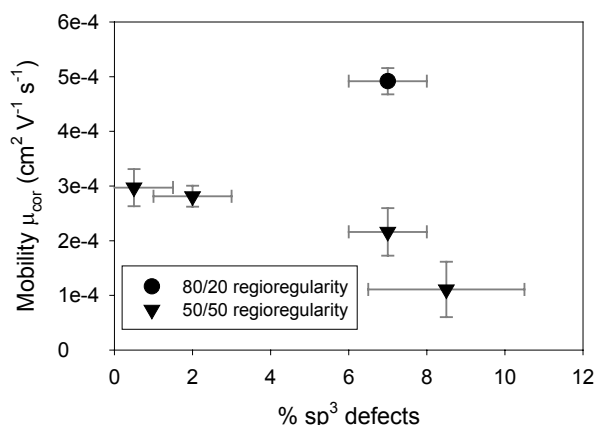
figure 3.12 Overview of the FET-mobility of the charge carriers corrected for the presence of a contact resistance determined via TFT's for the different MDMO-PPV batches

Within this figure, a considerable higher value for the mobility of the material with increased regioregularity (R-SUL) can be observed.

Within the group of regiorandom materials (A-SUL, B-SUL, C-SUL and N-GIL) a similar trend is observed as in figure 3.10, indicating a weak correlation of the mobility with the number of sp^3 defects. The trend line using the mobility values of the A-SUL, N-GIL and B-SUL MDMO-PPV material is characterized by a value for the intercept equal to 3.1 10^{-4} cm^2 V$^-$

[1] s^{-1} and a value for the slope equal to −1.3 10^{-5} cm^2 V^{-1} s^{-1} (% defects)$^{-1}$. A correlation coefficient R^2 equal to 0.99 could be reached. The C-SUL MDMO-PPV material is excluded of this process due to the high uncertainty on the defect level.

3.4.2   Conductivity results

The conductivity can be derived from a measurement of the drain-current during a drain-sweep, according to equation 3.5. Although in principle there is no difference in sensitivity of these measurements compared to the mobility measurements, a number of features complicate conductivity measurements in this set-up. The conductive channel scales in this case to the total thickness of the MDMO-PPV layer. However the exact determination of the thickness of the MDMO-PPV layer, localized in the channel, between source and drain is not always easy. This is even complicated by the occurrence of variations in thickness between different locations in one conductive channel and between different devices located on one substrate. As these measurements are performed in air, oxygen doping can occur at the surface, increasing the number of carriers. Furthermore the measured values for the drain-current (especially for low values of V_d) are considerably low compared to the detection limit of the measurement equipment.

The results of the calculation of the conductivity (according to equation 3.5) for one series of devices with different channel lengths and different MDMO-PPV materials layer are summarized in figure 3.13.
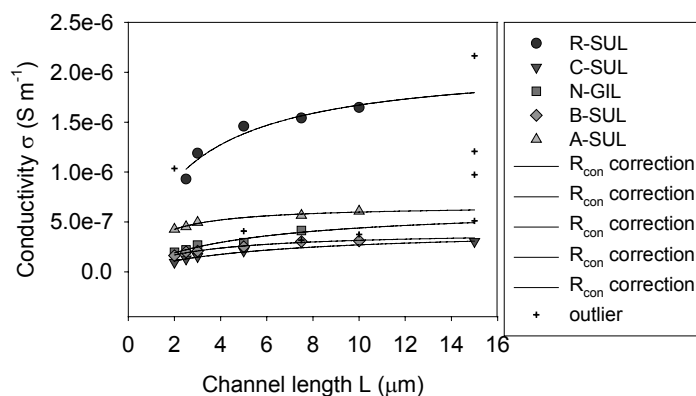

figure 3.13 Conductivity of the charge carriers as function of the channel length and modeling of a contact resistance

Within this figure, a significant higher value for the conductivity of the MDMO-PPV batch with increased regioregularity (R-SUL) compared to the regiorandom batches of MDMO-PPV (A-SUL, B-SUL, C-SUL and N-GIL) is

observed. This is in accordance with the observations made for the FET-mobility.

Within the group of regiorandom batches of MDMO-PPV, differences between batches become small and comparable with the detection limit. However, also in this case, a small influence of the number of sp^3 defects on the values of the conductivity can be observed.

A summary of the results of the modeling of this data according to equation 3.13 is given in table 3.2.

Code	σ_{corr} $(10^{-7}$ S m$^{-1})$	R_{con}/R'_{cha} (μm)	R^2
A-SUL	6.6 ± 0.2	1.1 ± 0.2	0.980
B-SUL	4.1 ± 0.2	2.7 ± 0.3	0.984
C-SUL	4.0 ± 0.1	5.7 ± 0.7	0.987
N-GIL	6.5 ± 1	4.9 ± 2	0.924
R-SUL	21 ± 2	2.6 ± 0.7	0.939

table 3.2 Summary of the results of the modeling according to equation 3.13 of the conductivity data for one series of transistors

Within this table, the reported error is the error determined by the fitting of the data according to equation 3.13 neglecting outliers. The real fault caused by a limited detection limit is supposed to be much higher and is estimated to be at least 2 10^{-7} S m^{-1}.
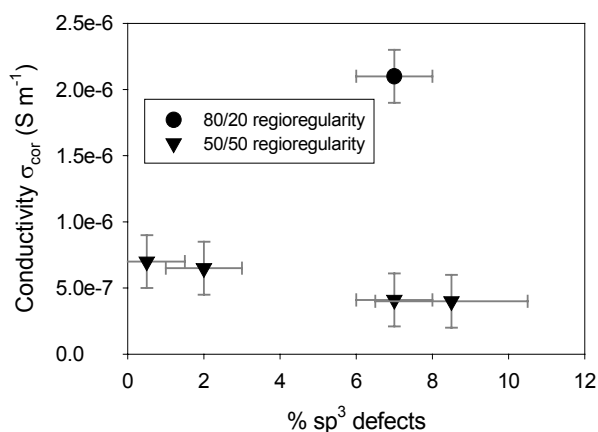

figure 3.14 Overview of the conductivity of the charge carriers corrected for the presence of a contact resistance for the different MDMO-PPV batches

The significant difference between the value for the conductivity of R-SUL MDMO-PPV and the regiorandom batches (A-SUL, B-SUL, C-SUL and N-GIL) is preserved by correction with the value for a contact resistance.

In figure 3.14, an overview of the contact resistance corrected values for the conductivity are plotted as function of the percentage of sp^3 defects.

Within this figure, the considerable higher value for the conductivity can be observed for R-SUL MDMO-PPV. Differences within the regiorandom group of MDMO-PPV batches are comparable to the estimated fault of the conductivity. However a first order trend line based on the values of the A-SUL, N-GIL and B-SUL MDMO-PPV material is fitted. This line is characterized by a value of the intercept equals to 7.3 10^{-7} S m^{-1} and a value of the slope equals to –4.5 10^{-8} S m^{-1} (% defects)$^{-1}$. A correlation coefficient of R^2 equals to 0.99 is obtained. Also in this case is the C-SUL MDMO-PPV material is excluded due to the high uncertainty on the defect level.

3.4.3   Gate-voltage dependency of the mobility

As indicated in section 3.3.2, the gate-voltage and temperature dependency of the FET-mobility can be understood by a hopping transport in the tail of a density-of-states[10]. Information on the parameters determining the density of states and about the tunneling process is preferably determined by temperature dependent measurements. However a rough estimation can be made via a linear fit of the logarithmic mobility at room temperature versus the logarithmic gate-voltage based on equation 3.9 yielding equation 3.14:

$$\log \mu = prefactor(\sigma_0, T_0, T, \alpha, B_c, C_i, \varepsilon_s) + 2\left(\frac{T_0}{T} - 1\right)\log V_g$$

equation 3.14 Estimation of the width(T_0) of the density of states
via a log-log plot of the mobility versus the gate voltage

This is exemplary depicted in figure 3.15 for the different MDMO-PPV batches deposited on devices with rather high channel lengths (e.g. 15 μm) to minimize the influence of a contact resistance.

Within this figure a linear regression of the data yields no strong differences between individual slopes. However, the R-SUL MDMO-PPV exhibits a somewhat lower value for this slope. On the other hand the values for the intercept exhibit stronger changes within our matrix of MDMO-PPV batches.
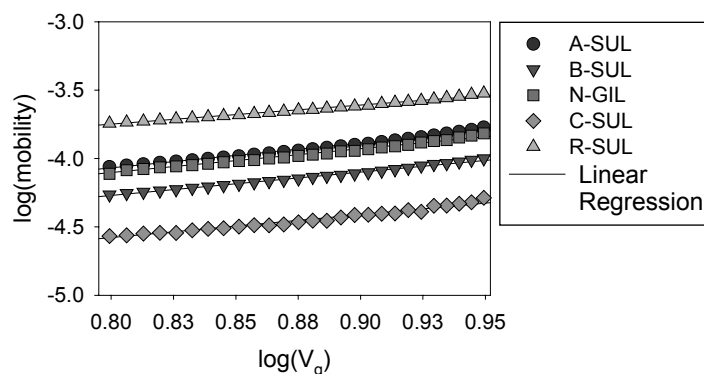
figure 3.15 Plot of the logarithmic mobility as function of the logarithmic gate-voltage for the different MDMO-PPV batches applied on an exemplary device with a high channel length

The slope of the linear regression depicted in figure 3.15 can be directly related with the width of the exponential distribution (T_0) as indicated in equation 3.9. The intercept however is related to more than one parameter, namely: a pre-exponential factor, the overlap parameter and the width of the distribution of localized states. Therefore, in table 3.3 the average value of the width of the exponential energy distribution of localized states (T_0) and the average value related with the intercept denoted as a pre-factor is given for high channel length devices (10 μm and 15 μm) of the different MDMO-PPV batches.

Code	T_0 (10^1 K)	Pre-factor (10^{-6} cm^2 V^{-1} s^{-1})
A-SUL	56.0 ± 0.5	2.9 ± 0.1
B-SUL	55 ± 1	2.3 ± 0.6
C-SUL	54 ± 2	1.4 ± 0.3
N-GIL	56 ± 2	2.1 ± 1
R-SUL	51.0 ± 0.4	12.3 ± 3

table 3.3 The average value of the width of the exponential energy distribution of localized states (T_0) and the average value related with the intercept denoted as a pre-factor

Although the presented method is limited and gives only an estimated value for T_0 and the pre-factor, within this table a significant difference of both values can be observed for the MDMO-PPV with increased regioregularity (R-SUL) compared to the regiorandom batches. Indeed a lower T_0 value for R-SUL (e.g. 510 K) compared to the other batches (A-SUL, B-SUL, C-SUL, N-GIL) (about 550 K) is shown. The increase of about one order of magnitude for the value of the pre-factor of R-SUL MDMO-

PPV (e.g. $1.2 \cdot 10^{-5}$ cm^2 V^{-1} s^{-1}) compared to the regiorandom batches ($1.4 - 2.9 \cdot 10^{-6}$ cm^2 V^{-1} s^{-1}) can be either interpreted in terms of an decreased T_0 value and/or an increased pre-exponential factor (σ_0) and/or increased value for the overlap parameter (α^{-1}). The latter one determines the tunneling process between different sites. Notice that this key parameter is absent in the multiple-trapping model. As the length scale α^{-1} is smaller than the size of the molecule one must be cautious not to interpret α^{-1} simply as the decay length of the electronic wave function. The size and shape of the molecules as well as the morphology of the film are expected to have an important influence. Vissenberg et al.[15] studied the temperature and gate-voltage dependent mobility of PTV and pentacene. They could attribute the two orders of magnitude higher mobility value of pentacene compared to PTV mainly due to a decreased overlap parameter of the latter. Martens et al.[19] compared the absolute values, temperature dependency and field dependency of the mobility determined via hole-only devices of MDMO-PPV (OC_1C_{10}); a PPV-derivative with instead of the methoxy side chain an additional (3'-7'-dimethyloctyloxy) side chain, namely $OC_{10}C_{10}$ and a copolymer of both monomer units. The $OC_{10}C_{10}$ material is due its symmetric substitution fully regioregular. The copolymer is partly regioregular. Although, the mobility is in the case of hole-only devices described by means of a hopping in a Gaussian site-energy distribution, similar parameters such as the width of the distribution, the average site separation and the localization length are determined. They observed a significant decrease of the energetic disorder of the $OC_{10}C_{10}$ material and the partly regioregular material compared to the standard MDMO-PPV. This observation is in accordance with the in this work observed lowering of the T_0 value for of the regioregular MDMO-PPV compared to the regiorandom MDMO-PPV batches. The result can be interpreted by an increased configurational freedom of the regiorandom materials, giving rise to a larger energetic spread between the electronic levels of individual chain segments. Furthermore, Martens et al. observed a similar value of the average site separation for the three materials, but an increased value for the localization length in the case of regioregular materials. This indeed can be interpreted by an enhancement of the ordering in the solid state (induced by an increased regioregularity), favoring charge delocalization. To some extend the parameters localization length and average site separation can be linked with the overlap parameter (α^{-1}) supposed by Vissenberg and Matters et al. As such, the increased localization length, similar average site separation and decreased energetic disorder for the regioregular $OC_{10}C_{10}$ and copolymer of OC_1C_{10}-$OC_{10}C_{10}$ compared to the standard MDMO-PPV are in accordance with our observations of a decreased T_0 value and an increased pre-factor for R-SUL MDMO-PPV compared to the regiorandom batches MDMO-PPV (A-SUL, B-SUL, C-SUL, N-GIL).

As seen in table 3.3, differences within the group of regiorandom materials are much smaller. In figure 3.16, an overview of the values for the width of the exponential distribution of localized-state energies is plotted as function of the percentage of sp^3 defects.
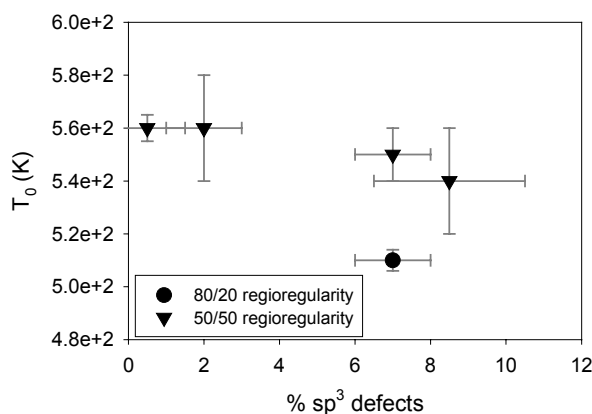
figure 3.16 Overview of the T_0 values of the different MDMO-PPV batches

Within figure 3.16, the lowered value of T_0 for R-SUL MDMO-PPV compared to the regiorandom batches of MDMO-PPV is shown. Furthermore, within the error bars, no significant differences between the T_0 values of the regiorandom batches are observed. The fitted trend line based on the values of A-SUL, N-GIL and B-SUL MDMO-PPV shows almost no dependency and is characterized by an intercept of 562 K and a slope equals to −1.7 K (% defects)$^{-1}$. A R^2 value equals to 0.95 is obtained. The C-SUL MDMO-PPV material is not taken into account to fit the linear trend line because of the poor estimation on the number of single bond defects.

In figure 3.17, an overview of the values for the pre-factor of the different MDMO-PPV batches is plotted as function of the percentage of sp^3 defects. The increased value of the pre-factor for R-SUL MDMO-PPV as compared to the regiorandom batches of MDMO-PPV is clearly shown. Furthermore, within the regiorandom batches, a very weak relation of the pre-factor with the number of sp^3 defects is observed. The fitted trend line for the values of the A-SUL, N-GIL and B-SUL MDMO-PPV is characterized by an intercept of 2.6 10^{-6} cm^2 V^{-1} s^{-1} and a slope equals to −5.9 10^{-8} cm^2 V^{-1} s^{-1} (% defects)$^{-1}$. A R^2 value equals to 0.23 is obtained, indicating a weak correlation. The C-SUL MDMO-PPV material is excluded of this process due to the high uncertainty on the defect level.
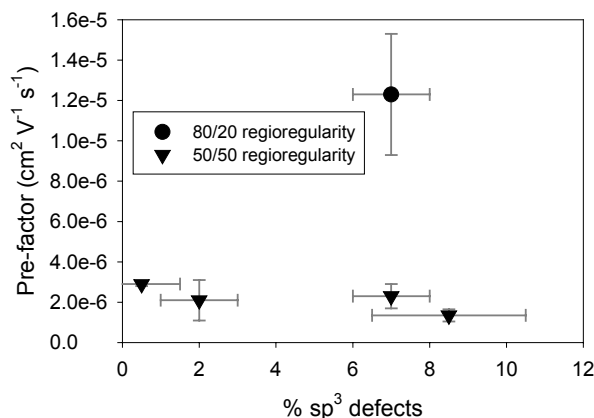
figure 3.17 Overview of the pre-factor values of the different MDMO-PPV batches

The normalized slopes of the trend lines fitted in figure 3.10, figure 3.12, figure 3.14, figure 3.16 and figure 3.17 are given in table 3.4.

Property	Trend line shown in figure	Normalized slope (% defects)$^{-1}$
μ_{obs}	figure 3.10	$-4.1 \cdot 10^{-02}$
μ_{cor}	figure 3.12	$-4.3 \cdot 10^{-02}$
σ_{cor}	figure 3.14	$-6.1 \cdot 10^{-02}$
T_0	figure 3.16	$-3.0 \cdot 10^{-03}$
Pre-factor	figure 3.17	$-2.2 \cdot 10^{-02}$

table 3.4 Normalized value of the slope for trend line obtained via a linear fit of the property as function of the % defects

Within this table, it is shown that the % of sp^3 defects in MDMO-PPV has a small influence on the mobility, conductivity and pre-factor. Within or measurement sensitivity, a negligible influence on the value for T_0 could be observed.

A comparison between the absolute values, the temperature dependency and field dependency of the mobility determined via hole-only devices of MDMO-PPV and a copolymer of MDMO-PPV units and (non-conjugated) phenylene-ethylidene units was made by Martens et al.[19] Also in this case parameters such as the width of Gaussian energy distribution of localized states, the average site separation and the localization length are derived. The strongest limitation of the hampered charge transport of the partly conjugated material is an increased inter-site distance. Furthermore, a very

small increase in disorder with decreasing conjugation could be observed. The localization length was similar in both cases.

The observed significant change in inter-site distance for the partly conjugated material is in accordance with our observations of a decreasing pre-factor, probably caused by a decreasing of the overlap parameter (α^{-1}) as function of the increasing number of conjugational defects. Furthermore, within our measurement sensitivity, there is no change in energetic disorder observed while Martens et al. observed a very small increase of the energetic disorder by decreasing conjugation. The decreased mobility influenced by a broken conjugation can be most likely interpreted by an effective dilution of the charge-transporting fraction of the material.

3.5   Conclusion

Concerning the relation between the microstructure of MDMO-PPV and its electrical properties, chapter 3 has led to two main observations.

The major observed difference is an increase (roughly by a factor of 2) of the electrical properties (FET-mobility and conductivity) for the regioregular (R-SUL) batch compared to the regiorandom (A-SUL, B-SUL, C-SUL, N-GIL) batches. Notice that the studied R-SUL MDMO-PPV is not fully regioregular (80/20 ratio between both monomers). These observations are understood in terms of a higher degree of order in the film induced by the more regular chemical structure of the individual polymeric chains. Although, studies of the mobility are reported in literature for regiorandom poly(3-hexylthiophene) compared to regioregular poly(3-hexylthiophene) and for regiorandom MDMO-PPV compared to regioregular $OC_{10}C_{10}$, within this work, it is the first time that a similar trend is shown for regiorandom MDMO-PPV compared to regioregular MDMO-PPV.

An estimation of a parameter proportional to the width of the distribution of energy site is determined. Comparison of the regiorandom batches of MDMO-PPV and the more regioregular material (R-SUL) indicates a lower width of this distribution of energy sites for the latter one. The higher degree of order for the R-SUL material will indeed lower the width of the distribution of energy sites as observed. An increased pre-factor is also in accordance with a higher degree of regularity governing an improved hopping between adjacent sites.

The observed differences within the regiorandom batches are much smaller and at the limit of our instrumental reproducibility. However a consistent trend line could be fitted for the mobility, conductivity and pre-factor, with a normalized value of about -4 10^{-2} (% defects)$^{-1}$. Within the group of sulfinyl MDMO-PPV (A-SUL, B-SUL and C-SUL) all measured devices clearly show decreased electrical properties as function of increased conjugational defects.

The batch N-GIL showed similar properties as the regiorandom sulfinyl batches, but is characterized by an increased irreproducibility and has in general a somewhat higher error bar than the sulfinyl batches. The reason for this feature is unclear, although the microstructure is somewhat more complex than in the sulfinyl case. On one hand, there are two types of bonds (e.g. triple bond and double bonds) that maintain the conjugation. On the other hand the number of defects as determined by Becker et al. and within our group shows a similar trend, but the exact values differ.

The observed differences within the group of regiorandom materials shows a weak relation with the number of conjugational defects.

Both observations and conclusions of chapter 3 emphasize the importance of the microstructure induced by differences in chemistry when studying and comparing different types of conjugated polymers.

3.6   *References*

[1]   C.D. Dimitrakopoulos, D.J. Mascaro, *IBM J. Res. & Dev.* (**2001**) 45, 11.

[2]   C.J. Drury, C.M.J. Mutsaers, C.M. Hart, M. Matters, D.M. de Leeuw, *Appl. Phys. Lett.* (**1998**) 73, 108.

[3]   Y.Y. Lin, D.J. Gundlach, S. Nelson, T.N. Jackson, *IEEE Electron device Lett.* (**1997**) 18, 606.

[4]   H. Sirringhaus, N. Tessler, R.H. Friend, *Science* (**1998**) 280, 1741.

[5]   a) A. Tsumura, H. Koezuka, T. Ando, *Appl. Phys. Lett.* (**1986**) 49, 1210. b) J.H. Burroughes, C.A. Jones, R.H. Friend, *nature* (**1988**) 335, 137. c) A. Assadi, C. Svensson, M. Willander, O. Inganäs, *Appl. Phys. Lett.* (**1988**) 53, 195. c)J. Paloheimo, E. Punkka, H. Stubb, P. Kuivalainen, *roceedings of NATO ASI Spetses Greece*, (ed. R.M. Mertzger) Ple*P*num Press, New York (**1989**). d) Z. Bao, A. Dobabalapur, A.J. Lovinger, *Appl. Phys. Lett.* (**1996**) 69, 4108.

[6]   a) G. horowitz, *Adv. Mater.* (**1998**) 10, 365. b) S.F. Nelson, Y.Y. lin, D.J. Gundlach, T.N. Jackson, *Appl. Phys. Lett.* (**1998**) 72, 1854.

[7]   a) A. J. lovinger, L.J. Rothberg, *J. Mater. Res.* (**1996**) 11, 1581. b) H.E. Katz, Z. Bao, *J. Phys. Chem. B* (**2000**) 104, 671. c) F. Garnier, *Chem. Phys.* (**1998**) 227, 253. d) A.R. Brown, C.P. Jarrett, D.M. de Leeuw, M. Matters, *Synth. Met.* (**1997**) 88, 37. e) H.E. Katz, *J. Mater. Chem.* (**1997**) 7, 369. f) N. Greenham, R.H. Friend, *Solid State Physics: Advances in Research and Applications, vol. 49* (eds. H. Ehrenreich, F. Spaepen) Academic Press, San Diego (**1995**) 1.

[8]   a) L. Torsi, A. Dobalapur, H.E. Katz, *J. Appl. Phys.* (**1995**) 78, 1088. b) G. Horowitz, R. Hajlaoui, R. Bourgouiga, *Synth. Met.* (**1999**) 101, 401. c) C.D. Dimitrakopoulos, A.R. Brown, A. Pomp, *J. Appl. Phys.* (**1996**) 80, 2501. d) C.D. Dimitrakopoulos, B.K. Furman, T. Graham, S. Hegde, S. Purushothaman, *Synth. Met.* (**1998**) 92, 47.

[9]   G. Horowitz, R. Hajlaoui, P. Delannoy, *J. Phys. III France*, (**1995**) 5, 355.

[10]   a) M. Matters, D.M. de Leeuw, M.J.C.M. Vissenberg, C.M. Hart, P.T. Herwig, T. Geuns, C.M.J. Mutsaers, C.J. Drury, *Optical Materials* (**1999**) 12, 189. b) M.J.C.M Vissenberg, M. Matters, *Phys. Rev. B* (1998) 57, 12964.

[11]   a) B. G. Streetman, Solid state electronic devicces, Prentice-Hall International, New Jersey (1995) edition 4, 288. b) R.F. Pierret, *Modular series on solid state devices*, Addison-Wesley Publishing compagny, Reading, Massachusetts (**1983**) vol. IV, 81.

[12]   G. Horowitz, X. Z. Peng, D. Fichou, F. Garnier, *J. Appl. Phys.* (**1990**) 67, 528.

[13]   G. Horowitz, R. Hajlaoui, H. Bouchrika, R. bourguiga, M. Hajlaoui, *Adv. Mater.* (**1998**) 10, 923.

[14]   G.E. Pike, C.H. Seager, Ph*ys. Rev. B* (**1974**) 10, 1421.

15   M.C.J.M. Vissenberg, *PhD Dissertation* (**1999**) Universiteit Leiden.

16   a) H.E. Katz, A.J. Lovinger, J. Johnson, C. Kloc, T. Siegrist, W. Li, Y.Y. Lin, A. Dodabalapur, *Nature* (**2000**) 404, 478. b) W. Geens, *PhD Dissertation* (**2002**) Universiteit Antwerpen.

17   J. Liu, Y. Shi, L. Ma, Y. Yang, *J. Appl. Phys.* (**2000**) 88, 605.

18   S. Jain, *IEE Proceedings Pt. I.* (**1988)** 135, 162.

19   a) H.C.F. Martens, P.W.M. Blom, H.F.M. Schoo, P*hys. Rev. B* (**2001**) 61, 7489. b) P.W.M. Blom, M.C.J.M. Vissenberg, *Materials Science and Engineering* (**2000**) 27, 53.

Chapter 4
Optical characterization

In chapter 4 general optical properties of the MDMO-PPV materials with various defect levels and types (e.g. regioregularity and single bond defects) are compared. A basic model used to understand the studied optical properties is described. A combination of the results obtained via photoluminescence efficiency measurements and time resolved fluorescence measurements provide a better understanding of the nature of the photoexcitation and the exciton motion. For the matrix of MDMO-PPV materials also the electroluminescent properties are studied.

4.1   Basic model

Many aspects of the photophysical properties of conjugated oligo(p-phenylenevinylene) are known in detail[1]. However, while the intrinsic properties of isolated conjugated oligomers are interesting by themselves, the changes in optical properties when condensing these well-defined molecules into solid-state macromolecular materials (or even blends consisting of a number of materials) are missing. The importance of three-dimensional order and mesoscopic structure on optical properties becomes progressively clear. As a result of interactions between conjugated chains in the solid phase, the optical properties of aggregates are considerably modified as compared to isolated or molecularly dissolved polymer chains[2]. A very simple model, used to understand the basic optical properties of conjugated polymers is depicted in figure 4.1. The relative rate of the radiative and nonradiative processes will determine the device efficiency. For example exciton migration to quenching defects increases the nonradiative decay rate and as such will lower the luminescence efficiency.
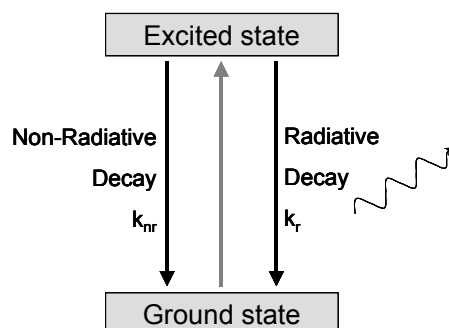
figure 4.1 Basic model used to describe the excitation of a conjugated polymer and the decay via a combination of radiative and nonradiative processes

The emitting species is in most cases the same whether optically or electrically generated. Within the scope of this thesis the major focus is on the material parameters of different batches of MDMO-PPV. To exclude complicating influences of metal barriers and contact or interface layers, it is easier to carry out experiments with optically excited ones. However in section 4.3 the electroluminescence spectra of the defined matrix of MDMO-PPV materials are determined.

Typical techniques used in this work are the determination of the photoluminescence efficiency (section 4.2) and time-dependent fluorescence spectroscopy (section 4.4). Combination of both measurements[19] gives a more profound understanding of the nature of the photoexcitation and the exciton motion in the studied materials (section 4.5).

4.2   External photoluminescence

Photoluminescence measurements are believed to put an upper limit on electroluminescence quantum efficiencies. As such, they form a relatively simple experimental technique to compare optical properties of different batches of conjugated polymers. Due to the easy sample preparation compared to the production of PLED's, determination of the external radiative quantum efficiency is widely used when screening potential PLED materials.

In this section, first a comprehensive discussion of the data acquisition and an improved experimental determination technique of external photoluminescence quantum efficiencies, as proposed by Mello et al.[4] will be given (section 4.2.1). During a 6 week traineeship the experimental set-up of this technique was built and tested at Philips, Natlab (Eindhoven, The Netherlands). Secondly in section 4.2.2, the results will be discussed of the value for the external photoluminescence quantum efficiency of our matrix of MDMO-PPV batches, determined with this improved technique.

4.2.1   Experimental technique and data acquisition

The external radiative quantum efficiency (η) is defined as depicted in equation 4.1.

$$\eta = \frac{number\,of\,emitted\,photons}{number\,of\,absorbed\,photons}$$

equation 4.1 External radiative quantum efficiency (η)

In a liquid, due to inherent disorder, an isotropic angular distribution for emission can be assumed. The detected amount of emitted light over a solid angle (Ω) can be assumed to be linearly proportional with the product of the detection solid angle and the total emitted light. Therefore, the external photoluminescence efficiency can simply be calculated by the ratio of the total emitted light (directly calculated from the detected light and detection solid angle) and the absorbed light (determined via an absorption spectrometer).

In thin solid films however, an anisotropy in the emission dipole moment can be observed. When thin-film conjugated polymer samples are spincoated on glass substrates, significant wave-guiding effects additionally contribute to this angularly distributed emission.

A standard and necessary technique for measuring thin film fluorescence quantum efficiencies involves the use of an integrating sphere[3]. An ideal

integrating sphere redistributes the emitted light isotropiccally over the sphere surfaces without any losses of photons.

Mello et al.[4] proposed an improved experimental determination technique by using an integrating sphere combined with CCD spectrometer. During a 6 week traineeship this experimental set-up was built at Philips, Natlab and used within the scope of this thesis.
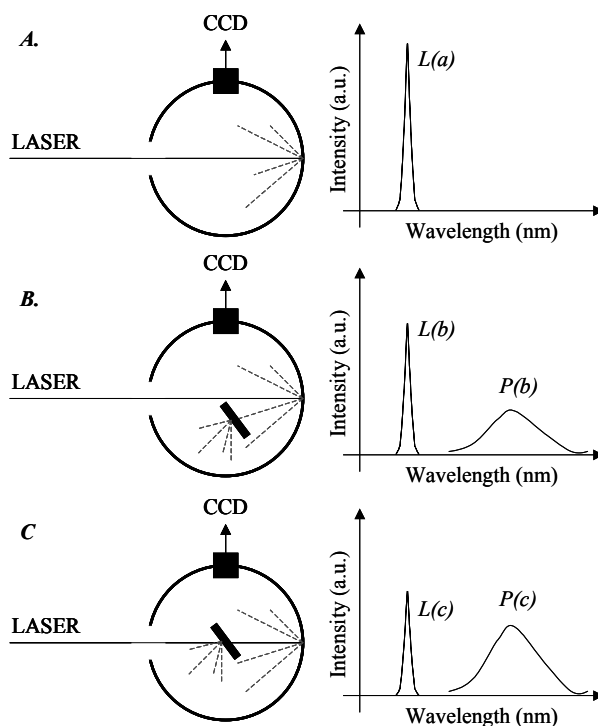
figure 4.2 Schematic representation of the measurement set-up and recorded spectra of the three subsequent measurements performed by the method proposed by Mello et al. [4] to determine external radiative quantum efficiencies

As depicted in figure 4.2, three subsequent measurements are performed. Firstly (A), a fraction of the laser light is measured in an empty sphere. Secondly (B), the sample is placed in the sphere and the laser beam is directed on the sphere wall. The CCD measures a signal proportional to the number of photons per wavelength interval. During the third measurement (C) the excitation laser beam is directly focused on the sample. Both the emission related to the laser light directly striking the sample and the emission caused by laser light, scattered from the wall of the sphere and subsequently striking the sample, contribute to the recorded emission spectra.

The sharp peaks indicated in the schematic representation of the recorded spectra in figure 4.2 correspond to the laser line. The area under the laser profile (e.g. $L_{(a)}$, $L_{(b)}$ and $L_{(c)}$) is proportional to the amount of unabsorbed light. As such, the absorption coefficient (A) can be calculated according to equation 4.2.

$$A = \left(1 - \frac{L_{(c)}}{L_{(b)}}\right)$$

equation 4.2 Calculation of the absorption coefficient (A) from the recorded laser profiles

The area under the emission profile, indicated as P(b) and P(c), is proportional to the amount of emitted light. The external fluorescence quantum efficiency can be subtracted out of the recorded spectra according to equation 4.3.

$$\eta = \frac{P_{(c)} - (1 - A)P_{(b)}}{L_{(a)}\, A}$$

equation 4.3 Calculation of the external fluorescence quantum efficiency (η) from the recorded emission and laser profiles (via the absorption coefficient (A))

The presented method is used to determine η for the different MDMO-PPV polymers.

4.2.2   Results and discussion

A study of the external photoluminescence properties of the matrix of MDMO-PPV materials, as described in section 2.4 is performed. Thin spincoated films (100 nm) on glass substrates prepared according to the conditions denoted in section 2.5.2 are examined. The photoluminescence spectra of the different batches of MDMO-PPV are depicted in figure 4.3. Photoexcitation occurred at 440 nm (λ_{ex}).

Photoexcitation at λ_{ex} = 440 nm gives for all regiorandom batches of MDMO-PPV (e.g. A-SUL, B-SUL, C-SUL and N-GIL) an emission maximum at 585 nm and vibronic shoulders at 629 nm and approximately around 700 nm. The observed peak positions for the batch N-GIL and B-SUL are in accordance with values presented in the literature[5].
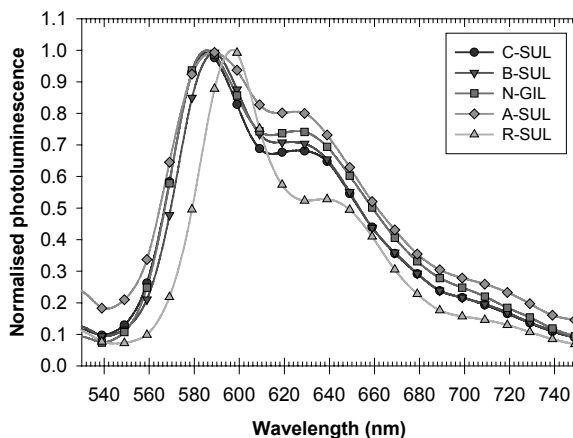
figure 4.3 Photoluminescence spectra of the matrix of MDMO-PPV materials (λ_{ex} = 440nm)

The major difference when comparing the different batches of MDMO-PPV is a clear red shift of 12 nm of the photoluminescence peaks observed for the regioregular material (e.g. R-SUL). This observation is most likely caused by an enhanced three-dimensional ordering. Aggregation of polymer chains is more likely in regioregular MDMO-PPV than in the co-polymer (the regiorandom batches of MDMO-PPV).

Differences in peak positions within the batch of regiorandom materials are small. This is in accordance with the results of Braun et al.[3a] They have seen the expected blue shift for the least conjugated MDMO-PPV, for materials with non-conjugated segments larger than 30 %.

Within figure 4.3 there is an increase on oscillator strength for the phonon peak at 630 nm with decreasing number of single bond defects. Most likely this can be understood in terms of aggregation.

Apart from the determination of the photoluminescence spectra, the external photoluminescence quantum efficiency is measured for the different MDMO-PPV batches, according to the experimental method described in section 4.2.1. In figure 4.4 a typical example of three subsequent measurements yielding an improved experimental determination of the photoluminescence efficiency is depicted.

A clear excitation peak of the argon ion laser (λ_{ex} = 458 nm) can be observed for all three subsequent measurements. A strong decrease of this peak induced by an increased absorption, according to equation 4.1 is shown when comparing measurement (A) with (B) and (B) with (C).
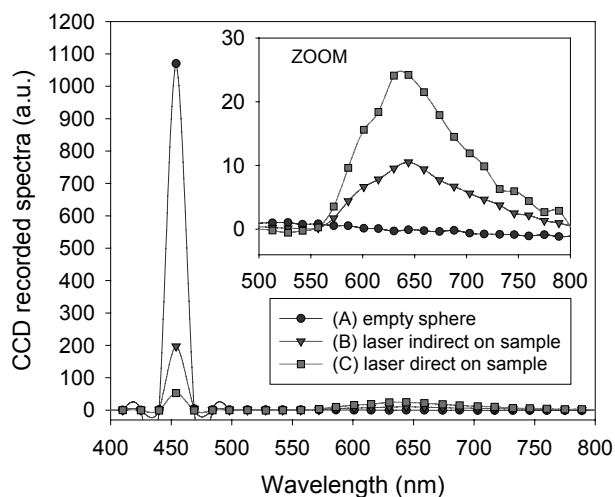
figure 4.4 Experimentally recorded spectra of N-SUL MDMO-PPV of the three subsequent measurements performed by the method proposed by Mello et al. [4]

Samples are made via spincasting of MDMO-PPV dissolved in chlorobenzene (according to the conditions described in section 2.5.2), on in isopropanol ultrasonically cleaned glass substrates. These samples are prepared and stored under inert atmosphere. As the experimental set-up is located under normal ambient conditions, samples are brought under these ambient conditions just preceding the actual measurements.

The absorption coefficient as defined by equation 4.2 has a similar value (0.75 ± 0.03) for all studied samples. This can easily be explained by means of the well-defined spincoating conditions yielding an equal thickness for all samples. All samples exhibit a strong absorption of the excited light.

The external photoluminescence quantum efficiency was determined via equation 4.3 for a number of samples of all different MDMO-PPV batches. A summary of the results is given in table 4.1.

Code	Photoluminescence efficiency
A-SUL	0.145 ± 0.007
B-SUL	0.15 ± 0.01
C-SUL	0.16 ± 0.02
N-GIL	0.15 ± 0.02
R-SUL	0.09 ± 0.02

table 4.1 The average value of the external photoluminescence quantum efficiency for the different batches of MDMO-PPV

The MDMO-PPV material with increased regioregularity (R-SUL) yields a considerable lower value for the external photoluminescence quantum efficiency (e.g. 0.09 ± 0.02) than the MDMO-PPV batches with a random 50/50 ratio of both regioregularity forms (A-SUL, B-SUL, C-SUL and N-GIL).

Most likely due to the enhanced order of the R-SUL MDMO-PPV compared to the fully regiorandom batches, the aggregated phase is more pronounced. Most likely, in this aggregated form a strongly non-emissive low energy state is present (e.g. an interchain dimer with exciton coupling).

Within the group of regiorandom (50/50) MDMO-PPV materials (A-SUL, B-SUL, C-SUL and N-GIL) differences in photoluminescence between the different batches are almost virtually and within the experimental error of this technique. However a small increasing trend of the photoluminescence as a function of the number sp^3 defects can be observed in figure 4.5. Most likely due to small changes in exciton mobility, quenching sites are more easily reached and thus a lowered photoluminescence quantum efficiency is observed for the low defect materials. However as observed in the photoluminescence spectra, influences of differences in aggregation may not be excluded.
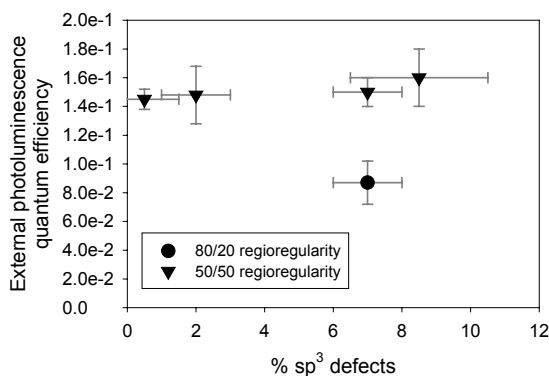
figure 4.5 External photoluminescence quantum efficiency versus the number of sp^3 defects for the different MDMO-PPV batches

Based on the values of the A-SUL, N-GIL and B-SUL MDMO-PPV material, a first order linear trend line is fitted. This regression is characterized by a value for the intercept equal to 0.146 and a value for the slope equal to 6.7 10^{-4} (% defects)$^{-1}$. A correlation coefficient R^2 equal to 0.84 could be reached. The observed slope of the first order polynomial trend line indicates no strong effect of the number of sp^3 defects on the external photoluminescence efficiency. Due to the high uncertainty in the defect level of the C-SUL material, this value is not used to fit the linear trend line. This indicates indeed that differences of exciton motion within the studied group of regiorandom MDMO-PPV batches are rather small.

The molecular weight, considerably higher for Gilch synthesized MDMO-PPV (N-GIL) does not seem to be influencing the values of the external photoluminescence quantum efficiency when compared to the sulfinyl synthesized MDMO-PPV batches (A-SUL, B-SUL and C-SUL).

4.3   Electroluminescence

As already mentioned in section 1.4.2, the discovery of electroluminescence (EL) from the conjugated polymer PPV, sandwiched between two injecting electrodes[6] boosted the research towards conjugated polymers. As such, PLED's are the first commercial application where conjugated polymers are used as active material in an electronic device.

The working principle of electroluminescence can be qualitatively described using the semiconductor band model (with its limitations), as depicted in figure 4.6. Injection of holes from the anode side and electrons from the cathode side, leads to a migration of the charge carriers and finally the formation of an exciton. This exciton can decay by emitting a photon. Electrically or optically excited excitons are considered as identical in properties.
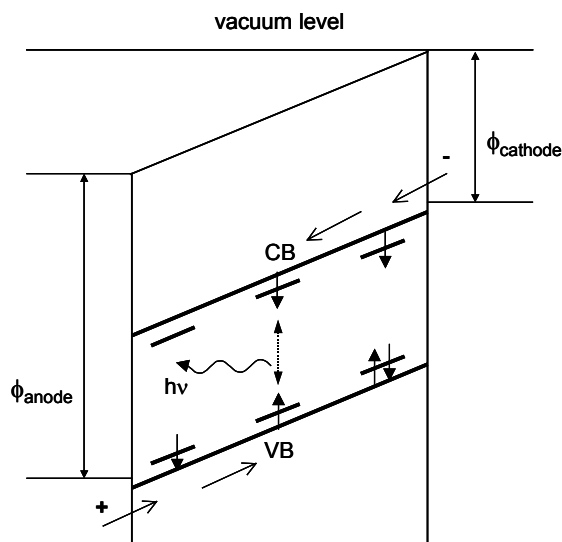
figure 4.6 Schematic band diagram of a PLED under forward bias

Three processes thus determine the operation of a PLED: charge injection, charge transport and recombination. More about this device can be found in a review article[7]. Actually two sets of parameters determine the performance of a PLED, namely the device characteristics (e.g. choice of electrodes, architecture of the layers, quality of the film, …) and the parameters directly linked with the active semiconductor layer (e.g. bandgap, defects, mobility, width of the density of states, …)

As both sets of parameters are equally important, it is difficult to compare intrinsic material properties in a limited number of PLED devices. Major observed differences could be easily attributed to influences of processing.

4.3.1   Device preparation

A typical PLED currently used, consists of four layers. On top of a glass substrate, a thin indium-tin oxide (ITO) layer is used as transparent anode. An additional conjugated polymeric anode, poly(ethylene-dioxythiophene) (PEDOT)[8], layer is used to increase stability and lifetime. A threefold function is attributed to this layer namely: smoothing of the electrode surface, a balancing of the charge injection between cathode and anode, and preventing oxygen migration from ITO. The next layer is the emissive layer, within the scope of this thesis MDMO-PPV. Finally a low work-function metal such as Ca or Ba is evaporated as cathode. The total set-up is encapsulated to prevent diffusion of water and oxygen into the active area. A schematic cross-section of the structure of a PLED is given in figure 4.7.
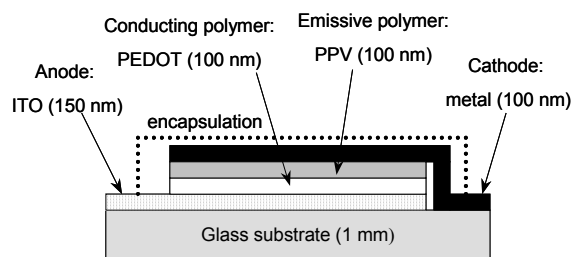
figure 4.7 Schematic structure of the cross-section of a PLED

For this study, pre-shaped glass substrates with an ITO stripe of 3 mm width are used. After an ultrasonic cleaning step of these substrates in isopropanol, a 100 nm PEDOT layer is spincoated on top of this structure. The solvent used for this step is a combination of water (2/3) and isopropanol (1/3). Solvent rests are removed after spincoating via a heat treatment (e.g. 150 °C, 900 s). MDMO-PPV dissolved in chlorobenzene is used to prepare a 100 nm thick emissive layer. The different batches of MDMO-PPV are spincasted via the conditions described in section 2.5.2. Within this work, a 6 nm Ba and a 40 nm Al layer are sequentially evaporated as cathode.

4.3.2   EL-results and discussion

A study of the electroluminescence spectra of the matrix of MDMO-PPV materials, as described in section 2.4 is performed. Devices are prepared

according to the conditions denoted in section 4.3.1. The electroluminescence output is plotted versus the detection wavelength in figure 4.8.
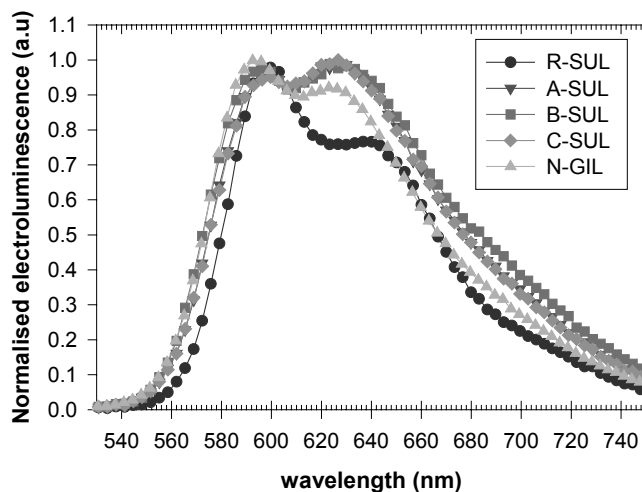
figure 4.8 Electroluminescence spectra of PLED devices prepared for the matrix of MDMO-PPV materials

The observed electroluminescence curves are similar to the photoluminescence curves as depicted in figure 4.3. An emission maximum at 585 nm and vibronic shoulder at 629 nm are clearly visible. The observed peak positions for the batch N-GIL and B-SUL are in accordance with values presented in the literature[9].

A small red shift of electroluminescence peaks of 10 nm is observed for the regioregular material (e.g. R-SUL). This shift is somehow more pronounced for the vibronic shoulder. Such a shift is most likely caused by an enhanced three-dimensional ordering. This is in accordance with the photoluminescence spectra.

Differences in peak positions within the batch of regiorandom materials are negligible within experimental error.

The optical electroluminescence properties are comparable to the photoluminescence data, indicating indeed an equal excited species in both cases.

4.4   Time resolved fluorescence

Time resolved fluorescence measurements are made by exciting the sample with a short light pulse and measuring the time-dependence of the luminescence. A number of detection techniques used to study conjugated polymers are reported. Common methods are time-correlated single photon counting (TCSPC)[10], streak cameras[11] and luminescence up-conversion in non-linear crystal[12].

Several picosecond photoluminescence studies have been performed on MEH-PPV[13,11b] to observe the energy relaxation of the excitons. Three main features can be observed. First, an extreme rapid rise in the luminescence extending across the entire spectral region. This is followed by a very fast decay of the high-energy luminescence tail within a few hundreds of femtoseconds. On a (sub-)picosecond timescale a red shift and narrowing of the luminescence peaks is observed. Thirdly, an overall decay of the luminescence can be seen.

These observations are understood by describing the conjugated polymer film sample as a series of smaller conjugated sub-units whose size (and thus energy) depends on the degree of chain alignment and conjugational defects.

The ultra fast rise in luminescence is attributed to the formation of excitons and their subsequent vibrational relaxation onto the lowest vibrational level of the first excited electronic state[14]. Exciton migration can occur prior to recombination via Förster transfer from less (higher energy) to more conjugated (lower energy) chain segments[14a]. Nguyen et al.[15] showed that intrachain transport is much slower than interchain transport as the dipoles are head-to-tail. This exciton motion explains the rapid removal of the high-energy luminescence tail. This can occur at a sub-picosecond time scale due to the presence of a large density of lower lying states. The excitons can migrate to sites in three dimensions[16]. On a (sub-) picosecond time scale, the migration is a slower diffusion. The excitons loose more and more energy and as such, there are fewer and fewer energetically available sites. This causes the observed red shift and narrowing of the luminescence peaks.

4.4.1   Experimental technique and data acquisition

In a time-correlated photon-counting set-up, pulse decay times are measured directly by recording the time evolution of the spectrally filtered sample emission. A typical TCSPC set-up is schematically depicted in figure 4.9.
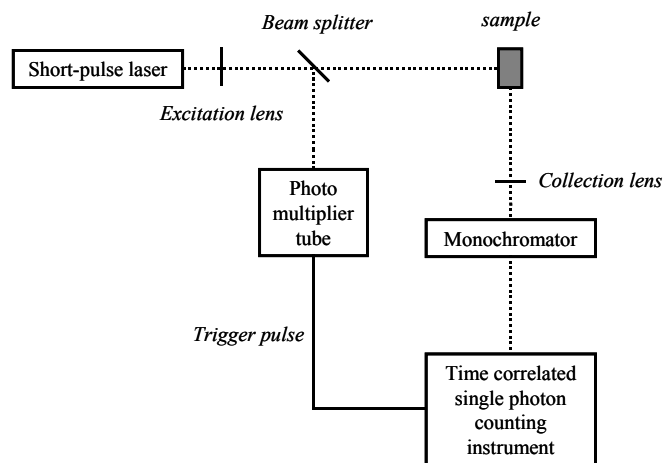
figure 4.9 Typical time-resolved photon counting set-up

In the time-resolved photon counting set-up, the output of a pulse laser is used to excite the sample. Fluorescence emission is collected and filtered with a monochromator before reaching the time-correlated-single-photon-counting instrument. The latter can be seen as a micro channel-plate photo multiplier tube (MCP PMT) that produces pulses that theoretically correspond to the arrival of individual photons. By counting the number of pulses produced within a series of discrete sequential time intervals after the excitation pulse (externally triggered) a time-resolved histogram of the sample emission at a certain emission wavelength can be produced.

The photoluminescence emission consists of a short intense flash followed by a slower decay described simply by equation 4.4.

$$I(t) = \left(\frac{1}{\tau}\right) \exp\left(\frac{-t}{\tau}\right)$$

equation 4.4 Time-resolved photoluminescence emission (I(t))
expressed in time (t) and the photoluminescence lifetime (τ)

Although this equation is fairly simple, difficulties occur when analyzing photoluminescence decay curves having multiple components. The emission from such a complex sample is described by the contributions from several molecules each having a different decay rate or from one molecule with different localized decay environments. This is mathematically described by equation 4.5, the more general version of equation 4.4.

$$I(t) = \sum_i \left(\frac{1}{\tau_i} \right) a_i \exp\left(\frac{-t}{\tau_i} \right)$$

equation 4.5 General version of the time-resolved photoluminescence emission (I(t)) expressed versus time (t) by several contributions a_i each with a different photoluminescence lifetime (τ_i)

However in cases where two or more components have lifetimes that differ only by a few tens of percent, it is difficult to distinguish different emission species. Conjugated polymers are an extreme version of the latter situation as the conjugated polymer film sample is described as a series of smaller conjugated sub-units whose size (and thus energy) depends on the degree of chain alignment and conjugational defects. As such, a single lifetime can hardly be distinguished on conjugated polymer samples. Often three or four components are used to fit the time-resolved decay function, although this discrete analysis has no physical background. A somewhat different approach is to fit the time-resolved fluorescence function by a continuous distribution of lifetimes. Within the scope of this thesis a Gaussian distribution of lifetimes is used as indicated by equation 4.6.

$$a(\tau) = \frac{1}{\sigma\sqrt{2\pi}} \exp\left(-\frac{\left(\tau - \tau_{avg}\right)}{2\sigma^2} \right)$$

equation 4.6 Gaussian distribution of lifetimes describing the contribution (a) of each conjugated sub-unit versus the lifetime of this sub-unit (τ) characterized by the averaged lifetime (τ_{avg}) and the variance of the distribution (σ^2)

Although this Gaussian distribution is chosen for its mathematical simplicity, no real physical background can be attributed. However, a complete random distribution of conformational defects and chain-alignment should lead by approximation to a Gaussian-like distribution of lifetimes. At least this type of model is the most reasonable for biological polymers like proteins[17].

Within the scope of this thesis samples of the matrix of MDMO-PPV materials are prepared via spincoating of polymer solutions on glass substrates according to the conditions described in section 2.5.2.
Measurement of the time-resolved fluorescence decay data is performed at the laboratories of prof. R.A.J. Janssen, University of Technology Eindhoven, The Netherlands. The experimental set-up is characterized by an excitation pulsed LED (400 nm) with an intensity of about 10 µW on the sample, a low temporal dispersion monochromator and an Edinburgh Instrument Ltd. Lifespec ps, time-correlated-single-photon-counting instrument. As such, this set-up has a typical time resolution of 10 ps. Detection at emission wavelengths of 550, 600 and 675 nm is performed.

Time base for the instrument response function is 0.005 ns for the instrument response function (IRF) and 0.012 ns for the fluorescence decays. The illumination area on the sample was about 2 by 8 mm.

Data were analyzed[18] with the Lifespec single decay analysis software and with the Globals analysis package (Globals Inc.) developed at the Laboratory for Fluorescence Dynamics (LFD) of the university of Illinois at Urbana Champaign (UIUC), USA. Gaussian fits with either linked center or linked width were carried out. No significant changes in the results were observed.

4.4.2   Results and discussion

The time-resolved fluorescence spectral properties of the matrix of MDMO-PPV materials as described in 2.4 are studied. In figure 4.10 typical decay curves for the different studied emission wavelengths (excitation wavelength 400 nm) are depicted.
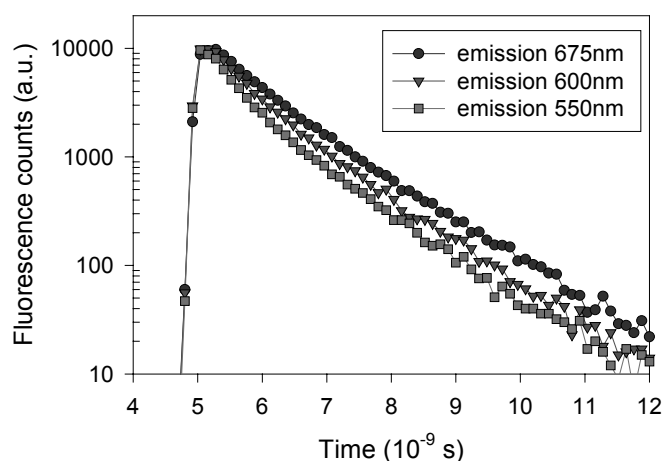
figure 4.10 Logarithmic representation of the time-resolved photoluminescence counts at different emission wavelengths for a typical MDMO-PPV sample (e.g. N-GIL)

A typical feature observed in the time-resolved fluorescence spectra is a dependency of the decay time of the emission wavelength. A faster decay is observed at higher energy emission wavelengths. This can be understood by describing the conjugated polymer film sample as a series of smaller conjugated sub-units whose size (and thus energy) depends on the degree of chain alignment and conjugational defects. Indeed high-energy excitons (shorter emission wavelengths) have more available sites with lower energy in their surrounding and as such will decay faster (shorter lifetime).

Although the curves are represented in a semi-logarithmic representation, no complete linear behavior can be observed. This indicates that the polymer sample has two or more fluorescence lifetimes. This indeed is in agreement with the model describing the conjugated polymer sample as a distribution of smaller conjugated sub-units each with different energy levels. A shown in figure 4.10 the best linear fit can be observed for the high-energy (e.g. 550 nm) detection wavelength.

A typical time-resolved fluorescence decay curve at an emission wavelength of 550 nm is depicted in figure 4.11 for the different batches of MDMO-PPV.
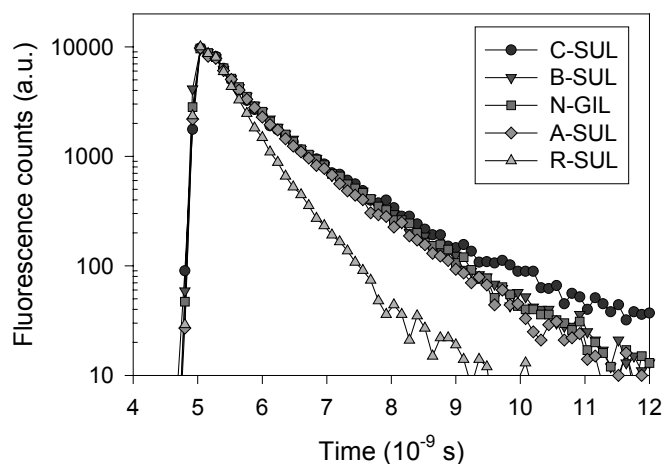
figure 4.11 Fluorescence decay curves of the different batches of MDMO-PPV as described in section 2.4

The time-resolved measurements clearly indicate a faster decay for the regioregular MDMO-PPV samples. The value of photoluminescence lifetime obtained via a simple monoexponential fit of the data-points according to equation 4.4 of the first nanoseconds is summarized in table 4.2.

The denoted typical error is estimated from the uncertainty on the fitted slope values.

The major difference between the individual MDMO-PPV batches is observed for the regioregular batch (e.g. R-SUL) compared to the regiorandom batches (e.g. A-SUL, B-SUL, C-SUL, N-GIL). This first order approach yields a two-times faster decay for the regioregular batch. The regiorandom MDMO-PPV batches have all a photoluminescence lifetime in the order of $0.8 \ 10^{-9}$ s. This is in accordance with literature values of MEH-PPV, a PPV derivative similar to the studied materials[19].

MDMO-PPV	Fluorescence lifetime (τ) (10^{-9} s)	Correlation coefficient (R^2)
A-SUL	0.77 ± 0.03	0.98
B-SUL	0.81 ± 0.03	0.98
C-SUL	0.84 ± 0.05	0.97
N-GIL	0.80 ± 0.03	0.98
R-SUL	0.46 ± 0.02	0.98

table 4.2 Table of the photoluminescence lifetime according to a mono-exponential fit of the time-resolved fluorescence decay curves at 550 nm emission wavelength for the different batches of MDMO-PPV

Within this group of regiorandom MDMO-PPV batches, differences are much smaller and at the limit of reproducibility. However, an increasing lifetime can be observed for batches with an increasing number of sp^3 defects. This photoluminescence decay time for all batches of MDMO-PPV is depicted versus the percentage of sp^3 defects in figure 4.12.
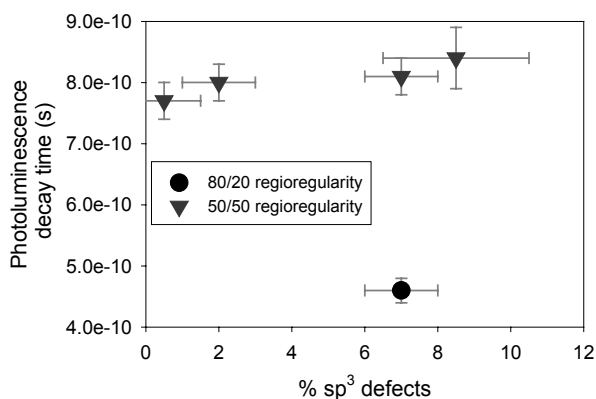
figure 4.12 Photoluminescence decay time obtained via a mono-exponential fit of the data versus the number of sp^3 defects for the different MDMO-PPV batches

A fitted linear trend line of the values of A-SUL, N-GIL and B-SUL MDMO-PPV is characterized by a value for the intercept of 7.8 10^{-10} s and a value for the slope of 5 10^{-12} s (% defects)$^{-1}$. A correlation coefficient R^2 equal to 0.70 could be reached. The observed slope of the first order polynomial trend line indicates no strong effect of the number of sp^3 defects on the first-order photoluminescence decay time. Notice that the C-SUL material is not taken into account to calculate the trend line.

Although the obtained results give already a clear indication, the fit is not fully satisfying. Therefore a fit with a Gaussian distribution of lifetimes as indicated by equation 4.6 is performed.

An overview of the values for the center of this Gaussian distribution of lifetimes is given in table 4.3 for the studied matrix of MDMO-PPV materials.

MDMO-PPV	Center of distribution at detection wavelength 550 nm (10^{-10} s)	Center of distribution at detection wavelength 600 nm (10^{-10} s)	Center of distribution at detection wavelength 675 nm (10^{-10} s)
A-SUL	6.0 ± 0.3	6.6 ± 0.3	7.7 ± 0.3
B-SUL	7.3 ± 0.3	7.3 ± 0.3	8.4 ± 0.3
C-SUL	8.3 ± 0.5	7.4 ± 0.5	8.2 ± 0.4
N-GIL	6.5 ± 0.2	7.0 ± 0.2	7.9 ± 0.2
R-SUL	3.4 ± 0.2	3.3 ± 0.3	3.4 ± 0.2

table 4.3 The value of the center of the Gaussian distribution of lifetimes used to fit the time-resolved photoluminescence decay curves detected at three different wavelengths for the matrix of MDMO-PPV materials

As already shown via the first-order approach, a clear distinction can be observed between the regiorandom batches and the regioregular batch. Within the group of regiorandom batches the differences are much smaller and also similar to the first-order approach. All batches show an increase of the center of lifetimes with increasing detection wavelengths. However this feature is not pronounced for the regiorandom batch. Besides differences in the center of the distribution of lifetimes, a significantly smaller width of the distribution of lifetimes could be observed for the R-SUL material (typical 4 10^{-10} s) compared to the regiorandom batches (typical 1 10^{-10} s).

Most likely due to the enhanced order of the R-SUL MDMO-PPV compared to the fully regiorandom batches, the aggregated phase is more pronounced. In this aggregated form a strongly non-emissive low energy state might be present (e.g. an interchain dimer with exciton coupling). The differences within the group of regiorandom MDMO-PPV materials are understood in terms of differences in exciton mobility.

4.5   Decay model

A number of studies presented in the past were focused on the exact nature of the excitation[19,20]. Either interchain or intrachain (excimer) excitations are formed on conjugated polymers. Samuel et al.[19] showed how a combination of measurements of luminescence efficiency and time-resolved fluorescence could help to understand the nature of photoexcitation of conjugated polymer. Furthermore, a general kinetic model was proposed giving insight in the different situations observed for different polymers. Within this section, first in paragraph 4.5.1 it is explained how a combination of photoluminescence measurements yields information on the radiative and nonradiative luminescence lifetime. Secondly, in paragraph 4.5.2, a general kinetic model is briefly discussed. Finally the results of section 4.2 and 4.4 are combined and interpreted giving insight into the nature of the photoexcitation of the studied batches of MDMO-PPV.

4.5.1   Natural radiative lifetime

A natural radiative lifetime (τ_r) is defined, as the lifetime the luminescence would have in absence of any nonradiative decay processes. A combination of photoluminescence efficiency measurements and time-resolved photoluminescence measurements can give insight into that natural radiative lifetime of a chromophore.

Assume a simple model whereby an excited state can decay radiatively (with a rate constant k_r) and nonradiative (with rate constant k_{nr}). As such, the natural radiative lifetime (τ_r) and nonradiative lifetime (τ_{nr}) can be expressed in these rate constants.

$$\tau_r = \frac{1}{k_r} \quad \& \quad \tau_{nr} = \frac{1}{k_{nr}}$$

equation 4.7 Expression of the natural radiative lifetime and nonradiative lifetime versus their rate constants assuming unimolecular decay processes

Time-resolved photoluminescence decay measurements as described in section 4.4 yield a photoluminescence decay time or radiative lifetime (τ) determined via a radiative and nonradiative contribution. Assuming single excited species and unimolecular decay processes, this radiative lifetime can also be expressed in both rate constants.

$$\tau = \frac{1}{k_r + k_{nr}}$$

equation 4.8 Expression of the radiative lifetime or photoluminescence decay time determined via time-resolved photoluminescence experiments versus the radiative and nonradiative rate constant

Experiments to determine the external photoluminescence efficiency, as described in section 4.2 are used in combination with the time-resolved measurements to get a distinction between the radiative and nonradiative processes. The photoluminescence efficiency (η) is given by the fraction of excitations decaying radiatively.

$$\eta = \frac{k_r}{k_r + k_{nr}} = \frac{\tau}{\tau_r} = \frac{1}{1 + \dfrac{\tau_r}{\tau_{nr}}}$$

equation 4.9 Expression of the photoluminescence efficiency versus the rate constants and lifetimes

Insight in the radiative and nonradiative photophysical properties is used to get detailed information on the nature of excitations in conjugated polymers. Within the scope of this thesis, this combined interpretation of time-resolved photoluminescence and efficiency measurements is used in section 4.5.3 for the studied MDMO-PPV batches.

4.5.2   General kinetic model

A more general kinetic model[19], schematically depicted in figure 4.13 was proposed to explain the excited state kinetics in conjugated polymers. Within the scope of this thesis, this model is briefly discussed. More detailed information can be found in the work of Samuel et al.[19]

Two kinetically distinct species, namely an intrachain excitation (A*) and an interchain excitation (B*) are described. Interconversion is expressed via two rate constants, k_{AB} and k_{BA} (although the latter is only written for completeness). The initially excited state (X*) leads to the population of both, the intrachain and interchain excitation, described via k_{XA} and k_{XB}. However if k_{AB} and k_{XB} compete efficiently with k_{XA}, it will look within the time-scale of our experiment, as if a direct excitation of B* is observed. Both states can decay either radiatively or nonradiatively with rate constants $k_{R,A}$ and $k_{NR,A}$ for the intrachain excitation and $k_{R,B}$ and $k_{NR,B}$ for the interchain excitation.
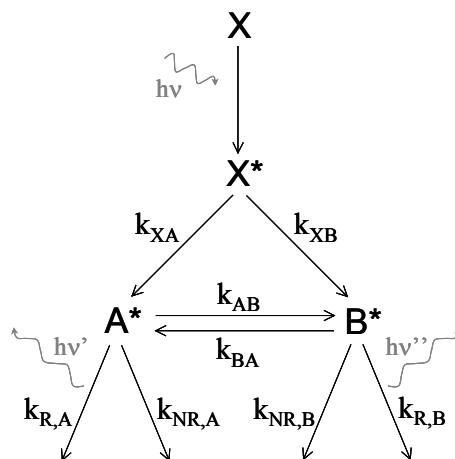
figure 4.13 Kinetic scheme for a general model proposed to explain the excited state kinetics of conjugated polymers[19]

As MEH-PPV is a well-known example in the literature and chemically close to MDMO-PPV, a comparison with the properties of MEH-PPV is given.

MEH-PPV in a good solvent has well separated polymer chains and as such the formation of interchain excitations is precluded. Within the described model this is understood via a value of k_{xa} much greater than k_{xb} and an extremely small value for k_{ab}. There is little or no emission of X* observed. Notice that the state X* is similar in nature as A*. Typical values for MEH-PPV found in the literature[21] are a natural radiative lifetime ($1/k_{R,A}$) of $1\ 10^{-9}$ s and a nonradiative lifetime ($1/k_{NR,A}$) of $0.5\ 10^{-9}$ s.

However MEH-PPV in film shows a different behavior. The interchain excitation formation (k_{AB} and k_{XB}) is competing efficiently with $k_{r,a}$ and $k_{nr,a}$. The lifetime of A* ($1/[k_{AB} + k_{R,A} + k_{NR,A}]$) is short and only limited emission is seen from this state. Therefore, the measured natural lifetime is that of B*, the interchain excitation. Typical values of MEH-PPV found in the literature are a natural radiative lifetime of $5\ 10^{-9}$ s and a nonradiative lifetime of $0.8\ 10^{-9}$ s. The value of the natural radiative lifetime is about one order of magnitude higher than in solution and is consistent with an excited state delocalized over neighboring chains.

4.5.3   Results and discussion

The data from the time-resolved photoluminescence measurements and photoluminescence efficiency measurements are combined in order to obtain the natural radiative and nonradiative lifetime of the studied batches of MDMO-PPV.

The photoluminescence efficiency values as described in table 4.1 and the values of the radiative lifetime obtained via the first-order fit on the time-resolved decay curves as described in table 4.2 are combined to generate information on radiative and nonradiative processes. The natural radiative lifetime and nonradiative lifetime determined according to equation 4.8 and equation 4.9 are summarized in table 4.4 for the MDMD-PPV batches.

MDMO-PPV	Natural radiative lifetime (τ_r) (10^{-9} s)	Nonradiative lifetime (τ_{nr}) (10^{-9} s)
A-SUL	5.3 ± 1	0.90 ± 0.15
B-SUL	5.4 ± 1	0.95 ± 0.15
C-SUL	5.2 ± 1	1.00 ± 0.15
N-GIL	5.3 ± 1	0.94 ± 0.15
R-SUL	5.1 ± 1	0.50 ± 0.15

table 4.4 The natural radiative lifetime and nonradiative lifetime of the studied MDMO-PPV batches

The absolute value of the natural lifetime as denoted in table 4.4 shows clearly coincidences with the MEH-PPV in film case. It can be concluded that all studied regiorandom batches of MDMO-PPV have an interchain excited state. The R-SUL MDMO-PPV has a much faster nonradiative decay compared to the regiorandom batches. This significant difference in rate constant for the nonradiative decay is most likely understood in terms of a different excited state present in the regioregular material (for example an interchain dimer with exciton coupling). Therefore, in the kinetic scheme as presented in figure 4.13 an additional state should be added, namely C*, typical for the R-SUL MDMO-PPV material. This second type of intrachain excitations would have a rather fast nonradiative decay time ($k_{NR,C}$ greater then $k_{R,C}$). Both intrachain excitations compete efficiently with each other.

Differences within the group of regiorandom batches are almost negligible. However, a higher nonradiative decay rate could be found versus a decreasing number of sp^3 defects (Although this is within the experimental error). Most likely this could also be explained by small differences in excited state dynamics (e.g. exciton mobility).
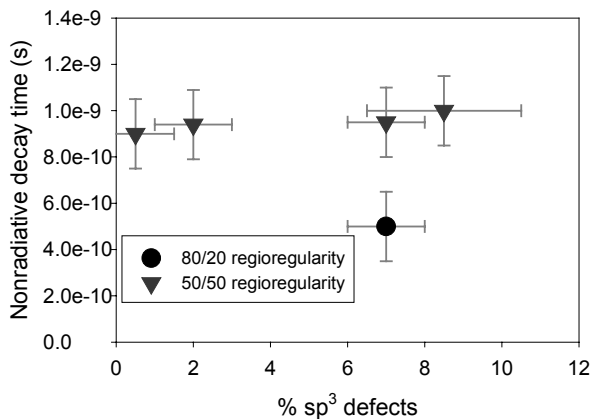
*figure 4.14 Nonradiative decay time versus the number of sp3
defects for the different studied MDMO-PPV batches*

The determined nonradiative lifetimes for the matrix of MDMO-PPV materials are depectid in figure 4.14. A fitted first order trend line based on the values of the A-SUL, N-GIL and B-SUL material is characterized by an intercept equal to $9.1 \cdot 10^{-10}$ s, a slope equal to $6.2 \cdot 10^{-12}$ s (% sp^3 defects)$^{-1}$ indicating only a very weak dependency and a correlation coefficient of only 0.65. The C-SUL MDMO-PPV material is excluded of this process because of the high uncertainty on the value for the defect level.

The molecular weight, considerably higher for Gilch synthesized MDMO-PPV (N-GIL) does not seem to be influencing the values of the natural radiative lifetime and nonradiative lifetime when compared to the sulfinyl synthesized MDMO-PPV batches (A-SUL, B-SUL and C-SUL).
When using the center of the Gaussian distribution of photoluminescence decay times obtained via the time-resolved experiments, a similar result is obtained. The values of the natural radiative decay time are equal within experimental error. The values of nonradiative lifetime show an almost negligible increase versus the number of sp^3 defects.

4.6   Conclusion

Summarizing chapter 4 two main observations can be made concerning the relation between the chemical structure of MDMO-PPV and its optical properties.

The major observation is a clear distinction between the optical properties of the regioregular MDMO-PPV and the regiorandom batches. A clear red shift in the photoluminescence spectra indicates a higher degree of order in the R-SUL MDMO-PPV film. Both the photoluminescence efficiency and photoluminescence radiative lifetime is considerably lower in this material. Combination of both observations leads to the conclusion that the partly regioregular material has an equal natural radiative lifetime compared to the regiorandom materials but a significantly faster nonradiative decay time. This two times faster decay observed for the R-SUL material is understood in terms of the presence of a strongly nonemissive low energy state (e.g. an interchain dimer with exciton coupling). Besides a difference in radiative lifetime, also a decrease of the width of the Gaussian distribution, used for the time-resolved photoluminescence data is observed.

Within the group of regiorandom materials differences are small. However, a very small but consistent increase of the photoluminescence efficiency and photoluminescence decay time is observed as the number of sp^3 defects increases.

Combination of efficiency and time-resolved measurements yields a natural radiative lifetime of $5 \; 10^{-9}$ s. This value is equal to the value observed for the regioregular MDMO-PPV material. A slightly faster decay is observed for the batches with a lower number of defects. Most likely, this can be explained via a slightly higher exciton motion. A normalized slope indicates approximately a decrease in exciton motion of $-0.008 \; (\% \; \text{defects})^{-1}$.

The molecular weight, considerably higher for Gilch synthesized MDMO-PPV (N-GIL) compared to the sulfinyl synthesized MDMO-PPV batches (A-SUL, B-SUL and C-SUL), has no significant influence on the optical properties of MDMO-PPV.

4.7   References

[1]   a) R.A.J. Janssen, *Primary Photo excitations in conjugated polymers: Molecular exciton versus semiconductor band model, (Ed. N.S. Sariciftci)* World Scientific Publishing, S (**1998**) 18, 524. b) D. Beljonne, J. Cornil, D.A. dos Santos, Z. Shuai, J.L. Bredas, *Primary Photo excitations in conjugated polymers: Molecular exciton versus semiconductor band model, (Ed. N.S. Sariciftci)* World Scientific Publishing, S (**1998**) 19, 559.

[2]   a) M. Yan, L.J. Rothberg, E.W. Kock, T.M. Miller, *Phys. Rev. Lett.* (**1995**) 75, 1992. b) U. Lemmer, S. Heun, R.F. Marht, U. Scherf, M. Hopmeier, U. Siegner, E.O. Göbel, K. Müllen, H. Bässler, *Chem. Phys. Lett.* (**1995**) 240, 373.

[3]   a) D. Braun, E.G.J. Staring, R.C.J.E. Demandt, G.L.J. Rikken, Y.A.R.R. Kessener, A.H.J. Venhuizen, *Synth. Met.* (**1994**) 66, 75. b) N.C. Greenham, I.D.W. Samuel, G.R. Hayes, R.T. Philips, Y.A.R.R. Kessener, S.C. Moratti, A.B. Holmes, R.H. Friend, *Chem. Phys. Lett.* (**1995**) 89.

[4]   J. Mello, H. Wittmann, R. Friend, *Adv. Mat.* (**1997**) 9, 230-232.

[5]   L. Lutsen, P. Adriaensens, H. Becker, A.J. Van Breemen, D. Vanderzande, J. Gelan, *Macromolecules* (**1999**) 32, 6517.

[6]   J.H. Burroughes, D.D.C. Bradley, A.R. Brown, R.N. Marks, K. Mackay, R.H. Friend, P.L. Burn, A.B. Holmes, *Nature* (**1990**) 347, 539.

[7]   P.W.M. Blom, M.C.J.M. Vissenberg, *Materials Science and engineering* (**2000**) 27, 53.

[8]   H. Spreitzer, H. Becker, E. Kluge, W. Kreuder, H. Schenk, R. Demandt, H. Schoo, *Adv. Mater.* (**1998**) 10(16), 1340.

[9]   L. Lutsen, P. Adriaensens, H. Becker, A.J. Van Breemen, D. Vanderzande, J. Gelan, *Macromolecules* (**1999**) 32, 6517.

[10]   a) I.D.W. Samuel, B. Crystall, C.J. Collison, *Phys. Rev.* (**1995**) B 52; 11573. b) W.J. Feast, I.S. Millichamp, R.H. Friend, M.E. Horton, D. Philips, S.D.D.V. Rughooputh, G. Rumbles, *Synth. Met.* (**1985**) 10, 181. c) S.A. Jenekhe, J.A. Osaheni, *Science* (**1994**) 265, 765. d) G. Rumbles, I.D.W. Samuel, L. Magnani, K.A. Murray, A.J. de Mello, B. Crystall, S.C. Moratti, B.M. Stone, A.B. Holmes, R.H. Friend, *Synth. Met. (***1996***)* 76, 47.

[11]   a) U. Lemmer, R.F. Mahrt, Y. Wada, A. Greiner, H. Bässler, E.O. Göbel, *Appl. Phys. Lett.* (**1993**) 62, 28287. b) L. Smilowitz, A. Hays, A.J. Heeger, G. Wang, J.E. Bowers, *J. Chem. Phys.* (**1993**) 98, 6504.

[12]   a) G.R. Hayes, I.D.W. Samuel, R.T. Philips, *Phys. Rev.* (**1996**) B 54, 8301. b) R. Kersting, U. Lemmer, R.F. Mahrt, K. Leo, H. Kurz, H. Bässler, E.O. Göbel, *Phys. Rev. Lett.* (**1993**) 70, 3820.

[13]   a) I.D.W. Samuel, B. Crystal, G. Rumbles, P.L. Burn, A.B. Holmes, R.H. Friend, *Chem. Phys. Lett.* (**1993**) 213, 472. b) G.R. Hayes, I.D.W. Samuel, R.T. Philips, *Phys. Rev. B* (**1995**) 52, R11 569.

14   a) R. Kersting, U. Lemmer, R.F. Mahrt, K. Leo, H. Kurz, H. Bässler, E.O. Göbel, *Phys. Rev. Lett.* (**1993**) 70, 3820. b) M. Yan, L. Rothberg, B.R. Hsieh, R.R. Alfano, *Phys. Rev. B* (**1994**) 49, 9419.

15   T.Q. Nguyen, J. Wu, S.H. Tolbert, B.J. Schwartz, *Adv. Mater.* (**2001**) 13, 1053.

16   U. Lemmer, R.F. Mahrt, Y. Wada, A. Greiner, H. Bässler, E.O Göbel, *Chem. Phys. Lett.* (**1993**) 209, 243.

17   H. Frauenfelder, E. Gratton, *Meth. In Enzymology* (**1985**) 127.

18   J. M. Beechem, E. Gratton, M. Ameloot, J.R. Knutson, L. Brand, *Topics of fluorescence spectroscopy*, II, (Ed. J.R. Lakowicz, Ed.) (**1991**) 5, 241.

19   I.D.W. Samuel, G. Rumbles, R.H. Friend, *Primary Photo excitations in conjugated polymers: Molecular exciton versus semiconductor band model, (Ed. N.S. Sariciftci)* World Scientific Publishing, S (**1998**) 7, 140.

20   T.G. Bjorklund, S.-H. Lim, C.J. Bardeen, *J. Phys. Chem. B* (**2001**) 105, 11970.

21   I.D.W. Samuel, B. Crystall, G. Rumbles, P.L. Burn, A.B. Holmes, R.H. Friend, *Chem. Phys. Lett.* (**1993**) 213, 472.

Chapter 5
Photovoltaic devices

In chapter 5 the different MDMO-PPV materials with various defect levels and types (e.g. regioregularity and single bond defects) are investigated in organic solar cells. As Gilch MDMO-PPV based devices were for a long time 'state-of-the-art' solar cells with the highest reported efficiency among all polymeric based cells, it is extremely interesting to compare the various MDMO-PPV materials in a similar configuration. Typical for these devices is a blended active semiconductor layer making a direct correlation between photovoltaic performance and chemical defects more complicated. By using sulfinyl MDMO-PPV instead of Gilch MDMO-PPV a new efficiency record was obtained, being 15 % higher than the highest reported value (2.5 %) at that time. In this chapter, a brief introduction about organic solar cells, a description of the device preparation and data acquisition, the obtained results for the different MDMO-PPV batches and some conclusions are presented.

5.1   *Organic solar cells*

Applications involving conjugated polymers include a wide variety of solid-state electronic devices e.g. light emitting diodes, thin film transistors, sensors and photovoltaic devices. The need to develop inexpensive renewable energy sources stimulates the research towards low cost photovoltaic devices. As such, efficient and stable plastic solar cells can sustain that need.

If photoinduced free charge carrier generation is allowed at the same time, electroluminescence devices show light emission under forward bias and a

significant photocurrent under reversed bias[1]. However, these homogene devices should have a potential difference between the electrodes, high enough to overcome the coulomb attraction of the photo-generated excitons. Contrarily, under conditions of a low potential difference, the created excitons will mainly decay geminately.

The discovery of ultra fast photoinduced electron transfer in a composite of conjugated polymers as donor material and buckminsterfullerene (C_{60}) (figure 5.1) as acceptor material provided a molecular approach to high efficient photovoltaic conversion[2].
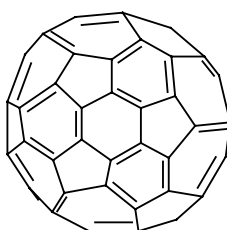
figure 5.1 Front view of the chemical structure of buckminsterfullerene

Typically, conjugated polymers are electron donors upon photoexcitation. Once the photo-excited electron is transferred to an acceptor unit (e.g. buckminsterfullerene), the resulting cation radical (positive polaron) species on the conjugated backbone is known to be highly delocalized, mobile and stable. Observations, clearly evidencing this ultra fast reversible metastable photoinduced electron transfer from conjugated polymers onto buckminsterfullerene are reported independently by Sariciftci et al.[3,2] and Yoshino et al.[4]

Early devices, based on a PPV/C_{60} bilayer, yielded limited photovoltaic performance[5]. Although diodes with high rectification ratios in the order of 10^4 could be reached, relatively low charge collection efficiencies are achieved.

A major increase in efficiency was obtained by blending the conjugated polymer directly with a soluble methanofullerene (e.g. (6,6)- phenyl-C_{61}butyricacidmetlyester, PCBM)[6] (figure 5.2).
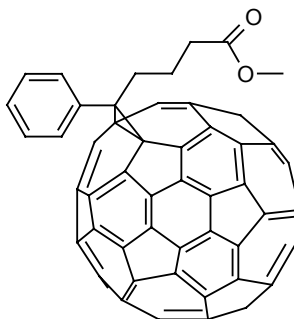
figure 5.2 Front view of the chemical structure of 1-(3-methoxycarbonyl)-propyl-1-phenyl-(6,6)C_{61} (PCBM)

Within these devices, a large interfacial region is formed. Because any photoexcitation in the composite is (in principal) within a few nanometers of a donor-acceptor interface, these devices are named as donor-acceptor bulk hetero junction solar cells.

The working principle of the bulk hetero junction photovoltaic devices can be qualitatively described using the semiconductor band model (with its limitations), as depicted in figure 5.3.
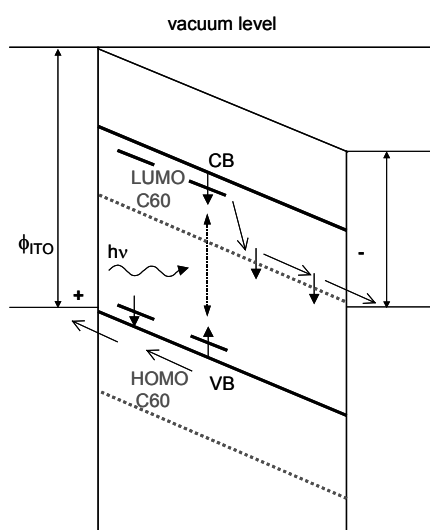
figure 5.3 Schematic presentation of the working principle of a bulk hetero junction photovoltaic device

A photoinduced electron transfer occurs from the conjugated polymer towards the C_{60} derivative. The resulting cation radical species (positive polaron) is known to be highly delocalized, mobile and stable. This will be driven out of the film under influence of the work function difference

between the ITO cathode layer and the metallic anode layer. The opposite is true for the negative polaron localized on C_{60}. It is already clear from this simple description that a good working solar cell needs a high number of excitons (e.g. good overlap with the solar spectrum), an efficient charge separation (e.g. bulk hetero junction), good transport of the separated charges (interplay of recombination and mobility) and a good charge collection (e.g. dedicated electrodes and interfacial layers).

Large area (3600 mm^2) flexible plastic solar cells based on a blend of MDMO-PPV and PCBM are reported with efficiencies (about 1%) equal to similar small area (typically 6 mm^2) photovoltaic devices[7], proving the ability for an easy up scaling.

It is shown that the power conversion efficiency of an organic photovoltaic cell is dramatically affected by the molecular morphology, caused by the casting conditions[8]. An optimization of the casting solvent yields an increase in efficiency from 1 % to 2.5 % by using chlorobenzene instead of toluene for the alkoxy-PPV:PCBM donor-acceptor bulk hetero junction solar cells. This result was interpreted in terms of differences in bulk morphology determined via Transmission Electron Microscopy (TEM) by Martens et al[9].

Recently, the focus is shifted from MDMO-PPV as donor-material towards thiophene derivatives. Thiophene derivatives have in general a higher mobility and a better overlap with the solar spectrum. Both properties are favorable in the development of high efficient photovoltaic devices up to 5 %[10].

Beside a strong tendency to develop and apply better donor materials, the same trend is observed towards the acceptor material. Photovoltaic bulk hetero junctions based on MEH-PPV and an acceptor-conjugated polymer have been reported[11].

A detailed overview about organic solar cells can be found in some excellent review articles[12].

In section 5.2, the typical device preparation and characterization are discussed. The described procedure is applied on the matrix of MDMO-PPV materials. The results are discussed in section 5.3. Finally this chapter is ended with a brief summary and some general conclusions (section 5.4).

5.2   Experimental techniques and data acquisition

For the solar cells as reported in this chapter MDMO-PPV as an electron donor and PCBM as electron acceptor are used. A description of the device preparation as used in this thesis is given. Furthermore a typical photovoltaic characterization is defined. Besides the more general photoelectrical properties of the solar cell, an important focus towards characterization of the bulk morphology is presented. It is shown that this morphology plays a crucial role towards the development of high performance plastic photovoltaic cells.

5.2.1   Device preparation

PCBM and MDMO-PPV show both a satisfactory solubility in a large number of organic solvents[13]. The enhanced solubility of PCBM compared to C_{60} allows a high ratio of the fullerene compared to the conjugated polymer. A typical ratio PCBM:MDMO-PPV of 4:1 by weight is used. This mixed solution is stirred over night and used to prepare the active bulk hetero junction layer in a photovoltaic device, via spincoating. The spincoat parameters as defined in section 2.5.2 were modified to obtain thin (typical 100 nm) bulk heterojunction layers. As PCBM acts as a sort of filler in the semiconductor layer, an increased spincoat velocity is used. Furthermore, the weight percentage MDMO-PPV in the solvent (typically between 0.5 wt % and 0.2 wt % of conjugated polymer in chlorobenzene) is decreased compared to the preparation of non-blended films.
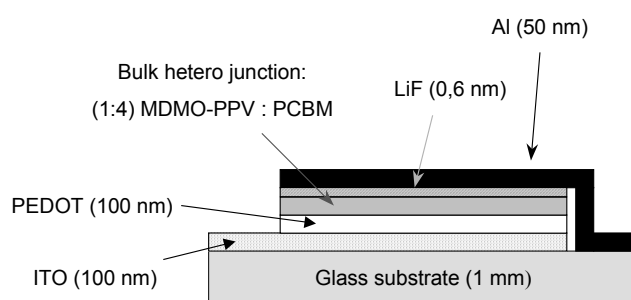

figure 5.4 Schematic representation of the device structure of a state-of-the-art bulk hetero junction solar cell

The typical structure of a solar cell used within this thesis is schematically depicted in figure 5.4. The detailed production of these devices, which consisted in all cases of 6 layers, is performed as described in literature[14]. An indium tin oxide layer positioned on a glass substrate is used as a transparent conductive oxide (TCO) layer. A PEDOT:PSS additional anode layer (poly(3,4-ethylene-dioxy-thiophene doped with polystyrene sulphonic acid) is spincasted from an aqueous solution on the ITO-substrate. A typical layer with an average thickness of 100 nm is applied. This causes a minimization of ITO surface roughness, an improvement of the electrical contact to the semiconducting polymer and a change in work function of the electrode. Furthermore, doping of the PPV with PSS is reported[15]. A number of procedures to reduce solvent rests in the PEDOT:PSS layer are commonly used. Within the scope of this thesis, the samples were dried under nitrogen atmosphere in a glove-box.

On top of these electrodes, the bulk hetero junction layer is spincoated. This is possible by making use of the difference in solubility properties between both mixtures (e.g. PEDOT:PSS soluble in water/isopropanol and MDMO-PPV:PCBM soluble in chlorobenzene).

The next layer is an ultra thin (only 0.6 nm) evaporated layer of LiF (as originally used for enhancing the efficiency of organic LED's). Brabec et al.[16] suggested that the observed increase of photovoltaic efficiency could be attributed to the formation of a dipole moment across the junction. This dipole either formed by orientation of the LiF or chemical reactions leading to a charge transfer across the interfaces, yields improved electrode properties (e.g. lowering of the metal work function or shifting the molecule levels towards higher energies).

Finally, the Al electrode is evaporated on the sample. The thickness of both vacuum depositions is monitored via a quartz balance. A typical pressure of less than 10^{-5} mbar was reached at the start of the thermal deposition. A shadow mask is used in order to define a well-controlled device area of either 1.5×3 mm^2 or 2×3 mm^2.

An overview of the two typical device layouts used within this thesis is depicted in figure 5.5.
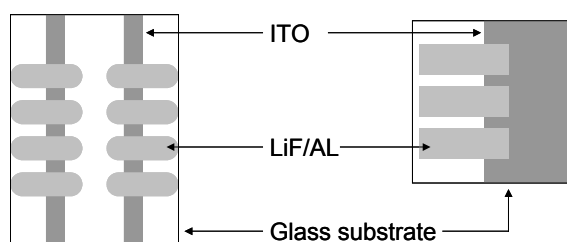
figure 5.5 Overview of the two typical substrate layouts as used to characterize the MDMO-PPV solar cells within the scope of this thesis

The active area of the photovoltaic devices is located at the cross-section of the ITO/PEDOT and the LiF/Al layers. This procedure allows the preparation of a number of solar cells with a well-defined active area, on a single substrate.

Storage time of the devices under dark and inert atmosphere conditions was minimized before characterization.

5.2.2   Photovoltaic characterization

A standard characterization of the photovoltaic devices is performed under AM1.5[a] simulated illumination (80 mW cm^{-2}) from a solar simulator (Solar Constant 575 with AM1.5 filter, K.H. Steuernagel Lichttechnik GmbH). A typical current-voltage characteristic in dark and under light is schematically depicted in figure 5.6.
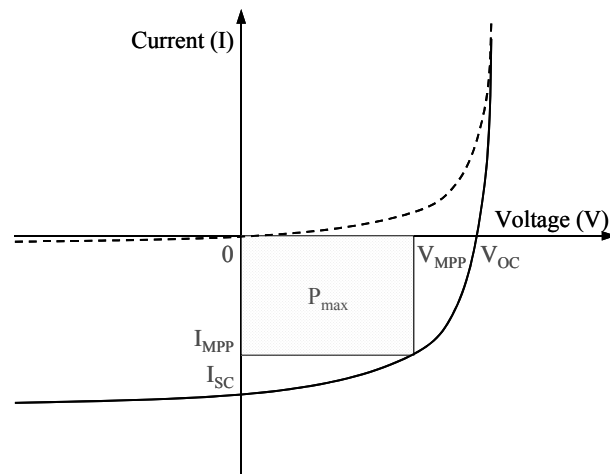
figure 5.6 Schematic representation of a current (I)-voltage (V) characteristic of a solar cell under illumination (solid line) and in dark (dashed line)

Within this figure, an important area is the so-called fourth quadrant. In this quadrant a positive voltage and a negative current can be observed for a device under illumination. An electrical energy gain is obtained, as the power sign is negative. The maximum power point (MPP) is the point amongst the current-voltage characteristic in the fourth quadrant with the maximum absolute product of current and voltage. The larger this area (P_{max}) is, the more the current-voltage characteristic resembles a rectangular with the area $V_{OC} \times I_{SC}$. This open-circuit voltage (V_{oc}) is the potential

---

[a] *AM0 is the solar spectrum above earth's atmosphere while AM1.5 is the standard spectrum at sealevel.*

difference measured between both electrodes of the studied photovoltaic device with an infinite resistance. It is represented as the cross-point of the zero current axes and the current-voltage characteristic. The short-circuit current (I_{sc}) is the current measured of a device under illumination with no load resistance. It is represented as the cross-point of the zero voltage axes and the current-voltage characteristic.

The ratio between both mentioned areas is a measure of the quality of the shape of the current-voltage characteristic. This ratio is called fill factor (FF) and is expressed via equation 5.1.

$$FF = \frac{P_{max}}{I_{sc} V_{OC}}$$

equation 5.1 Fill factor (FF) expressed versus the maximum output power, the short-circuit current and the open-circuit voltage

The higher the fill-factor is, the more the current-voltage characteristic resembles a constant current source with a maximum voltage and the more electric power can be extracted.

In practice, the photo-excited electron can decrease its potential energy by losing energy to photons until it reaches the lowest lying energy level. Since the photon energy dissipates into heat this process is called thermalisation.

The higher the bandgap of the used semiconductor, the higher the voltage can be. On the other hand, a low bandgap material can absorb more photons and as such lead to a higher photocurrent. This leads to the definition of an optimal bandgap with for a given light spectrum. For both AM0 and AM1.5 solar spectrum a semiconductor bandgap between 1.3 and 1.5 eV gives the highest power.[17]

In order to describe the power conversion efficiency under AM1.5 illumination ($\eta_{AM1.5}$), the maximum output power (P_{max}) has to be related to the incident light (P_{in}). As shown in equation 5.2, the power conversion efficiency can be expressed versus the fill factor, open-circuit voltage and short-circuit current using equation 5.1.

$$\eta_{AM1.5} = m \frac{P_{max}}{P_{in}} = m \frac{I_{sc} V_{oc} FF}{P_{in}}$$

equation 5.2 The power conversion efficiency expressed versus the typical solar cell parameters: short-circuit current, open-circuit voltage and fill factor

Within equation 5.2, the spectral mismatch factor (m) accounts for deviations in the spectral response to that of a reference cell[18]. For the measurements described within this thesis, P_{in} = 80 mW cm^{-2} and m = 0.753. However, not in all cases a solar simulator was used. For simplicity,

sometimes, a standard halogen lamp was used to compare different batches of solar cells.

Actually, a similar equation as equation 5.2 can be written but with a wavelength dependency of every parameter. However, often the incident photon per converted electron ratio (%) (IPCE) is defined. The definition of IPCE is expressed via equation 5.3.

$$IPCE = \frac{number\ of\ electrons\ in\ external\ circuit\ (\lambda)}{number\ of\ incident\ photons\ (\lambda)}$$

equation 5.3 Definition of the incident photon per converted electron ratio

The IPCE represents a true measure for the photon to current conversion efficiency.

5.2.3 Bulk hetero junction morphology

Increasing the interfacial area between the p-phase and n-phase of a hetero junction, has a beneficial effect on the efficiency of charge separation. Shaheen et al.[8] demonstrated the effect of the spincasting solvent on the solar cell efficiency. A study of the surface morphology with Atomic Force Microscopy (AFM) indicated a more uniform mixture of PCBM and MDMO-PPV when spincoated from a chlorobenzene solution compared to toluene casted films (yielding solar cell efficiencies of 2.0 % versus 0.9 %). Evidence of different bulk morphology was given by Martens et al.[9] using TEM. TEM images of the (1:4) MDMO-PPV:PCBM bulk hetero junction layer spincoated from chlorobenzene and toluene are depicted in figure 5.7.
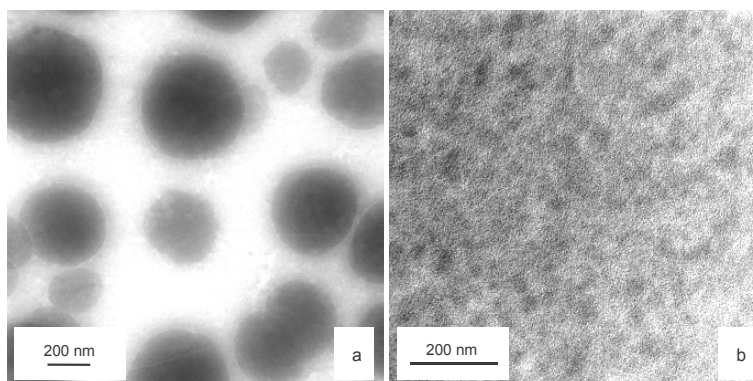

figure 5.7 TEM images of MDMO-PPV:PCBM (1:4) films spincoated from a toluene (a) and chlorobenzene solution (b)

The dark spots have been interpreted as regions with a high PCBM concentration whereas the white-gray regions in between consist of a

mixture of PCBM and MDMO-PPV. The average size of a PCBM cluster in the toluene cast film is significantly larger then in the chlorobenzene cast film.

Geens et al.[19] proposed a simplified model to describe the working principle of MDMO-PPV:PCBM bulk hetero junction solar cells. As the absorption of fullerene and its derivatives is weak in the visible range, the absorption of light is mainly localized in the MDMO-PPV:PCBM region (white-gray). It is taken into account that each absorbed photon creates a free electron-hole pair as the dissociation efficiency is near unity (forward electron transfer time less then 45 fs[20]).

Within this idea, only a limited volume of the total film is contributing towards the current depending on the diffusion length of the electrons and the number and distribution of PCBM channels. The depicted figure 5.7 a and b illustrate that information of the bulk morphology provided by TEM, gives a clear view how this distribution is influenced by the spincasting conditions.

On the other hand, a good electron and hole transport is needed in order to prevent recombination. Both are influenced by the bulk morphology. However it is expected from the morphology shown in figure 5.7 that the electron transport in the film is strongly influenced by the PCBM distribution via the presence of a percolation network.

Presently, this idea is not yet incorporated in the model proposed by Geens et al.

Both considerations yield somewhat conflicting demands towards the PCBM morphology, indicating an optimum structure.

Furthermore Martens et al.[21] showed that spincasting conditions (e.g. evaporation speed of solvent, concentration of the MDMO-PPV:PCBM mixture in a solvent, choice of solvent, …) have a clear influence on the morphology of the dry MDMO-PPV:PCBM blend. This makes it extremely difficult to compare different batches of MDMO-PPV in photovoltaic devices.

Martens et al. provide a more profound study on the MDMO-PPV:PCBM bulk hetero junction morphology which may lead to an improvement of the model proposed by Geens et al.

5.3   Results and discussion

In order to compare the photovoltaic performance of the matrix of MDMO-PPV batches described in section 2.4, a number of solar cells are made. These photovoltaic devices (prepared as described in section 5.2.1) have an approximately equal thickness of 100 nm and differ only by means of the nature of the donor material in the bulk hetero junction, the MDMO-PPV.
Gilch MDMO-PPV:PCBM based solar cells were for a long time the 'state-of-the-art' polymeric photovoltaic devices. An efficiency of 2.5 % under AM1.5 illumination is reported[8]. Therefore in section 5.3.1 these Gilch MDMO-PPV based devices are compared with cells based on the sulfinyl MDMO-PPV material with similar chemical defects (e.g. number of sp^3 interruptions and regioregularity), namely the B-SUL MDMO-PPV. Furthermore an extensive study of the thickness dependency of the photovoltaic performance of both materials is presented in section 5.3.2. The results described in section 5.3.1 and section 5.3.2 are obtained during a 6 week stay at the Christian Doppler Laboratory for Solar Cells, Johannes Kepler University (Linz, Austria) in the framework of the scientific exchange program 'Euromap'.

A more profound discussion of the photovoltaic performance of the regiorandom sulfinyl MDMO-PPV based solar cells will be the topic of section 5.3.3. Beside a comparison of the regiorandom batches, a comparison of the R-SUL and B-SUL MDMO-PPV based solar cells is made.
As already mentioned, differences in molecular weight yield different spincasting conditions to obtain an equal film thickness. However, differences in spincasting conditions yield also different morphologies. Therefore within section 5.3.4, an introductory morphology study is carried out using TEM. The obtained results will help in understanding the observed differences in photovoltaic performance.

5.3.1   'State-of-the-art' polymeric solar cells

Gilch MDMO-PPV:PCBM solar cells had for a long time the highest polymeric photovoltaic performance with a reported[8] efficiency of 2.5 %. A typical current-voltage characteristic in dark and under illumination with a solar cell simulator is depicted in figure 5.8.
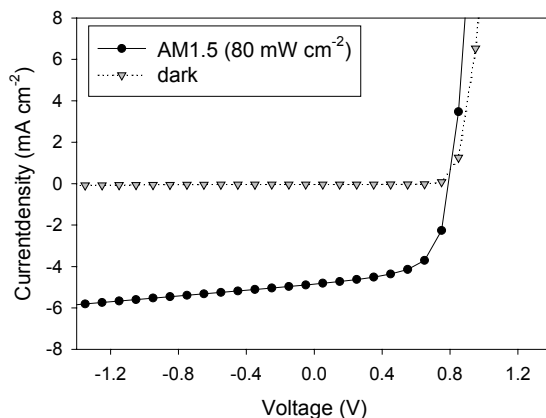
figure 5.8 Current density versus voltage characteristic of a typical bulk hetero junction MDMO-PPV:PCBM solar cell under light and in dark

As shown in figure 5.8, under light a negative current and positive voltage can be observed in the fourth quadrant, indicating an energy gain within this electrical system. Typical parameters (as defined in section 5.2.2) such as fill factor, open-circuit voltage, short-circuit current(-density) and efficiency can be easily extracted out of this data.

The photovoltaic performance of devices based on sulfinyl synthesized MDMO-PPV is compared with the reference 'state-of-the-art' cells based on Gilch synthesized MDMO-PPV. Therefore, a rather high number of cells with an approximately 100 nm thick active layer, based on B-SUL and N-GIL MDMO-PPV are characterized under AM1.5 illumination. These devices are prepared according to the description presented in section 5.2.1. The B-SUL MDMO-PPV material is chosen because it has a chemical defect structure (e.g. sp^3 interruptions and regioregularity) that resembles the chemical defect structure of N-GIL MDMO-PPV.

Summarizing these results, an overview listing the values for the solar cell parameters of the B-SUL and N-GIL MDMO-PPV devices is given in table 5.1.

	B-SUL MDMO-PPV	N-GIL MDMO-PPV
V_{oc} (V)	0.8	0.8
J_{sc} (mA cm^{-2})	4.7	4.2
FF (%)	62	59
$\eta_{AM1.5}$ (%)	2.9	2.5

table 5.1 Overview op the typical solar cell parameters obtained for N-GIL MDMO-PPV (reference) and B-SUL MDMO-PPV based photovoltaic devices

A nice result is the obtained efficiency of 2.9 % using B-SUL MDMO-PPV. At that moment this increase with 15 % in efficiency for the sulfinyl based solar cells compared to the Gilch based ones was a new efficiency record.
As shown in table 5.1, the increase in efficiency (2.9 versus 2.5 %) is obtained via both an increase in FF (62 versus 59 %) and an increase in J_{sc} (4.5 versus 4.2 mA cm^{-2}).
The incident photon per converted electron ratio (IPCE) as a function of wavelength is presented in figure 5.9 for a B-SUL and N-GIL MDMO-PPV:PCBM 100 nm bulk hetero junction solar cell.
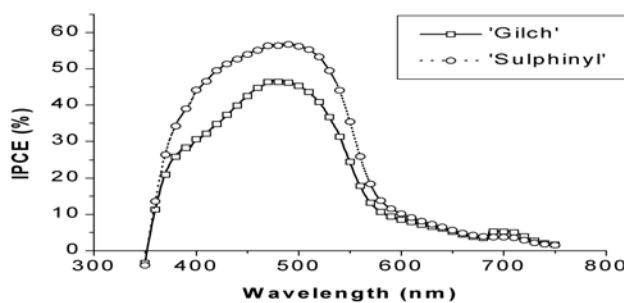
figure 5.9 The incident photon per converted electron ratio (%) (IPCE) versus the wavelength for a 100 nm N-GIL and B-SUL MDMO-PPV:PCBM bulk hetero junction photovoltaic device

It is shown that the sulfinyl MDMO-PPV based device is more efficient in converting photons to electrons than the Gilch one (a maximum value of 55 % versus 45 %). The maximum value is for both devices found at a wavelength of about 470 nm.
The N-GIL MDMO-PPV IPCE curve, the values for the fill factor, short-circuit current density, open-circuit voltage and power conversion efficiency are in accordance with reported values in literature[8].

Comparing the AM1.5 power conversion efficiency an increase of 15 % is observed for the 'sulfinyl' versus the 'Gilch' 100 nm 'state-of-the-art' solar cells. Although these results are close to the reproducibility, these values are observed for two totally separately prepared series of a significant population of samples. Furthermore these results are reproduced at the Energieonderzoek Centrum Nederland (ECN) (Petten, the Netherlands)[22].

5.3.2 Thickness dependency study for B-SUL and N-GIL MDMO-PPV

The reported increase of the photovoltaic performance for the B-SUL MDMO-PPV based cells compared to the widely used reference photovoltaic devices based on Gilch synthesized MDMO-PPV (e.g. N-GIL) clearly demonstrates that the sulfinyl route can lead to beneficial and promising results for plastic electronic applications. This is already an answer on one of the key questions at the start of this work.
A study of the dependency of the photovoltaic performance on the thickness of the active semiconductor layer is performed for the B-SUL and N-GIL MDMO-PPV based solar cells to get more insight in this phenomenon.
A large number of cells with a thickness variation of the active semiconductor layer between 50 and 200 nm is examined. The thickness of the active layer is measured via a photon absorption measurement at the λ_{max} value of MDMO-PPV. The calibration of this method is performed via a profile measurement perpendicular to a scratch in the bulk hetero junction layer, with an AFM equipment.

In figure 5.10 the thickness dependency of the photovoltaic efficiency under AM1.5 illumination (80 mW cm^{-2}) is plotted for cells based on both materials. The photovoltaic devices are prepared according to the conditions described in section 5.2.1. The typical solar cell parameters are determined via the formulas described in section 5.2.2. Each data point represents a single substrate with three individual solar cells. The variation between these individual photovoltaic devices is plotted as an error bar. These data points include two independently prepared series of solar cells based on either N-GIL or B-SUL MDMO-PPV.
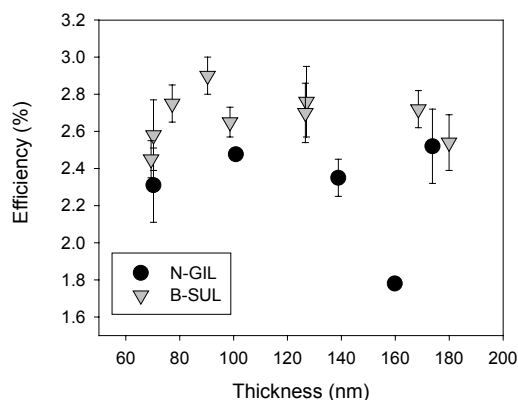
figure 5.10 The power conversion efficiency under AM1.5 illumination (80 mW cm^{-2}) for a significant population (total number of devices = 45) of N-GIL and B-SUL MDMO-PPV:PCBM bulk hetero junction solar cells

Evaluating the thickness dependency of the conversion efficiency it is shown that this difference between the N-GIL and B-SUL devices is somewhat decreasing with increasing thickness of the active layer. The major increase of efficiency of the B-SUL devices compared to the N-GIL devices can be observed for rather thin devices.

A highly interesting feature of these devices is their rather expressed thickness independent efficiency. A variation of nearly a factor three in the thickness results in no significant changes of the efficiency. This behavior is interpreted as one of the typical characteristics of thin film bulk hetero junction devices, where the photoactive layer comprises rather low transport mobility but outstanding high lifetimes for the charge carriers.

Although the efficiency is an important parameter expressing solar cell performance, it is only a sort of overall number. Therefore the J_{sc}, FF and V_{oc} are also examined versus the active layer thickness.

All studied samples yield a value for the V_{oc} of about 0.8 V. This is in accordance with the results of Brabec et al. indicating a linear correlation between acceptor strength and the V_{oc}[23].

In figure 5.11 the J_{sc} is presented versus the active layer thickness.
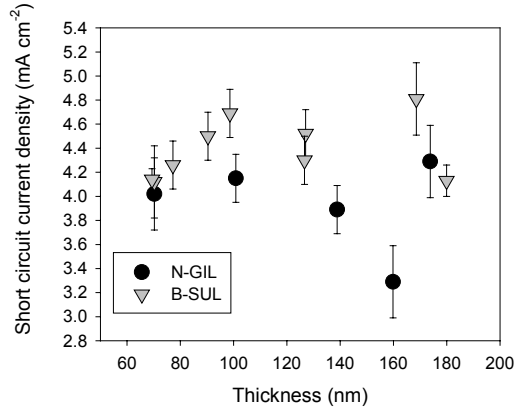
figure 5.11 The short-circuit current density under AM1.5 illumination (80 mW cm^{-2}) for a significant population (total number of devices = 45) of N-GIL and B-SUL MDMO-PPV:PCBM bulk hetero junction solar cells

As shown in figure 5.11 a clear increase of can be observed versus the thickness. At about 100 nm this increasing trend starts to saturate. This is understood in terms of a change from an absorption-limited regime to a mobility-limited regime. This effect is more pronounced for the B-SUL material. Similar to the trend observed for the efficiency, also in this case the major increase in J_{sc} for the B-SUL MDMO-PPV based devices is observed for rather thin devices (90-120 nm).

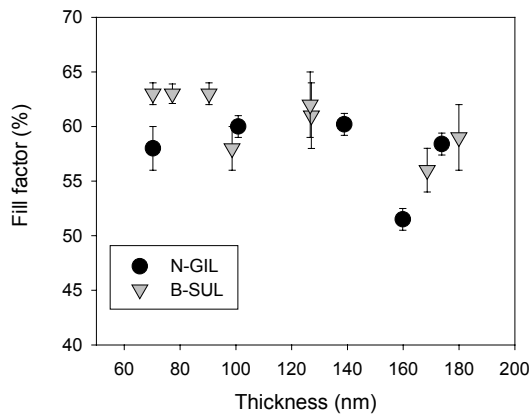In figure 5.12, the fill factor versus the thickness of the active layer is plotted.

figure 5.12 Fill factor under AM1.5 illumination (80 mW cm^{-2}) for a significant population (total number of devices = 45) of N-GIL and B-SUL MDMO-PPV:PCBM bulk hetero junction solar cells

The fill factor starts to decrease as function of the thickness at about 140 nm. This behavior is understood in terms of a limited mobility of the charge carriers, favoring more recombination. Within this data, a similar behavior as already observed for the J_{sc} can be observed, namely: some higher values for the B-SUL MDMO-PPV cells more pronounced for the thin devices and a decreasing difference between the photovoltaic performance of both materials for the thicker devices.

It can be concluded that the major difference between the photovoltaic performance of both N-GIL and B-SUL MDMO-PPV is more pronounced for rather thin devices. Both the J_{sc} and the FF have higher values for the B-SUL MDMO-PPV batch. An overview of these values was given in table 5.1. The sulfinyl (e.g. B-SUL) MDMO-PPV based devices are more efficient in converting photons to electrons than the Gilch (e.g. N-GIL) ones. This behavior cannot be understood via the parameters determined in chapter 3 and chapter 4. At least the higher FET-mobility of the pure N-GIL material is either no representative measure for the actual active layer or this effect is compensated by a secondary effect. A hypothesis is indeed that due to the higher molecular weight of the N-GIL MDMO-PPV a different morphology of the bulk hetero junction is obtained.

5.3.3   The sulfinyl MDMO-PPV based solar cells

Based on the results described in the previous sections, two interesting studies within the group of sulfinyl based MDMO-PPV materials can be made. Firstly, the three regiorandom MDMO-PPV materials (e.g. A-SUL, B-SUL and C-SUL) with similar molecular weights and small differences in mobility are compared in photovoltaic devices. Secondly, the R-SUL material with clearly different material properties (e.g. mobility) (chapter 3 and chapter 4) is examined and compared with the B-SUL MDMO-PPV. As indicated in table 2.1 both materials have a similar number of sp^3 interruptions but difference in regioregularity.

5.3.3.1 Regiorandom sulfinyl MDMO-PPV

In this paragraph, a small set of regiorandom sulfinyl MDMO-PPV (e.g. A-SUL, B-SUL and C-SUL) based solar cells prepared at the 'Instituut voor Materiaal Onderzoek' (IMO) at the 'Limburgs Universitair Centrum' (LUC) are compared.

A set of rather thick photovoltaic devices (250 nm) is prepared according to the conditions described in section 5.2.1. The data plots consist of two independently prepared populations of photovoltaic devices of A-SUL, B-SUL and C-SUL MDMO-PPV as varied parameter. In figure 5.15 the power conversion efficiency under AM1.5 illumination (80 mW cm^{-2}) is depicted for the different regiorandom sulfinyl MDMO-PPV based solar cells.
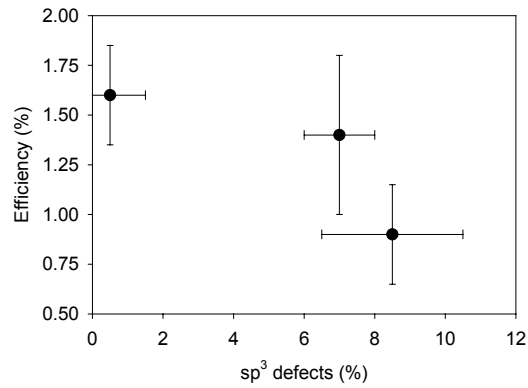
figure 5.13 The power conversion efficiency under AM1.5 illumination (80 mW cm^{-2}) for a significant population of the regiorandom sulfinyl synthesized MDMO-PPV:PCBM bulk hetero junction solar cells (e.g. A-SUL, B-SUL and C-SUL) as function of the number of sp^3 defects

As shown in figure 5.13 a small decreasing trend as function of the number of sp^3 defects is observed. The differences between A-SUL and B-SUL are rather small. The obtained error bars indicate that the observed trend is at the limit to be significant.

The lower efficiency values compared to the one presented in section 5.3.2 can be explained in terms of the higher thickness of the bulk hetero junction layer combined with differences in preparation and characterization (e.g. differences in calibration of the solar simulator) between both research locations (LUC versus Linz). Due to these differences, in this section, there is no focus on the absolute value of the photovoltaic resuls but more on the the relative trend.

Beside the efficiency more specific values are extracted out of the data. In figure 5.14 and figure 5.15 the J_{sc} and FF are presented as function of the number of sp^3 defects.
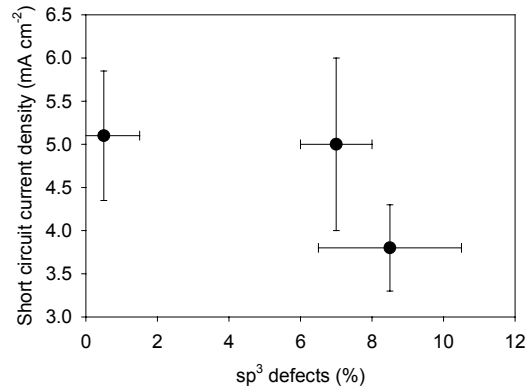
figure 5.14 The short-circuit current density under AM1.5 illumination (80 mW cm^{-2}) for a significant population of the regiorandom sulfinyl synthesized MDMO-PPV:PCBM bulk hetero junction solar cells (e.g. A-SUL, B-SUL and C-SUL) as function of the number of sp^3 defects
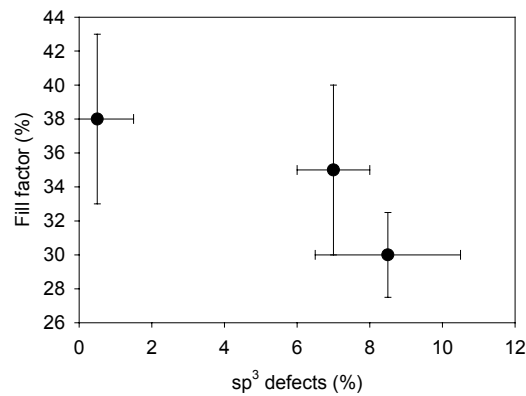
figure 5.15 The fill factor under AM1.5 illumination (80 mW cm^{-2}) for a significant population of the regiorandom sulfinyl synthesized MDMO-PPV:PCBM bulk hetero junction solar cells (e.g. A-SUL, B-SUL and C-SUL) as function of the number of sp^3 defects

The decrease in efficiency as function of the increase in sp^3 defects as observed for the regiorandom sulfinyl synthesized MDMO-PPV solar cells in figure 5.13 is caused by both a decrease of the FF (figure 5.15) and a decrease of the Jsc (figure 5.14).

As the studied devices are rather thick, the observed differences can indeed be explained via a decreasing trend in the mobility with an increasing number of sp^3 defects.

5.3.3.2 *Regioregular sulfinyl MDMO-PPV*

An overview of the values for the typical solar cell parameters of the R-SUL compared to the B-SUL MDMO-PPV based devices (thickness 250 nm) prepared at the LUC is indicated in table 5.2.

	B-SUL MDMO-PPV	R-SUL MDMO-PPV
V_{oc} (V)	0.8	0.5
J_{sc} (mA cm^{-2})	5.0	4.0
FF (%)	36	33
$\eta_{AM1.5}$ (%)	1.5	0.8

table 5.2 Overview op the typical solar cell parameters obtained for B-SUL MDMO-PPV and R-SUL MDMO-PPV based photovoltaic prototype devices as prepared at the LUC

The major observed difference is a decrease in the value for the V_{oc} of the R-SUL material. Besides this strong decrease, a limited decrease is observed for all other typical solar cell parameters (e.g. J_{sc} and FF). This results in a very weak overall photovoltaic efficiency. In spite of the promising properties for the FET-mobility of the R-SUL material, this could not be recognized in the solar cell performance.

5.3.4   Morphology

When comparing B-SUL and N-GIL only minor differences in the previously studied parameters (chapter 3 and chapter 4) could be obtained. However, a higher solar cell performance for the B-SUL MDMO-PPV based photovoltaic devices compared to the reference devices based on N-GIL MDMO-PPV was observed. Beside some limited differences in chemical defect structure, these MDMO-PPV materials have a major difference in molecular weight (table 2.2). The N-GIL material has approximately a double weight-average molar mass (M_w) compared to the B-SUL MDMO-PPV. As a consequence difference in viscosity behavior are observed. When spincoating the in chlorobenzene solved mixture of PCBM:MDMO-PPV a sort of phase separation occurs. An influence of the viscosity of the polymeric fraction (MDMO-PPV) on the via phase separation induced morphology can be expected.

Therefore, the morphology of the bulk hetero junction is studied by means of TEM techniques.
Thin freestanding samples are prepared via drop casting of the MDMO-PPV:PCBM solution in chlorobenzene on a cupper grid. Although this method will not fully represent the active bulk hetero junction layer

obtained via spincasting, it is a good method to compare qualitatively the different morphologies caused by different MDMO-PPV batches. The TEM images (magnification 53000×) of the different batches of MDMO-PPV are depicted in figure 5.16.
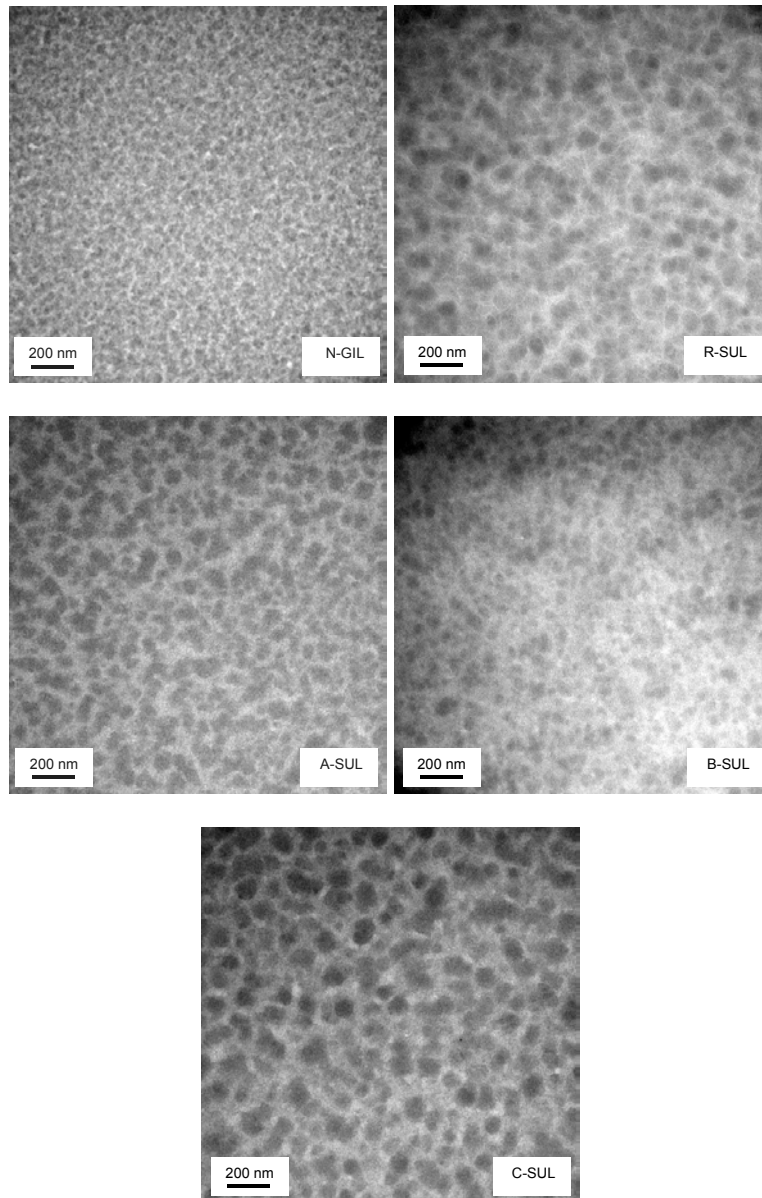
figure 5.16 TEM images (53000×) of thin freestanding films prepared via dropcasting of MDMO-PPV:PCBM solutions in chlorobenzene

A number of observations could be made. First of all, a spatial dependency of the morphology could be observed. Thinner places have in general somewhat smaller PCBM regions (black regions) than thicker places. The information on the morphology of the different MDMO-PPV derivatives mixed with PCBM, as depicted in figure 5.16 is obtained for spatial regions more or less equal in thickness. Information of the spatially dissolved thickness could be obtained via a measurement of the beam intensity at the backside of the specimen.

The major observed difference is between the sulfinyl and Gilch synthesized MDMO-PPV batches. The PCBM regions are clearly (about a factor of two) smaller when using Gilch MDMO-PPV. Within the group of sulfinyl synthesized batches differences are not that pronounced. However two batches have somewhat bigger PCBM regions, namely the R-SUL and the C-SUL batches of MDMO-PPV.

A summary of the differences in morphology is indicated in table 5.3.

MDMO-PPV	Estimation of the PCBM region (nm)	M_w $(10^3$ g mol$^{-1})$ *(Extracted from table 2.2)*
A-SUL	50-110	820
B-SUL	50-110	615
C-SUL	70-140	504
N-GIL	30-90	1386
R-SUL	70-140	554

table 5.3 Summary of the values for the size of the PCBM regions for the different MDMO-PPV batches blended with PCBM in a 1 to 4 ratio

As denoted in table 5.3, a clear inverse correlation between the size of the PCBM channel and the molecular weight of the MDMO-PPV batch is observed. The highest molecular weight (and as such the highest viscosity) MDMO-PPV batch (e.g. N-GIL) yields the smallest PCBM phase separated regions. The lowest molecular weight (e.g. C-SUL MDMO-PPV) shows the largest PCBM regions. However, the R-SUL MDMO-PPV has also some large PCBM regions although the molecular weight is somewhat more intermediate. This is understood in terms of more pronounced interactions between the individual MDMO-PPV chain segments.

This introductory morphology study gives somewhat more insight in the observed solar cell performance for the matrix of MDMO-PPV materials:
First of all the difference in morphology between the N-GIL and B-SUL material can be used to explain the difference in solarcell performance. This should mean that the morphology of the sulfinyl material blended with

PCBM is a more optimized morphology with respect to conerting photons to electrons.

Comparison of the regiorandom sulfinyl materials yielded a somewhat worse performance for the C-SUL MDMO-PPV based photovoltaic devices. Besides the already mentioned lower mobility of this material also the slightly larger PCBM regions can contribute to this results.

The higher mobility of the regioregular material is explained in terms of an enhanced interaction between the individual chain segments. Blending the R-SUL with PCBM most likely induces a reduction of these interactions and/or leads to a different composition of MDMO-PPV:PCBM matrix in between of the dark PCBM regions. As at the moment no good physical model is available including morphology and composition of intermediate phases. Allthough this hypothesis is most likely, it could be quantified within the timeframe of this work.

As shown, useful information of the morphology of the MDMO-PPV:PCBM blend is obtained via a limited TEM research. However, a number of remarks should be made when using these results to interpret the photovoltaic performance of the different batches of MDMO-PPV.

Martens et al.[21] showed that the film preparation technique has an omnipresent influence on the morphology of the blend. Therefore the observed results should be used preferable in a qualitative and relative way rather than quantitative.

Secondly, besides the size of the PCBM channels, another important parameter is the ratio of PCBM and MDMO-PPV in the with-gray regions. Unfortunately within this limited morphological study no information of the compounding of the matrix, was obtained.

5.4   Conclusions

The major observation within chapter 5 is the improvement of the reference N-GIL MDMO-PPV solar cell efficiency (under AM1.5 illumination 80 mW cm^{-2}) with about 15% by using sulfinyl MDMO-PPV with a low or intermediate number of sp^3 defects (e.g. A-SUL or B-SUL).

An overview of the obtained efficiencies related to the 'state-of-the-art' photovoltaic devices based on Gilch synthesized MDMO-PPV is given in a relative way in figure 5.17.
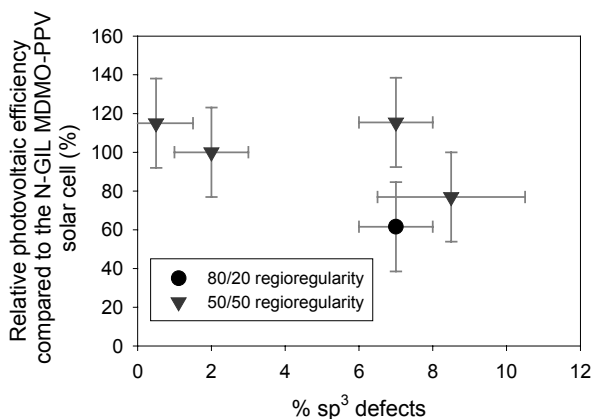
figure 5.17 The relative photovoltaic efficiency compared to the N-GIL MDMO-PPV

A thickness dependency study of the value of J$_{sc}$, FF and efficiency could not totally clarify the observed differences. However indications where found that the performance increase can be understood in terms of differences in morphology. Especially the differences observed for the rather thin photovoltaic devices can be understood in terms a higher collection and conversion capacity of the sulfinyl morphology. However no physical model including this morphology differences is available at the moment. Within our group, Martens et al. take these observations as input in a more profound research trying to clarify this relation between morphology and photovoltaic performance.

In order to exclude the rather high morphological differences a comparison of the regiorandom sulfinyl synthesized MDMO-PPV based solar cells was performed. This indicates a small trend of increasing performance with decreasing number of sp^3 defects. Although also within this result a morphology effect could not be totally excluded.

Finally the comparison of the R-SUL MDMO-PPV based cells with the B-SUL ones indicates a very weak performance of the (promising) regioregular material.

A comparison of the matrix of MDMO-PPV materials in photovoltaic devices indicates a rather complex balance between the individual material parameters in order to obtain a high performance bulk hetero junction solar cell. As the morphology of the active layer plays an omnipresent role, research is even more complicated by a strong influence of the processing parameters. On one hand this give an enormous opportunity for optimization of the polymeric solar cells. On the other hand control of this morphology will be a key-issue in getting an industrial successful processing.

From more scientific point-of-view a major challenge is the development of a physical model including the major material parameters and the morphological parameters either related to the material properties or the processing.

5.5   *References*

[1]   G. Yu, K. Pakbaz, A. J. Heeger, *Appl. Phys. Lett.* (**1994**) 64, 3422.

[2]   N.S. Sariciftci, L. Smilowitz, A.J. Heeger, F. Wudl, *Science* (**1992**) 258, 1474.

[3]   a) L. Smilowitz, N.S. Sariciftci, R. Wu, C. Gettinger, A.J. Heeger, F. Wudl, *Phys. Rev B* (**1993**) 47, 13835. b) B. Kraabel, J.C. Hummelen, D. Vacar, D. Moses, N.S. Sariciftci, A.J. Heeger, F. Wudl, *J. Chem. Phys.* (**1996**) 104, 4267. c) N.S. Sariciftci, A.J. Heeger, *Int. J. Mod. Phus. B* (**1994**) 8, 237. d) N.S. Sariciftci, *Prog. Quant. Electr.* (**1995**) 19, 131. e) X. Wei, Z.V. Vardeny, N.S. Sariciftci, A.J. Heeger, *Phys. Rev. B* (**1996**) 53, 2187.

[4]   a) S. Morita, A.A. Zakhidov, K. Yoshino, *Solid State Commun.* (**1992**) 82, 249. b) K. Yoshino, X.H. Yin, S. Morita, T. Kawai, A.A. Zakhidov, *Solid State Commun.* (**1993**) 85, 85. c) S. Morita, A.A. Zakhidov, K. Yoshino, *Jpn. J. Appl. Phys.* (**1993**) 32, L873. d) K. Yoshino, T. Akashi, K. Yoshimoto, S. Morita, R. Sugimoto, A.A. Zakhidov, *Solid State Commun.* (**1994**) 90, 41.

[5]   a) J.J.M. Halls, K. Pichler, R.H. Friend, S.C. Moratti, A.B. Holmes, *Appl. Phys. Lett.* (**1996**) 68, 3120. b) J.J.M. Halls, R.H. Friend, *Synth. Met.* (**1997**) 85, 1307. c) N.S. Sariciftci, D. Braun, C. Zhang, V.I. Srdanov, A.J. Heeger, G. Stucky, F. Wudl, *Appl. Phys. Lett.* (**1993**) 62, 585.

[6]   G. Yu, J. Gao, J.C. Hummelen, F. Wudl, A.J. Heeger, *Science* (**1995**) 270, 1789.

[7]   C.J. Brabec, F. Padinger, J.C. Hummelen, R.A.J. Janssen, N.S.Sariciftci, *Synth.Met.* (**1999**) 102/1-3, 861.

[8]   S.E. Shaheen, C.J. Brabec, N.S. Sariciftci, F. Padinger, T. Fromherz, J.C. Hummelen, *Appl.Phys.Lett.* (**2001**)78/6, 841.

[9]   T. Martens, J. D'Haen, T. Munters, Z. Beelen, L. Goris, J. Manca, M. D'Olieslaeger, D. Vanderzande, L. De Schepper, R. Andriessen, *Synth. Met.* (**2003**) 138, 243.

[10]   *Presseabteilung* Siemens, G. Weber (**2004**) Informationsnummer CT200309.001d

[11]   a) M. Granstorm, K. Petritsch, A.C. Arias, A. Lux, M.R. Andersson, R.H. Friend, *nature* (**1998**) 395, 257. b) G. Yu, A.J. Heeger, *J. Appl. Phys.* (**1995**) 78, 4510

[12]   a) C.J. Brabec, S.N. Sariciftci, *Monatshefte für chemie* (**2001**) 132, 421. b) C.J. Brabec, N.S. Sariciciftci, J.C Hummelen, Adv. Funct. Mater. (**2001**) 11(1), 15.

[13]   J.C.Hummelen, B.W.Knight, F.Lepec, F.Wudl, J. Yao, C.L. Wilkins, *J.Org.Chem.* (**1995**) 60, 532.

[14]   C.J.Brabec, F.Padinger,N.S.Sariciftci,J.C.Hummelen, *J. Appl. Phys. Lett.* (**1998**) 73, 1185.

15 A.C. Arias, M. Gränström, D.S. Thomas, K. Petritsch, R.H. Friend, *Phys. Rev. B* (**1999**) 60, 1854.

16 C.J. Brabec, S.E. Shaheen, C. Winder, N.S. Sariciftci, *Appl. Phys. Lett.* (**2002**) 80(7), 1288.

17 M.A. Green, *Solar Cells- Operating principles, technology and system applications*, University of Sout Wales, Kensigton (**1992**)

18 P.M. Sommeling, H.C. Rieffe, J.A.M. van Roosmalen, A. Schonecker, J.M. Kroon, J.A. Wienke, A.Hinsch, *Solar Energy Materials and Solar Cells*, (**2000**) 62/4, 399.

19 W. Geens, *Ph.D Dissertation* (**2002**) Universiteit Antwerpen.

20 C.J. Brabec, G. Zerza, G. Cerullo, S. De Silvestri, S. Luzzati, J.C. Hummelen, N.S. Sariciftci, *Chem. Phys. Lett*. (**2001**) 340, 232.

21 T.Martens, J. D'Haen, T. Munters, L. Goris, Mat. Res. Soc. Symp. Proc. (2002) 725, 7.11.1.

22 www.ecn.nl or info@ecn.nl

23 C.J. Brabec, A. Cravino, D. Meissner, N.S. Sariciftci, M.T. Rispens, L. Sanchez, J.C. Hummelen, T. Fromherz, *Thin Solid Films* (**2002**) 403-404, 368.

Chapter 6
Structure-property relations and conclusions

In chapter 6, the structure-property relations as described separately in the individual chapters will be brought together yielding general conclusions. I) The single bond defects causing conjugational interruptions have within the studied range of variations only a limited effect on the macroscopic MDMO-PPV properties due to the occurrence of slow, morphology dependent, interchain charge transfer processes. A more significant effect of the level of sp³-defects is demonstrated for the intrachain mobility with introductory time-resolved microwave-conductivity (TRMC) measurements. II) The major effect on the macroscopic electro-optical properties of MDMO-PPV is regioregularity. The presence of an enhanced structural order in the regioregular MDMO-PPV film used to explain the performance difference is proven via TEM.

Two type of defects related to asymmetrically substituted PPV-derivatives, such as the 'workhorse' material MDMO-PPV can be distinguished: defects related with interruptions of the conjugated system at the vinylene double bond (single bond defects**)** (also denoted as sp^3 defects) and defects related with the position of the side-chains (regioregularity). It is shown that the sulfinyl precursor route exhibits a versatile chemistry and can control both mentioned defects. The main goal of this work was to examine the relation between both mentioned defects (e.g. regioregularity and single bond defects) of MDMO-PPV and its semiconducting performance (structure-property relation). This information should lead to a fine-tuning of the

synthetic strategies for future generations of sulfinyl synthesized semiconducting polymers.

Firstly, in section 6.1 the structure-property relations of the single bond defects on the performance of MDMO-PPV, as described separately in the previous chapters is discussed. In this work, there was a strong focus on macroscopic properties of the individual devices. However, in section 6.1.2 very promising preliminary results obtained from a collaboration with the TU-Delft describing intrachain electronic properties are presented.

As described in the individual chapters, regioregularity is the most powerful tool to tune the electrical and optical semiconducting properties of MDMO-PPV. Besides a discussion about this structure-property relation (section 6.2.1), an additional Transmission Electron Microscopy (TEM) diffraction study will give insight in the exact nature of the enhanced order in the regioregular MDMO-PPV film (section 6.2.2).

Finally, some overall conclusions of this work and advises for future synthetic strategies are highlighted. Additionally, two general scientific prospectives towards future electronic applications are formulated.

6.1   Single bond defects

6.1.1   Structure-property relation

Within the presented variation in conjugational defects, only limited differences in semiconducting performance of MDMO-PPV could be observed.

The observed differences for the electrical properties within the regiorandom batches are small and at the limit of our instrumental reproducibility. However a consistent trend line could be fitted for the mobility, conductivity and pre-factor, with a normalized value of about -4 10^{-2} (% defects)$^{-1}$ for the A-SUL, B-SUL and N-GIL MDMO-PPV material.

The optical observations within the group of regiorandom materials indicate an extremely small difference at the limit of reproducibility. Only a very small increase op the photoluminescence efficiency and photoluminescence decay time could be observed as function of the number of sp^3 defects. This is explained via a slightly higher exciton motion as observed with the electrical measurements. However influences of differences in aggregation cannot totally be excluded. A normalized slope indicates approximately a decrease in photoluminescence properties of –7 10^{-3} (% defects)$^{-1}$.

Although the individual trends of the measured performance as function of the percentage single bond defects are rather small and hardly significant, the overall trend is consistent throughout both optical and electrical properties determined in this work. Within the scientific community,

similar trends are observed for both the electrical and optical parameters of related conjugated polymers. It is shown by Johansson et al. that through the insertion of methoxy groups as side chains and low polymerization temperatures BOP-PPV and BOPM-PPV could be obtained with a decrease of the content of defects, resulting in higher electroluminescence yields in LED's. The decrease in TBB content for BOP-PPV (from 5.8 % to 3.5 %) and BOPM-PPV (from 2.0 % to < 1.0 %) increased the electruminescence yield from 1.23 % to 1.34 % and 0.45 % to 1.74 % respectively[1]. It is furthermore known from the literature that shortening of the conjugation length improves the photoluminescence yields by decreasing the probability of exciton diffusion to defects, where nonradiative decay to the ground state can occur[2]. Braun et al.[3] have observed for a series of O-PPV polymers, with controlled fractions of non-conjugated segments (m<50%), an increase of PL efficiency with the fraction of non-conjugated segments due to the decrease in intrachain mobility.

The observed electrical properties within the group of regiorandom MDMO-PPV materials are somehow similar to the results of Martens et al.[4] who studied the field dependency of the mobility determined via hole-only devices of MDMO-PPV and a copolymer of MDMO-PPV units and (non-conjugated) phenylene-ethylidene units. was made by. The strongest limitation of the hampered charge transport of the partly conjugated material is an increased inter-site distance.

When blending these regiorandom materials with PCBM in order to examine the photovoltaic performance new effects occur. The main result in this work is a 15% higher solar cell performance for the sulfinyl MDMO-PPV ($\eta_{AM1.5}$ 2.9 %) based photovoltaic devices compared to the widely accepted Gilch ones ($\eta_{AM1.5}$ 2.5 %). The latter were for a long time the best polymeric solar cells within the scientific community. Via a TEM morphology study, the influence of the molecular weight (considerably higher for the Gilch synthesized MDMO-PPV) on the bulk morphology is proven. Indications of an omnipresent influence of the morphology on the photovoltaic performance could be found.

The differences in photovoltaic properties between the Gilch MDMO-PPV based cells compared to the sulfinyl MDMO-PPV based cells are mainly observed for the sulfinyl batches with a relatively small number of defects. This indicates a secondary parameter namely the MDMO-PPV bulk mobility. Excluding the molecular weight effect by comparison of regiorandom sulfinyl synthesized MDMO-PPV batches, a weak trend similar as the one observed for the mobility is shown for the photovoltaic performance.

6.1.2   Electronic intrachain properties

Regarding the small effect of the level of sp[3]-defects on the FET-mobility it is important to emphasize the macroscopic nature of this type of measurements. In FET-measurements and DC-measurements in general, the charge carriers drift throughout the bulk material under the influence of an applied electric field over macroscopic distances. As a consequence, the charge transport that is probed involves not only motion along the polymer chains but also much slower, morphology dependent, processes such as the transfer of charge between neighbouring chains and migration across grain boundaries and/or defects[5]. A powerful tool to study the intrinsic mobility of charge carriers is the time-resolved microwave-conductivity (TRMC) technique, which is based on the absorption of high frequency (~30 GHz) microwaves and uses an electrode-less measurement described in detail elsewhere[6]. In order to study the influence of the level of sp[3]-defects in MDMO-PPV on the intrinsic mobility, a collaboration has started with the group of Prof. dr. J. Warman and Prof. dr. L. Siebbeles at the Radiation Chemistry Department (IRI) of the Delft University of Technology. The initial measurements using the pulse radiolysis time-resolved microwave conductivity (PR-TRMC) technique have been performed on 3 materials from the studied MDMO-PPV-matrix : A-SUL, B-SUL and C-SUL MDMO-PPV. In the table below the preliminary intrachain hole mobility results are presented as obtained by ir. P. Prins and dr. L. Candeias on the materials dissolved in benzene (concentration 0.1 mM).

MDMO-PPV	Intrachain hole mobility ($cm^2 V^{-1} s^{-1}$)
A-SUL	1.20
B-SUL	0.75
C-SUL	0.52

table 6.1 Preliminary intrachain hole mobility values obtained with PR-TRMC on a set of MDMO-PPV materials dissolved in benzene (referentie : The measurements have been performed at the Radiation Chemistry Department, IRI, Delft University of Technology by ir. P. Prins and dr. L. Candeias)

These initial results show a high intrachain hole mobility for all materials and a clear inverse relation between the level of sp[3]-defects and the intrachain hole mobility. Further experiments have to be performed in order to determine the definitive values of the intrachain hole mobility for the various MDMO-PPV-materials, but it is clear also from investigations of other conjugated polymers that the presented technique is extremely suitable to obtain this information.
From the obtained DC-results and the considerations made above it can be concluded that the effect of the level of sp[3]-defects on the macroscopic

transport properties is rather small due to the occurrence of slow, morphology dependent, interchain charge transfer processes. A more significant effect of the level of sp^3-defects is expected for the intrachain mobility. In order to obtain a fundamental understanding of the relation between the level of sp^3-defects and the intrinsic mobility it is highly recommended to continue this work. The initiated collaboration in this field between TU-Delft and LUC is extremely promising since it allows to study systematically a set of materials with 'tunable' defect levels obtained through state-of-the-art synthesis with unique and powerful measurement techniques which assess directly the intrinsic mobility of charge carriers.

6.2   Regioregularity

6.2.1   Structure-property relation

A large influence of the regioregularity is observed via a comparison of a regioregular (80/20) sulfinyl synthesized MDMO-PPV batch with the regiorandom, either Gilch or sulfinyl synthesized MDMO-PPV. Notice that within the scope of this thesis not a fully regioregular material is chosen in order to have a compromise between pure material properties and the processing properties of that material. This already indicates a potential for further optimization of this approach.

An increase of about a factor of two for the values of the electrical properties (mobility and conductivity) for the regioregular material compared to the regiorandom batches is observed.

A similar result is shown for the optical properties. A clear red shift in the photoluminescence spectra is observed for the regioregular material. Either the photoluminescence efficiency and photoluminescence radiative lifetime of the regioregular MDMO-PPV compared to the regiorandom batches is about a factor of two lower. Combination of both observation lead to the conclusion that the partly regioregular material has an equal natural radiative lifetime compared to the regiorandom materials but a significantly faster nonradiative decay time. This indicates an alternative nonradiative pathway not present (or only very limited) in the regiorandom batches. Most likely this is an aggregated species. In section 6.2.2 the results of a TEM diffraction study giving insight in the exact nature of this aggregated species for the regioregular MDMO-PPV is presented.

When mixing this promising regioregular material with PCBM in order to form bulk hetero junction organic solar cells performance drops down till a level even beneath the regiorandom materials. As indeed the high mobility is induced via chain segment interactions, blending the regioregular material with other compounds (such as PCBM for organic solar cell applications) can detrimentally influence this interaction.

6.2.2   TEM diffraction study

The observed differences described above can be interpreted in terms of enhanced chain interactions. Indications that this is indeed the case are obtained via a limited transmission electron microscopy diffraction study of the regioregular material.

Bao et al. reported a diffraction study of 100/0 regioregular poly(3-hexylthiophene) (P3HT) TFT's with high mobility (e.g. $5 \ 10^{-2} \ cm^2 \ V^{-1} \ s^{-1}$)[7].

Within this work a transmission electron diffraction pattern for the regioregular P3HT, showing strong diffraction around 3.7 Å is presented. This is interpreted as thiophene rings in their stacks formed between adjacent chains. This preferred orientation might help account for the relatively high mobility, since it would place the transport direction parallel to the substrate. Besides this stack, well-organized lamellar structures with an intermolecular spacing of 16,4 Å are found.

A diffraction study on a number of MDMO-PPV batches is performed in order to quantify this kind of order. However, a number of features complicate such a study on amorphous MDMO-PPV films. First of all, the absence of the relatively heavy elements (e.g. sulfur in P3HT) in MDMO-PPV yields a poor ratio between the elastic and inelastic contribution to the diffraction pattern, decreasing the signal to noise ratio. Secondly, within this work, the R-SUL MDMO-PPV batch exhibits only an enhanced regioregularity, as the ratio between both monomers is 80/20. Thirdly, the 3-7-dimethyloctyloxy side chain posses an asymmetrically substituted carbon atom at the 3-position. The substitution of this carbon atom is random for all studied batches of MDMO-PPV including the R-SUL MDMO-PPV batch. Most likely, this will suppress the formation of well-organized lamellar structures as present in P3HT.

Transmission diffraction patterns are recorded for the different MDMO-PPV batches. The 100 nm freestanding films needed in this experiments are prepared via 'peeling' of spincoated MDMO-PPV films on glass substrates. The specimen are placed on a dedicated cupper grid and inserted in a Philips CM12 transmission electron microscope (TEM) working in diffraction mode. Images are taken via a 'Gaton' digital camera with various integration times.

All samples were completely amorphous. Some very weak amorphous rings could be observed for all batches of MDMO-PPV at 1.2Å and 2.1 Å.

Transmission electron diffraction patterns of B-SUL and R-SUL MDMO-PPV thin films are exemplary shown in figure 6.1
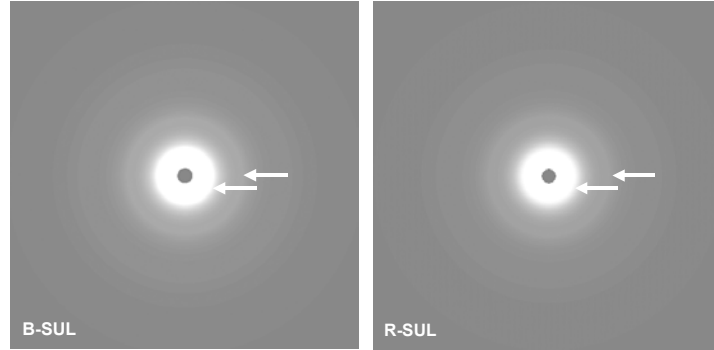
figure 6.1 Transmission electron diffraction pattern of a thin film of B-SUL and R-SUL MDMO-PPV

As electron diffraction suffers from a huge inelastic contribution, diffraction rings are very weak compared to this background and difficult to distinguish. Therefore a simple method to correct for this inelastic background is applied.

The inelastic differential cross-section ($\partial\sigma_{inel}/\partial\Omega$) can be described via equation 6.1[8].

$$\frac{\partial \sigma_{inel}}{\partial \Omega} = \frac{\lambda^4 \left(1 + E/E_0\right)^2}{4\pi^4 a_H^2} \frac{Z\left\{1 - \dfrac{1}{\left(1 + \left(\theta/\theta_0\right)^2\right)^2}\right\}}{\left(\theta^2 + \theta_E^2\right)^2}$$

equation 6.1 Description of the inelastic differential cross-section as function of the diffraction angle (θ) with Z the atomic number, λ wavelength of the electrons, E the energy of the electrons, a_H the Bohr radius, θ_0 the characteristic angle responsible for the decrease of the elastic differential cross-section (typical 10 mrad), θ_E the characteristic angle responsible for the decrease in inelastic differential cross-section (typical 0.1 mrad)

The total inelastic contribution (σ_{inel}) can be calculated via equation 6.2 as function of the diffraction angle (θ).

$$\sigma_{inel} = \int \frac{\partial \sigma}{\partial \Omega} \pi \sin \theta \, \partial \theta$$

equation 6.2 Total inelastic contribution as function of the diffraction angle and inelastic differential cross-section

The result of equation 6.1 and equation 6.2 gives a relation for the inelastic contribution as function of the diffraction angle and three independent fit parameters. This relation is used to fit the diffraction signal, as exemplary

shown for B-SUL MDMO-PPV in figure 6.2 as function of the diffraction angle.
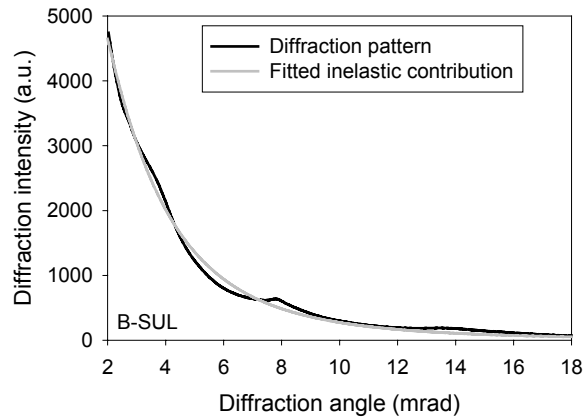
figure 6.2 Example of diffraction pattern and fitted inelastic contribution (B-SUL MDMO-PPV)

The residuals of this fit are plotted in figure 6.3 as function of the reciprocal diffraction angle, the diffraction distance (d) for the regiorandom sulfinyl material (B-SUL MDMO-PPV), the regiorandom Gilch material (N-GIL MDMO-PPV) and the regioregular sulfinyl material (R-SUL MDMO-PPV).
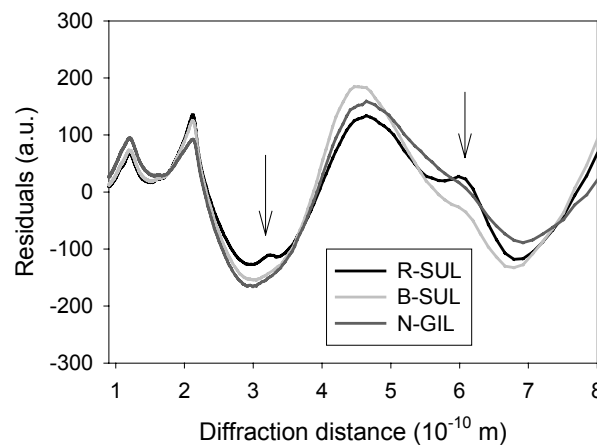
figure 6.3 Residuals of the diffraction pattern fitted with an inelastic contribution for the N-GIL, B-SUL and R-SUL material

The weak amorphous rings hardly visible in figure 6.2 are clearly shown in figure 6.3. Typical rings are observed for all samples at 1.2 Å, 2.2 Å and 4.4 Å. The latter is most likely a higher order ring of the 2.2 Å amorphous ring. The nature of these amorphous rings is not completely understood. All

regiorandom samples (e.g. A-SUL, N-GIL, B-SUL and C-SUL) exhibit an almost identical pattern.

The biggest difference observed is between the regioregular (e.g. R-SUL) and regiorandom batches of MDMO-PPV. An additional amorphous ring at 3.3 Å is observed for these samples. Most likely this ring can be interpreted in terms of additional order present within this material. The physical nature of this ring is not clear, however most likely it is related to some π–stacking between adjacent chains.

The TEM diffraction study with application of this correction method should be seen as a qualitative technique to indicate additional order in the R-SUL MDMO-PPV films compared to the regiorandom batches. For a complete quantitative analysis, the described technique is suffering from the very high inelastic scattering and as such is not useful.

6.3   General conclusion

The successful development at the 'Instituut voor Materiaal Onderzoek' (IMO) of the 'Limburgs Universitair Centrum' (LUC) of a new synthetic precursor route, the sulfinyl route allows the synthesis of organic semiconductor materials with a better-controlled structure and number of chemical defects. As this highly selective chemistry can control defects related to interruptions of the conjugated system at the vinylene double bond (single bond defects) and defects related to the position of the side-chains (regioregularity), new basic scientific questions appear: 'How to use these new synthetic possibilities to obtain high performance semiconducting organic polymers? What is the influence of regioregularity on the semiconductor properties? What is the influence of sp^3 defects (single bond defects) in the conjugated chain on the semiconductor properties?' Within this thesis these questions became progressively clear for a workhorse material MDMO-PPV, via a multidisciplinary approach, combining chemistry, physics and device engineering.

It can be concluded that the amount of regioregularity is the most powerful tool to tune the macroscopic electrical and optical semiconducting properties of pure MDMO-PPV materials. The regioregular MDMO-PPV material as used in this work is a promising material for a number of applications such as organic transistors. In these applications it can be used in a pure form for its high mobility properties. Disadvantage is a morphology dependency of this property complicating this method when blending this material or going to industrial processes. Therefore studying regioregular materials in bulk heterojunction photovoltaic devices requires a further optimization of the total morphology of the blend.
The single bond defect level can be used for a fine-tuning of the macroscopic semiconducting performance of MDMO-PPV. A small increase of the FET-mobility and a very weak influence on the optical properties could be observed. Depending on the desired application a sulfinyl MDMO-PPV material can be synthesized with either a high mobility (transistor and solar cell applications) or a high photoluminescence (PLED's).

These insights will be used to orient future extensions of the sulfinyl route to produce high performance conjugated polymers. The basic future synthetic strategy based on the outcome of this thesis would be to control and strengthening the interchain interactions. This should lead to materials with even higher mobilities. However potential new materials should combine excellent solubility properties (for processing) with these enhanced chain interactions. Besides a control of the interchain interactions, a control of the morphology of the bulk heterojunction is

needed for high performance solar cells. Currently, intensive effort is spent at LUC, by a.o. Martens et al. on a profound study of the MDMO-PPV:PCBM bulk hetero junction morphology which may lead to an improved insight in the morphology-performance relation of these photovoltaic devices.

It is shown that a combination of multiple disciplines (chemistry, physics and device engineering) is a key factor in solving structure-property relations in today's research fields such as plastic electronics. The structure-property relations clarified in this work emphasize the importance of a well-controlled chemistry to make semiconducting polymers successful in future products. The sulfinyl procedure can provide such a versatile and controllable chemistry.

6.4   Prospectives

Within this section two main directions for a further exploration of this work will be mentioned. The first, an increased stability through a reduction of TBB defects, can be situated in the nearby future as the first commercial applications of semiconducting polymers are appearing. For the second one, namely a transition from plastic electronics towards molecular electronics, commercial exploitation will be situated much farther in future. However this trend will lead to scientific excitement for at least the coming decades.

6.4.1   Increased reliability through reduction of TBB defects

The two major challenges in the field of organic based electronics are the increase of performance and the increase of reliability/stability of organic based semiconductor devices. While in this work we have mainly focused on the role of defects on the electro-optical performance of various semiconductor devices, it is important to emphasize that the presented 'sulphinyl' route can also play an important role towards plastic electronics with improved stability.

It has been demonstrated by Becker et.al. that the defect level within Gilch PPVs can have a strong influence on the operational lifetime of PLED's. They have shown that by decreasing the TBB content by a factor of ~2 leads to an increase in the lifetime by a factor of ~30. This is illustrated in the next figure, showing electroluminescence vs time curves during accelerated ageing for PLED's based on two polymers with similar emission color and luminance efficiency but a different TBB content : Ph-PPV P3 (TBB : 6 %) vs copolymer P5 (TBB : 2.5 %). These observations have been explained by a self-accelerating process in which a low mobility, related to the number of conjugation breaks, may lead to charge carrier build up and therefore to a higher probability of additional conjugation breaks. This self-accelerating mechanism implies that even slight decrease in the TBB content may lead to greatly increased lifetimes. Johansson et al confirmed that a reduction in TBB content for their BOP-PPV and BOPM-PPV resulted in PLED's with longer lifetime. In this context the sulphinyl-route which allows a close control over defects, can be a powerful tool towards improved stability.

6.4.2 From plastic electronics towards Molecular Electronics

As already discussed in chapter 1, impressive progress has been made during the last 10 years in the development of semiconductor applications based on organic electronic materials. This progress has not only led to successful electronic prototype devices to demonstrate proof-of-principle but also to real commercial products. Throughout this thesis it has been demonstrated with prototype FET's, LED's and solar cells that the sulphinyl route is very promising for the plastic electronics of tomorrow. But also towards a farther future, in the era of 'Molecular Electronic' the sulphinyl route can play a very important role.

According to Moore's Law, by the year 2020 the dimensions of integrated circuit components will have been reduced to approximately 10 nm. The interconnecting wires within such circuits will by then have approached the ultimate limit ; that of a linear array of single atoms. Potential candidates for such semiconductive 'molecular wires' are σ-bonded chains of silicon and π-bond conjugated chains of carbon[9]. As mentioned before, a powerful tool to study the intrinsic mobility of charge carriers in individual chains is the time-resolved microwave-conductivity (TRMC) technique. In the following table hole mobility results as obtained with this technique by Grozema et al are listed for a number of polymers :

Material	Intrachain hole mobility $(cm^2\ V^{-1}\ s^{-1})$
DEH-PF	0.74
MEH-PPV	0.43
MeLPPP	0.16
P3HT	0.02

table 6.2 Hole mobility values for different polymers as obtained by Grozema et al using TRMC

Comparing the hole mobility results listed in this table with the results obtained on the sulphinyl MDMO-PPV one comes to the very important observation that the low defect level MDMO-PPV shows the highest mobility value of them all. Since conjugational defects have a strong impact on the intrachain mobility, the sulphinyl synthesis route provides the possibility to develop materials with improved intrachain mobility, interesting for future molecular wires, through a careful control and reduction of defect levels.

6.5   *References*

[1]   D. M., Johansson, X. J. Wang, *Macromolecules* (**2002**) 35, 4997.

[2]   A. Kraft, A.C. Grimsdale, A.B. Holmes, *Angew. Chem., Int. Ed. Engl.* (**1998**) 37, 402.

[3]   D. Braun, E.G.J. Staring, R.C.J.E. Demandt, G.L.J. Rikken, Y.A.A.R. Kessener, A.H.J. Venhuizen, *Synt.Met*. (**1994**) 66, 75.

[4]   a) H.C.F. Martens, P.W.M. Blom, H.F.M. Schoo, P*hys. Rev. B* (**2001**) 61, 7489. b) P.W.M. Blom, M.C.J.M. Vissenberg, *Materials Science and Engineering* (**2000**) 27, 53.

[5]   F.Grozema, P.Th. van Duijnen, Y.A. Berlinc, M.A. Ratner, L.D.A. Siebbeles, *J. Phys. Chem. B* (**2002**) 106, 7791.

[6]   a) P.P. Infelta, M.P. de Haas, J.M. Warman, *Radiat. Phys. Chem.* (**1977**) 10, 353. b) J.M. Warman, M.P. de Haas *Pulse Radiolysis ed Y. Tabata*, Boca Raton, Fl. Chemical Rubber Company Ress. (**1990**) chapter 6. c) P.G. Schouten, J.M. Warman, M.P. de Haas, *J.Phys.Chem.* (**1993**) 97, 9863.

[7]   Z. Bao, A. Dodabalapur, A.J. Lovinger, *Appl. Phys. Lett*. (**1996**) 69, 4108.

[8]   L. Reiner, *Transmission Electron Microscopy, Physics of image formation and microanalysis,* Springer-Verlag Berlin Heidelberg New York (**1989**).

[9]   F.C. Grozema, L.D.A. Siebbeles, J.M. Warman, S. Seki, S. Tagawa, U. Scherf, A*dv. Mat* (**2002**) 14, 3, 228.

Summary

Since the beginning of the nineties precursor routes towards semiconducting polymers are examined at the 'Instituut voor Materiaal Onderzoek' (IMO) part of the 'Limburgs Universitair Centrum' (LUC). Besides the successful development of a new synthetic precursor route, the so-called sulfinyl route, chemical and physical characterization techniques are used to better understand the structure-property relation. A widely used 'workhorse' conjugated polymer, MDMO-PPV (a PPV derivative) can be synthesized via this sulfinyl route. Two chemical defects related to asymmetrically substituted PPV-derivatives, such as the 'workhorse' material MDMO-PPV can be distinguished: defects related with the position of the side-chains (regioregularity) and defects related with interruptions of the conjugated system on the vinylene double bond (single bond defects).

It is shown that the sulfinyl precursor route exhibits a versatile chemistry and can control both mentioned defects. This allows the preparation of a number of different batches of MDMO-PPV with various defect types and levels. In this context, some new basic scientific questions appear, namely: How to use these new synthetic possibilities to obtain high performance semiconducting organic polymers? What is the influence of regioregularity on the semiconductor properties? What is the influence of sp^3 defects (single bond defects) in the conjugated chain on the semiconductor properties?

The aim of this thesis is to clarify a relation between defects of MDMO-PPV and the performance of devices prepared with this material (structure-property relation), via physical parameters.

Beside the sulfinyl procedure to synthesize MDMO-PPV, a widely used synthetic procedure, namely the Gilch procedure is used as a reference in this work.

In chapter 2, a brief discussion is presented on the different defects expected for the two precursor routes of the 'workhorse' material MDMO-PPV. Besides a description of the basic synthetic procedure and chemical

characterization of the MDMO-PPV materials and films, a matrix with five model compounds is defined. Differentiation is made between the synthetic procedure used to prepare MDMO-PPV (Gilch - sulfinyl), the number of sp^3 defects (0.5; 2; 7 and 7-10 %) and the regioregularity fraction (50/50; 80/20). The comparitive characterization of this matrix can be considered as the general thread in this thesis. Besides the definition of the different materials, a description is provided on general methods and critical parameters to ensure a well-controlled sample and device preparation.

In chapter 3 the matrix of MDMO-PPV materials is used as semiconductor layer in field effect transistors in order to obtain information on the FET-mobility of the charge carriers. A first important result obtained with these measurements is that the regioregular material has a significantly higher FET-mobility compared to the regiorandom materials, namely $5 \ 10^{-4} \ cm^2 \ V^{-1} \ s^{-1}$ versus approximately $2.5 \ 10^{-4} \ cm^2 \ V^{-1} \ s^{-1}$. This result is explained in terms of the higher degree of order in the bulk of the polymer film for devices based on this regioregular material, which will be proved in chapter 6 with TEM. Secondly, a much smaller effect of the single bond defects on the field effect mobility was observed. A slight increase in mobility via a decrease in conjugational defects could be observed. This effect is quantified via a first order approximation characterized by a slope equal to $-1.3 \ 10^{-5} \ cm^2 \ V^{-1} \ s^{-1}$ (% defects)$^{-1}$. Regarding this relatively small effect it is important to emphasize the macroscopic nature of this type of measurements. The charge transport that is probed using FET-devices involves not only motion along the polymer chains but also much slower, morphology dependent, processes such as the transfer of charge between neighboring chains. A powerful tool to study the intrinsic mobility of charge carriers is the time-resolved microwave conductivity (TRMC) technique which is introduced in chapter 6 and which initial results show significant differences between the various materials together with a clear inverse relationship between the single bond defect level and the intrachain mobility. Furthermore comparing the hole mobility with the values obtained for other polymers (MEH-PPV, P3HT, ...) one comes to the very important observation that the low defect level MDMO-PPV shows the highest mobility value of them all.

In chapter 4, an extended optical characterization is carried out on the matrix of MDMO-PPV materials. A rather high difference in optical performance between the group of regiorandom MDMO-PPV materials and the regioregular MDMO-PPV could be observed. Besides a clear red shift in the photoluminescence and electroluminescence peaks, a lower photoluminescence efficiency and faster decay time determined via time-resolved photoluminescence measurements are found for the regioregular materials. An improved set-up to measure the photoluminescence quantum efficiency was built during a 6 week traineeship at Philips Natlab, the Netherlands. The as determined external photoluminescence quantum

efficiency for the regioregular material (equal to 0.08) is approximately a factor two lower then for the regiorandom MDMO-PPV materials (approximately 0.15). Within the group of regiorandom materials a small increase in external photoluminescence quantum efficiency as function of the number of sp^3 defects is observed. A first order linear trend line is characterized by a slope equal to 7×10^{-4} (% defects)$^{-1}$. Similar observations are made when studying the photoluminescence lifetime via time resolved photoluminescence measurements. A photoluminescence lifetime equal to 0.46×10^{-9} s is determined for the regioregular MDMO-PPV. This is an approximately a factor of two lower then the average lifetime of the regiorandom MDMO-PPV materials (equal to 0.81×10^{-9} s). Within the group of regiorandom batches a small increase for this photoluminescence lifetime is observed as function of the number of single bond defects. This effect is quantified via a first order trend line characterized by a slope equal to 5×10^{-12} s (% defects)$^{-1}$.

Combination of both observations by applying a simple decay model allows the determination of both radiative and nonradiative lifetime of the excited state. Within the group of studied MDMO-PPV materials an almost equal radiative lifetime of 5×10^{-9} s is observed. A large difference in nonradiative lifetime is observed for the regiorandom materials (average 0.9×10^{-9} s) compared to the regioregular material (equal to 0.5×10^{-9} s). This is understood in terms of an additional state for the regioregular MDMO-PPV material. This state is then characterized by a rather fast nonradiative decay time. Differences for the nonradiative lifetime within the group of regiorandom materials are small. An increase of the nonradiative lifetime as function of the number of single bond defects, characterized by a slope of 6×10^{-12} s (% defects)$^{-1}$ (first order approximation) is observed. This is understood in terms of a higher exciton motion for the MDMO-PPV materials with lower sp^3-defect levels.

The photovoltaic responses of the different materials are discussed in chapter 5. By using sulfinyl MDMO-PPV with a low or intermediate number of sp3 defects (e.g. 0.5 % or 7 %) an improvement of about 15 % compared to the reference N-GIL MDMO-PPV solar cell efficiency (under AM1.5 illumination 80 mW cm^{-2}) is demonstrated. This solar cell efficiency equal to 2.9 % was at that time the highest reported efficiency for polymeric solid-state photovoltaic devices. These results were partly obtained during an 8 week traineeship at the Christian Doppler Laboratory for Solar Cells, Johannes Kepler University (Linz, Austria).

In the qualitative comparison of the regiorandom sulfinyl synthesized MDMO-PPV based solar cells, a small increase of the performance when decreasing the number of sp^3 defects could be observed. Surprisingly, the so-far promising regioregular material performs less good than the regiorandom materials most probably due to a less effective phase separation when blended with PCBM. A comparison of the photovoltaic

performance of the devices prepared with the complete matrix of MDMO-PPV indicates a rather complex balance between the individual material parameters and the morphology of the blended active layer. As the morphology of the active layer plays such an omnipresent role, photovoltaic studies of organic materials are also complicated by a strong influence of the processing parameters.

Finally in chapter 6, the conclusive structure-property relation with respect to single bond defects and regioregularity are discussed. In order to understand the important differences observed throughout the thesis for the regioregular material compared to the regiorandom materials, an additional TEM diffraction study has been performed which indicates enhanced order the in regioregular MDMO-PPV. This feature is used to explain the large influence of regioregularity on the structure-property relation of MDMO-PPV.

As a general conclusion one can state that among both studied defects, namely: conjugational defects: and regioregularity, the latter is the most powerful to tune the macroscopic electrical and optical semiconducting properties of PPV based due to enhanced morphological order. The sulfinyl route can therefore via a control of the regioregularity play an important role in the development of the next generation of conjugated polymers for plastic electronics.

Although the reduction of conjugational defects have only slight beneficial effect on the electro-optical properties of the investigated materials, two important prospectives can be formulated. A first prospective is related to the improvement of the reliability of PLED's. Since an inverse relationship has been demonstrated between the defect level of TBB defects and lifetime of PLED's, the sulfinyl route can be a powerful tool towards improved stability of devices. A second prospective can be formulated related to future molecular electronics. Since conjugational defects have a strong impact on the intrachain mobility, the sulfinyl synthesis route provides via a careful control and reduction of the defect levels the possibility to develop materials with improved intrachain mobility, interesting for future molecular wires, … but that is a different story.

Samenvatting

Aan het 'Instituut voor Materiaal Onderzoek' (IMO), onderdeel van het 'Limburgs Universitair Centrum' (LUC) wordt er onderzoek verricht naar precursor routes voor de synthese van halfgeleidende polymeren. Dit resulteerde in een succesvolle ontwikkeling van een nieuwe precursor route (sulfinyl route) bruikbaar voor de synthese van een grote variëteit geconjugeerde polymeren. Daarnaast worden er chemische en fysische karakteriseringstechnieken gebruikt voor een beter begrip van de structuur-eigenschap relatie van deze gesynthetiseerde polymeren in halfgeleider toepassingen te verkrijgen. MDMO-PPV is in vele onderzoeksinstituten en -groepen een algemeen gebruikt referentie materiaal. Dit asymmetrisch gesubstitueerd PPV derivaat kan eveneens gesynthetiseerd worden via de sulfinyl route. Bij een polymeer met een dergelijke chemische monomeerstructuur kunnen twee belangrijke types van defecten onderscheiden worden, namelijk: defecten met betrekking tot de positie van beide zijgroepen in relatie tot de aangrenzende monomeereenheid (regioregulariteit) en defecten met betrekking tot een onderbreking in het geconjugeerd systeem ter hoogte van de vinylbinding (enkelvoudige binding defect). In tegenstelling tot een in de industrie veel gebruikte synthese route voor MDMO-PPV, de Gilch route, kan de sulfinyl route beide defecten in sterkere mate controleren. Dit geeft aanleiding tot nieuwe wetenschappelijke vragen, zoals: Hoe moeten deze synthese mogelijkheden aangewend worden om halfgeleider polymeren met een goede performantie te verkrijgen? Wat is de invloed van regioregulariteit op de halfgeleider eigenschappen van geconjugeerde polymeren? Wat is de invloed van het enkelvoudige binding defect op de halfgeleider eigenschappen van geconjugeerde polymeren?
De antwoorden op deze vragen zijn nodig om de nieuwe synthese mogelijkheden van de sulfinyl route ten volle te benutten en toekomstig synthese strategieën te bepalen.
Met de sulfinyl route kunnen er verschillende types van het MDMO-PPV materiaal gesynthetiseerd worden met een verschillende concentratie aan

beide defecten. Het doel van deze thesis is dan ook om de relatie tussen beide defecten aanwezig in het MDMO-PPV materiaal en de eigenschappen van halfgeleider structuren gemaakt met dit materiaal te onderzoeken. Tevens is de Gilch route in dit werk bestudeerd als een referentie synthese route.

In hoofdstuk 2 wordt er dieper ingegaan op de verschillende defecten en de manier van controleren voor beide synthese routes. Naast een beschrijving van de synthese routes wordt er een matrix van vijf verschillende MDMO-PPV materialen gedefinieerd. Merk op dat al deze materialen een gelijke monomeer voorstelling hebben. In deze matrix is het enkelvoudige binding defect gevarieerd (0.5; 2; 7 en 7-10 %) en de regioregulariteitsfractie (50/50 – 80/20). De karakterisering van de halfgeleider structuren, met als actieve laag de MDMO-PPV materialen zoals beschreven in de matrix, vormt de rode draad in dit werk. Tenslotte wordt er in hoofdstuk 2 de specimenpreparatie beschreven en enkele kritische parameters bepaald.

In hoofdstuk 3 wordt de matrix van MDMO-PPV materialen zoals gedefinieerd in hoofdstuk 2 gebruikt als actieve halfgeleider laag in een veld-geïnduceerde-transistor (FET). Hierdoor wordt de mobiliteit van ladingsdragers bepaald in het beperkt interactiegebied net boven de oxidelaag. Een eerste belangrijk resultaat is een significant grotere FET-mobiliteit voor het regioregulair materiaal in vergelijking met de regiorandom types ($5 \cdot 10^{-4}$ cm^2 V^{-1} s^{-1} in vergelijking met $2.5 \cdot 10^{-4}$ cm^2 V^{-1} s^{-1}). Dit resultaat wordt verklaard door een grotere orde van het regioregulaire MDMO-PPV in de actieve laag. Deze toegenomen orde zal via een TEM diffractie studie bewezen worden in hoofdstuk 6. Een klein effect van het enkelvoudige binding defect op de FET-mobiliteit is eveneens vastgesteld. Dit effect is gekwantificeerd door een eerste orde benadering die een afname van de mobiliteit als functie van een stijgend aantal enkelvoudig binding defecten beschrijft. De helling is gekarakteriseerd als $-1.3 \cdot 10^{-5}$ cm^2 V^{-1} s^{-1} (% defecten)$^{-1}$. Aangezien dit effect relatief klein is, is het belangrijk om de macroscopische benadering van het begrip mobiliteit bepaald via transistor metingen te benadrukken. Deze metingen geven niet enkel informatie over de beweging van de ladingsdragers langsheen de polymeerketens maar vooral over morfologie afhankelijke processen zoals de overdracht van ladingsdragers tussen naburige keten(-segmenten). Een interessante techniek om de intrinsieke mobiliteit van de ladingsdragers binnen de keten te bepalen zijn tijdsopgeloste microgolf geleidingsmetingen (TRMC). In hoofdstuk 6 worden enkele inleidende resultaten die significante verschillen aantonen tussen de verschillende sulfinyl MDMO-PPV materialen besproken. Een duidelijk inverse relatie tussen enerzijds de intrinsieke intra-keten mobiliteit en anderzijds het enkelvoudige binding defect niveau kon worden waargenomen. Tevens, is de waarde voor de intra-keten mobiliteit van het sulfinyl MDMO-PPV met

het laagste enkelvoudige binding defect niveau de hoogste in vergelijking met soortgelijke waardes voor andere halfgeleider polymeren (MEH-PPV, P3HT, ...).

In hoofdstuk 4 worden de optische eigenschappen van de vijf types van MDMO-PPV bepaald. Ook wat betreft de optische eigenschappen is er een groot verschil tussen het regioregulair MDMO-PPV materiaal in vergelijking met de regiorandom types. Er wordt een duidelijke roodverschuiving vastgesteld van het fotoluminescentie en elektroluminescentie spectrum. Tevens wordt er een kleinere fotoluminescentie efficiëntie en een sneller verval van de aangeslagen toestand gemeten via tijdsopgeloste fotoluminescentie metingen.

Een verbeterde opstelling voor het bepalen van de fotoluminescentie efficiëntie is opgebouwd gedurende een 6 weken durende stage in Philips Natlab, Nederland. Een externe fotoluminescentie waarde van 0.08 werd gemeten voor de regioregulaire MDMO-PPV films. Dit is ongeveer een factor twee lager dan voor de niet regioregulaire MDMO-PPV materialen (gemiddelde 0.15). Binnen deze groep van niet regioregulaire materialen werd een stijgende fotoluminescentie efficiëntie waarde als functie van een stijgend aantal enkelvoudige binding defecten vastgesteld. Een eerste orde trendlijn met een helling gelijk aan $7 \cdot 10^{-4}$ (% defecten)$^{-1}$ karakteriseert dit effect. Gelijkaardige waarnemingen zijn gedaan in een studie naar de fotoluminescentie levensduur van de aangeslagen toestand door middel van tijdsopgeloste fluorescentie technieken. Een fotoluminescentie levensduur gelijk aan $0.46 \cdot 10^{-9}$ s werd bepaald voor het regioregulaire MDMO-PPV materiaal. Ook hier is deze waarde ongeveer een factor twee lager dan de gemiddelde levensduur van de aangeslagen toestand van de niet regioregulaire MDMO-PPV materialen (gelijk aan $0.81 \cdot 10^{-9}$ s). Binnen deze groep kan er een stijgende fotoluminescentie levensduur van de aangeslagen toestand vastgesteld worden als functie van een stijgend aantal sp^3 defecten. Dit eerder beperkte effect is gekarakteriseerd door middel van een eerste orde benadering met helling $5 \cdot 10^{-12}$ (% defecten)$^{-1}$.

Combinatie van de fotoluminescentie efficiëntie waarde en de waarde voor de fotoluminescentie levensduur van de aangeslagen toestand geeft, door middel van de toepassing van een eenvoudig verval model, inzicht in de radiatieve en niet-radiatieve levensduur van de aangeslagen toestand. Voor elk van de bestudeerde MDMO-PPV monsters werd een radiatieve levensduur gelijk aan $5 \cdot 10^{-9}$ s vastgesteld. Een groot verschil tussen enerzijds de niet-radiatieve levensduur van het regioregulaire MDMO-PPV materiaal (gelijk aan $0.5 \cdot 10^{-9}$ s) en anderzijds het gemiddelde van de waarden voor de niet regioregulaire MDMO-PPV materialen (de gemiddelde waarde gelijk aan $0.9 \cdot 10^{-9}$ s) werd vastgesteld. Meest waarschijnlijk is dit verklaard door de aanwezigheid van een additionele toestand in de regioregulaire materialen. Deze toestand is dan gekenmerkt door een snel niet radiatief verval.

Verschillen binnen de groep van niet regioregulaire materialen zijn eerder klein. Een toename van de niet-radiative levensduur van de aangeslagen toestand als functie van een stijgend aantal enkelvoudige binding defecten werd vastgesteld. Een eerste orde benadering is gekarakteriseerd door een helling gelijk aan 6 10^{-12} s (% defecten)$^{-1}$. Dit effect is verklaard door verschillen in exciton mobiliteit.

De zonnecel eigenschappen van de verschillende materialen zijn bestudeerd in hoofdstuk 5. Hiervoor werden buiten het gebruik van het MDMO-PPV materiaal gelijke zogenaamde bulk heterojunctie zonnecellen gemaakt. In deze topologie bestaat de actieve laag uit een blend van het elektron gevende MDMO-PPV en het elektron accepterende PCBM (een C_{60} derivaat). Het belangrijkste resultaat is een verhoging van de zonnecel efficiëntie (onder AM1.5 verlichting 80 mW cm^{-2}) met 15%, ten opzichte van de referentie Gilch MDMO-PPV zonnecel, voor specimen met als actief materiaal de sulfinyl gesynthetiseerde materialen met laag of gemiddeld niveau van enkelvoudige binding defecten (bijvoorbeeld 0.5 % of 7 %). De gerapporteerde zonnecel efficiëntie was op dat ogenblik de hoogste gerapporteerde efficiëntie voor een polymeer gebaseerde bulk hetero junctie organisch fotovoltaïsche cel. Deze resultaten zijn gedeeltelijk bekomen gedurende een 8 weken durende stage aan het Christian Doppler Laboratory for Solar Cells, Johannes Kepler University (Linz, Oostenrijk). In een kwalitatieve studie binnen de groep van sulfinyl materialen werd er een dalende trend van de fotovoltaïsche respons vastgesteld als functie van een stijgend aantal enkelvoudige binding defecten.
Tot onze verrassing was de zonnecel performantie van het veel belovende regioregulaire materiaal minder goed dan deze van de niet regioregulaire materialen. Dit is waarschijnlijk te verklaren door een minder efficiënte morfologie die bepaald wordt door de fasescheiding gedurende het spincoaten van de actieve laag. De vergelijking van de verschillende MDMO-PPV materialen gebruikt in zonnecellen geeft aan dat de fotovoltaïsche eigenschappen bepaald zijn door een complexe balans van enerzijds echte materiaal eigenschappen zoals mobiliteit en anderzijds de morfologie van de bulk hetero junctie blend. Dit impliceert echter dat er tevens een sterke invloed is van typische proces parameters.

In hoofdstuk 6 tenslotte wordt de structuur eigenschap relatie met betrekking op beide bestudeerde defecten namelijk regioregulariteit en enkelvoudige binding defect samenvattend besproken. De regioregulariteit is duidelijk de sterkste parameter om de eigenschappen van het MDMO-PPV te beïnvloeden. Een additionele TEM diffractie studie beschrijft kwalitatief de gepostuleerde verhoogde regelmaat in de regioregulaire MDMO-PPV film. Deze eigenschap wordt dan ook gebruikt om de grootste geobserveerde verschillen tussen eigenschappen van regioregulair MDMO-PPV versus niet regioregulaire MDMO-PPV materialen te verklaren.

Van de beide bestudeerde defecten (enkelvoudige binding defecten en regioregulariteit) is de regioregulariteit de sterkste parameter om de eigenschappen van PPV derivaten te sturen. De sulfinyl route kan door een controle van de regioregulariteit dan ook een belangrijke bijdrage leveren aan de ontwikkeling van nieuwe generaties van geconjugeerde polymeren.

Ondanks het feit dat de reductie van de enkelvoudige binding defecten slechts een beperkt effect heeft op de bestudeerde elektrische en optische eigenschappen kunnen er twee interessante perspectieven geformuleerd worden. Ten eerste is er een inverse relatie aangetoond tussen het TBB-defect en de levensduur van PLED's. De sulfinyl route kan via een sterkere controle over dit type van defecten dan ook een belangrijke stap zijn in de richting van een verbeterde betrouwbaarheid van PLED's. Een tweede perspectief van dit werk is gerelateerd met moleculaire elektronica. Door een reductie van de defect niveaus worden er hogere intra-keten mobiliteiten waargenomen. De sulfinyl route biedt dan een ook een potentieel voor de ontwikkeling van toekomstige moleculaire elektrische draden, … maar dat is een ander verhaal.